先端エネルギー材料理工共創研究センター第9回ワークショップ

# 東北大学金属材料研究所
# 先端エネルギー材料理工共創研究センター
# 第9回ワークショップ

## Institute for Materials Research, Tohoku University
## Collaborative Research Center on Energy Materials (E-IMR)
## E-IMR International Workshop 2024
## November 2024

令和６（二〇二四）年十一月　東北大学金属材料研究所

TOHOKU UNIVERSITY

令和６（2024）年11月

Research

Opening address

As a satellite of the Summit of Materials Science (SMS) to be held at the Institute for Materials Research (IMR), Tohoku University on 27th and 28th November 2024, the E-IMR Centre (Collaborative Research Centre on Energy Materials, IMR) is going to hold the “E-IMR International Workshop 2024 (E-IMR IWS 2024)” on the 26th November, the day before SMS.

The recent issues of energy and global warming/climate change have increased the importance of solving these problems, and the research and development of mechanisms for securing new energy sources, energy conversion and storage materials have become urgent tasks. The development of new materials for energy has become an essential issue and is currently a priority area of focus in IMR.

The activities of IMR, which was established in April 2015, will enter its ninth year in FY2024, and from FY2022, when the “Fourth Medium-Term Goals and Plans” of MEXT began, the E-IMR Centre was reorganized, expanded and strengthened as the second phase of its mission. The E-IMR centre was reorganized into four research units: 1. Solar Energy Conversion Materials Research Unit, 2. Energy Storage Materials Research Unit, 3. Materials Evaluation and Analysis Research Unit, and 4. Novel materials unit towards social implantation. In particular, Materials Evaluation and Analysis Research Unit has been newly established, with a team structure that can carry out quantum beam analysis using synchrotron radiation and neutrons, first-principles calculations, as well as materials evaluation and prediction using materials informatics (MI).

Each research unit, which is composed of researchers from the fields of science and engineering, promotes world-class materials research by exploring the research frontiers in the field of energy materials, and employs three specially appointed assistant professors to foster young researchers with advanced research skills in interdisciplinary fields. In addition, we are promoting research in areas not completely covered by IMR, with the participation of faculty members and researchers from research organizations not only inside but also outside IMR, including the Graduate School of Engineering, the Advanced Institute for Materials Research (AIMR), and the International Center for Synchrotron Radiation Innovation Smart (SRIS).

Our mission is to establish innovative energy materials and composite module creation that contributes to maximizing solar energy utilization and the three storages of “heat, electricity, and hydrogen”. Through these research topics, we intend to contribute to the construction of a green energy society using solar energy towards carbon neutrality.

26th Nov. 2024(R6).

Head, E-IMR Centre
Institute for Materials Research, Tohoku University
Professor Dr. Tetsu ICHITSUBO

# 「E-IMR International Workshop 2024」
# Contents

【Research Publication】


1. **On the dynamics of magnets and ferroelectrics**
   Bauer Gerritt E.W [Solar Energy Conversion Materials Research Unit / Advanced Institute for Materials Research Professor] ····· 1

2. **Recent Progresses in Skyrmionic Materials and Devices**
   Wanjun Jiang [Tsinghua University Professor] ····· 3

3. **Dissociative Oxygen Adsorption and Incorporation in $Co_3O_4$-Dispersed PCFC Cathodes**
   Hitoshi Takamura [Energy Storage Materials Research Unit / School of Engineering Tohoku University Professor] ····· 17

4. **Revealing the Surface Termination Effect of Perovskite for Oxygen Exchange Reaction**
   Di Chen [Tsinghua University Associate Professor] ····· 27

5. **Mobility and clustering of O and anion vacancies in perovskites as energy materials**
   Francesco Cordero [CNR-ISM Istituto di Struttura della Materia Primo Ricercatore] ····· 29

6. **Nanostructure and chemical state imaging of energy materials by coherent X-ray diffraction**
   Yukio Takahashi [Materials Evaluation and Analysis Research Unit / International Center for Synchrotron Radiation Innovation Smart Professor] ····· 49

7. **Layered Manganese Dioxide as a Heat-Storage Material Utilizing Environmental Water Vapor**
   Norihiko Okamoto [Solar Energy Conversion Materials Research Unit / Institute for Materials Research Associate Professor] ····· 55

8. **A new AB3-based alloy with reversible hydrogen absorption and desorption reactions and lessdegradation**
   Toyoto Sato [Energy Storage Materials Research Unit / Institute for Materials Research Associate Professor] ····· 63

9. **Interface Design for Room-Temperature Rechargeable Magnesium Batteries with Transition Metal Oxide Cathodes**
   Hongyi Li [Energy Storage Materials Research Unit / Institute for Materials Research Project Assistant Professor] ····· 69

10. **Recent advances of silicon cystal for solar cells**
    Deren Yang [Zhejlang University Professor] ····· 75

11. **Probing the Multipolar Structure of Berry Curvature in Magnetization Space by the In-plane Anomalous Hall Effect**
    Dazhi Hou [University of Science and Technology of China Professor] ····· 101

12. **Formation Rate as a Key Factor in Enhancing the Stability of Anode-Less Lithium Metal Batteries**
    Michael De Volder [University of Cambridge Professor] ····· 115

# 【 Research Publication 】

# On the dynamics of magnets and ferroelectrics

Gerrit Bauer, バウアー・ゲリット, 包格瑞

Alexander von HUMBOLDT STIFTUNG  AIMR  E-IMR  キメラ準粒子

1

## With thanks to:

Haiming Yu c.s.
Eiji Saitoh c.s.
**Kenichi Uchida c.s.**
Bart van Wees c.s.
Joseph Heremans c.s.
Toeno van der Sar c.s.
Olivier Klein c.s.
Yaroslav Blanter c.s.
Kei Yamamoto/Hide Kurebayashi c.s.
Guoqiang Yu/Peng Yan c.s.
Shunsuke Fukami c.s.
Zhicheng Zhong c.s.
Sergio Rezende c.s.
…



2

## Contents

- Magnets and ferroelectrics
- Dynamics of magnets: Magnonics
- Dynamics of ferroelectrics: Ferronics

PRApplied

PHYSICAL REVIEW APPLIED **20**, 050501 (2023)
Perspective

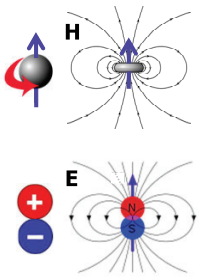


3

## Magnetic materials of interest

CoFeB

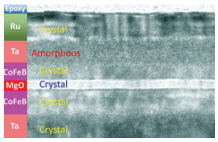


Hematite, $Fe_2O_3$ (Lebrun *et al.*, 2020)

NC-AFM

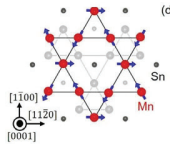


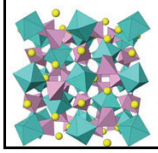

Yttrium iron garnet (YIG)

$Y_3^{(3+)}\,Fe_2^{(3+)}\,(Fe^{(3+)}O_4^{(2-)})_3$

$CrPS_4$ (de Wal *et al.*, 2023)

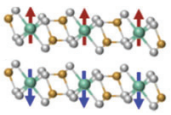

4

## Ferroelectric materials of interest

hopping protons

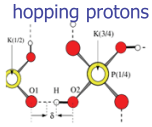

$NaNO_2$: $T_c$ ~ 450 K

molecular dipoles

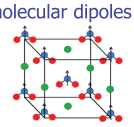

$KH_2PO_4$: $T_c$ ~ 122 K

soft optical phonons

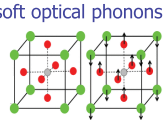

$BaTiO_3$: $T_c$ ~ 400 K

shift in polar bilayers (Yasuda et al., 2020)

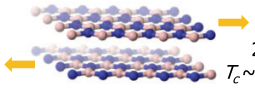

2BN
$T_c$~1000 K

Moiré charge-transfer (Zheng et al. 2020; Niu et al., 2022)

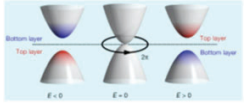

BLG
$T_c$~
100 K

5

## Applications of magnets and ferroelectrics

Information and communication technologies

| Technology | Magnets | Ferroelectrics |
|---|---|---|
| non-volatile memories | tapes, disks, M-RAMs | F-RAM |
| sensors and actuators | magnetic fields etc. | vibrations etc. |
| electronics | inductors | capacitors |
| computing | p-bits, spin wave interconnects | polarization waves |

Energy/heat management

| Heat managing | Magnets | Ferroelectrics |
|---|---|---|
| quasi-equilibrium/reversible cooling | magnetocalorics | electrocalorics |
| non-equilibrium/irreversible | Nernst/Ettingshausen effect | ? |
| | spin-dependent and spin Seebeck/Peltier effect | polarization Seebeck/Peltier effect GB et al. (2022) |
| heat switches | K. Uchida c.s. (2023) | Wooten et al. (2023) |

6

## Spin polarization waves and magnons

Landau-Lifshitz equation: $\frac{d\mathbf{M}}{dt} = -\gamma \mathbf{M} \times \mathbf{B}_{\text{eff}}$; $\mathbf{B}_{\text{eff}} = -\frac{\delta F[\mathbf{M}]}{\delta \mathbf{M}}$

free energy

Linearized solution (exchange spin waves):

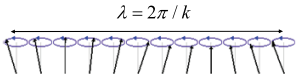


$\hbar\omega_k = \hbar\omega_0 + Ak^2$

$\omega_0 = \gamma B_{\text{eff}}$

Charles Kittel (1916-2019)

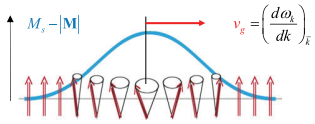


**Magnons** are the quanta of spin waves with $M_k \simeq -\mu_B$ (Bosons):

$$n_k = \frac{1}{e^{\frac{\hbar\omega_k}{k_B T}} - 1}$$

7

## Electric polarization waves and ferrons (displacive)

Landau-Khalatnikov equation: $\frac{1}{\varepsilon_0 \omega_p^2}\frac{d\mathbf{P}}{dt} = E_{\text{eff}}[\mathbf{P}]$; $\omega_p^2 = \frac{1}{\varepsilon_0 V_0}\sum_i \frac{Q_i^2}{M_i}$; $E_{\text{eff}} = -\frac{\delta F[\mathbf{P}]}{\delta \mathbf{P}}$

Linearized solution (polarization waves):

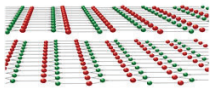

$\hbar\omega_k = \hbar\omega_0 + Ak^2$

$\omega_0 = \sqrt{\varepsilon_0 \omega_p^2 E_{\text{eff}}}$

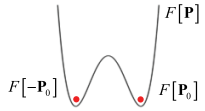


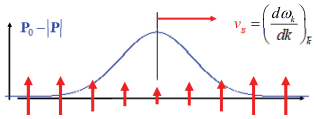


**Ferrons** are the quanta of polarization waves with Planck statistics:

$$n_k = \frac{1}{e^{\frac{\hbar\omega_k}{k_B T}} - 1}$$

8

## Hellmann-Feynman theorem for magnons and ferrons

**Magnon:** a quasiparticle that carries a magnetic dipole

Zeeman interaction: $\mathcal{H}_Z = \mathcal{H}_0 - \mathbf{M}\cdot\mathbf{B}$ and $\mathcal{H}_Z\psi_i = \varepsilon_i\psi_i$

$$\Rightarrow \quad \langle \mathbf{M} \rangle_i = -\frac{\partial \varepsilon_i}{\partial \mathbf{B}} = O(\mu_B)$$

**Ferron:** a quasiparticle that carries an electric dipole

Stark interaction: $\mathcal{H}_S = \mathcal{H}_0 - \mathbf{P}\cdot\mathbf{E}$ and $\mathcal{H}_S\psi_i = \varepsilon_i\psi_i$

$$\Rightarrow \quad \langle \mathbf{P} \rangle_i = -\frac{\partial \varepsilon_i}{\partial \mathbf{E}} = ?$$

Optical phonons in inversion symmetric systems are not ferrons: $\omega_{OP}(E) = \omega_{OP}(-E) \Rightarrow \langle \mathbf{P} \rangle_{OP} = 0$

9

## First experiments: thermal conductivity

Wooten et al. (OSU, 2023)

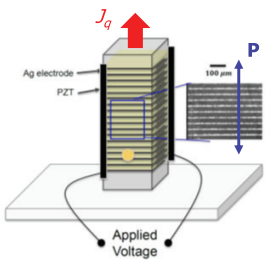


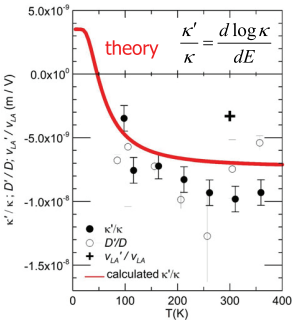


10

## Ferroelectric drag effect (P. Tang *et al.*, 2023)

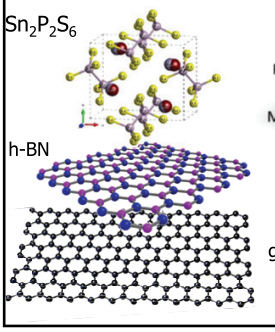


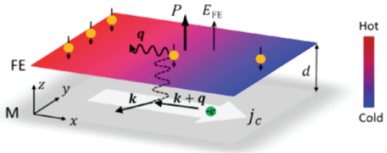


$$ZT = \frac{G_{\text{graphene}} S^2 T}{K_{\text{FE}}}$$

11

## Magnonic vs. ferronics

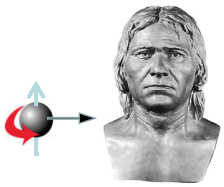

magnonics

ferronics

12

# Towards Functional Skyrmion Racetrack Memory

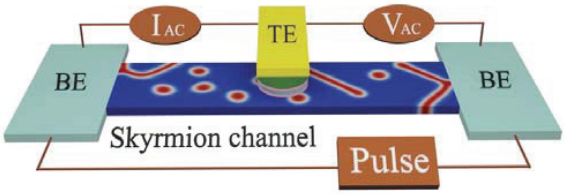


Wanjun Jiang

Department of Physics, Tsinghua University, Beijing

jiang_lab@tsinghua.edu.cn

## Outline

1: Background

2: Emerging materials and Topological physics

3: Deterministic generation and long-distance transportation of skyrmions

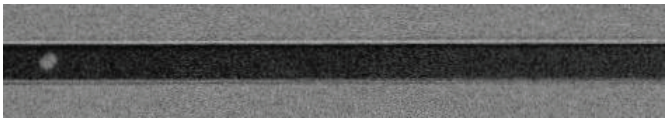

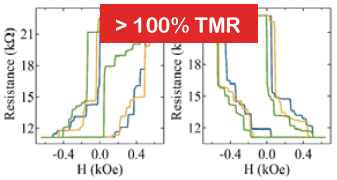


4: Optimization of skyrmionic MTJ

5: Conclusion and outlook

# Application of magnetism

**Information technology**

**Electronics**

**Electric vehicle**

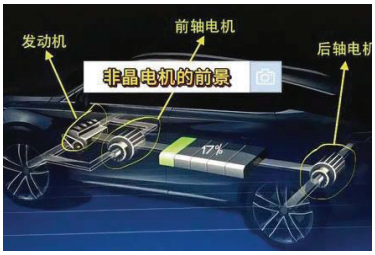


**Transportation**

**Life science**

**Defense technology**




# Spintronics

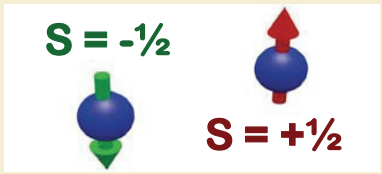


Spin up (1)

Spin down (0)

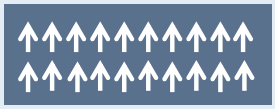

**Ferromagnetism**
$M = \Sigma s \neq 0$

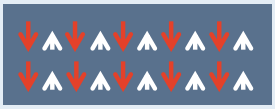

**Ferrimagnetism**
$M = \Sigma s \neq 0$

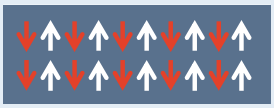

**Antiferromagnetism**
$M = \Sigma s = 0$

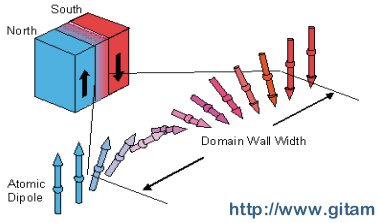


**Nanoscale spin textures**

# Racetrack: from domain wall to skyrmion

NiFe
Large size: 200-nm

Larger current density
$10^{7-8}$ A/cm$^2$

Spin transfer torque

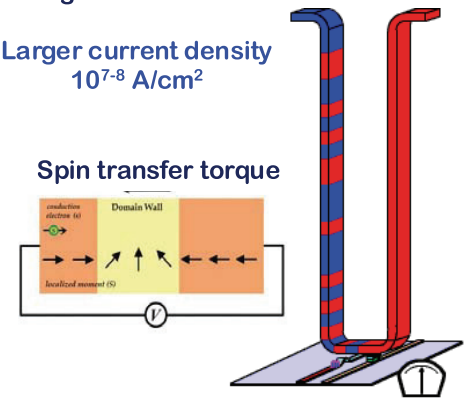


**Domain wall** racetrack memory

S. Parkin et. al., Science (2008)

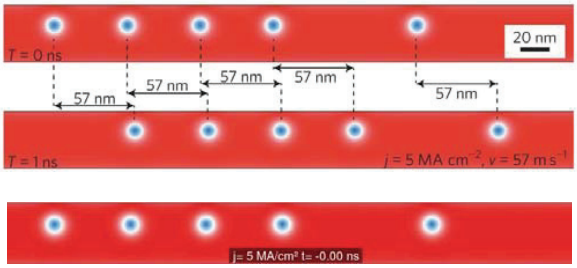


| | |
|---|---|
| Non-volatile | (topological protection) |
| Ultra-efficient | (spin-orbit torques) |
| Ultra-dense | (0.5 - 5 nm) |
| C-MOS compatible | (thin film) |

**Skyrmion** racetrack memory

Albert Fert et al., Nat. Nano. (2013)



# Néel skyrmions in magnetic multilayer

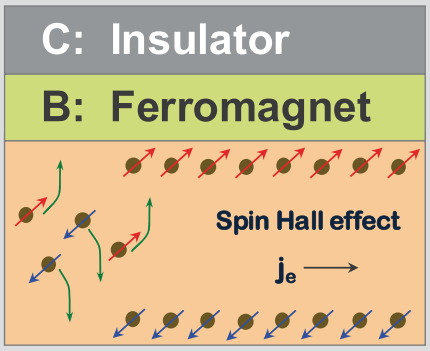


Néel skyrmion

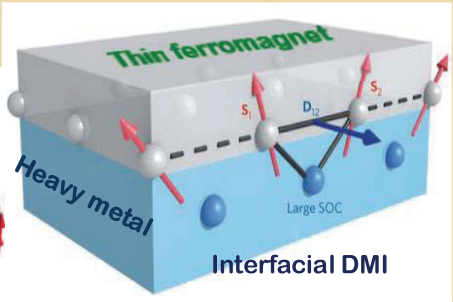


Pt/CoFeB/MgO, Ir/Fe/Pd, Ta/CoFeB/TaOx

Albert Fert et al., Nat. Nano. (2013)

Q. Liu et al., Science (2012)
For a Review: Axel Hoffmann,
IEEE Trans. Mag. 49, 5172 (2013)

**Promising**

(room temperature, few nanometers skyrmion,
novel driving mechanism, massive production,)

# Nano size and low-power consumption

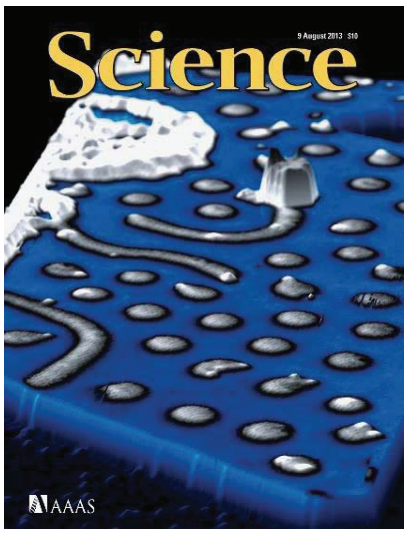


Romming et al., Science, 2013

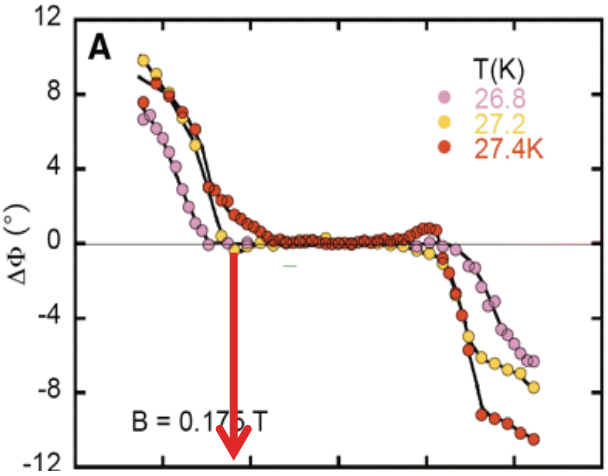


$J_c$ ($2 \times 10^2$ A/cm$^2$)

Jonietz et al, Science, 2010

**5 nm, 20 K**

**0.0001 of MRAM devices, 30 K**



# Outline

1: Background

2: Emerging materials and Topological physics

3: Deterministic generation and long-distance transportation of skyrmions

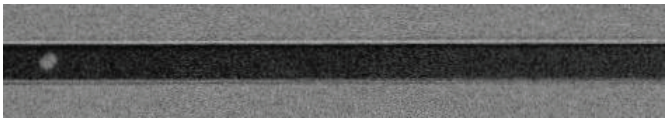

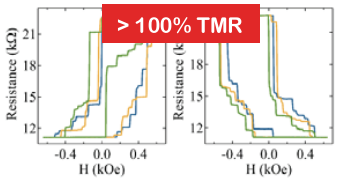


4: Optimization of skyrmionic MTJ

5: Conclusion and outlook

# A simple multilayer: Ta/CoFeB/$TaO_x$

UHV Sputtering system

Insulator

Ferromagnet

Heavy metal


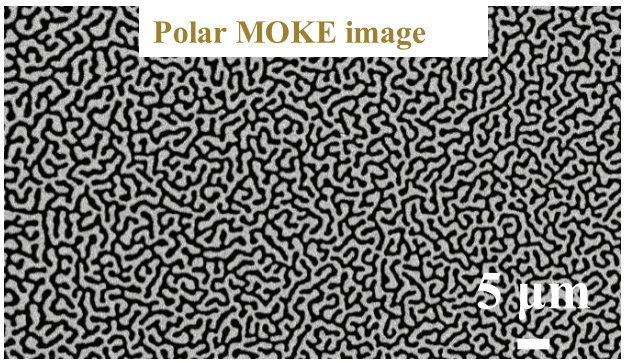




# Blowing skyrmion bubbles by currents


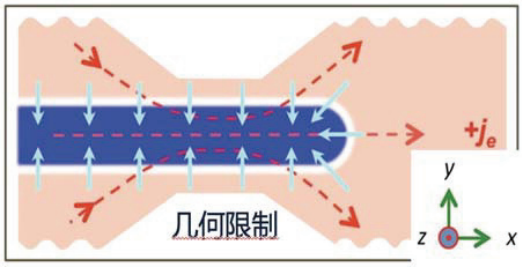


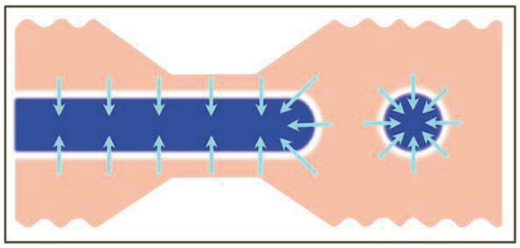

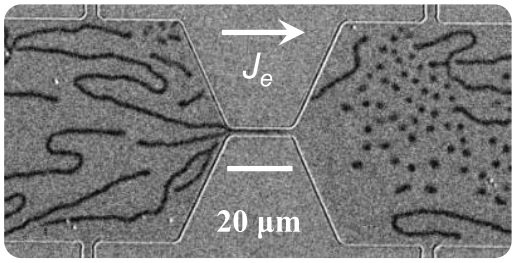


Ta/CoFeB/$TaO_x$, current density ~$7\times10^4$ A/cm$^2$

"Blowing" **Néel-type** skyrmions at room temperature

W. Jiang, et al., Science 349, 283 (2015), postdoc work at Argonne.

# Emerging skyrmion materials

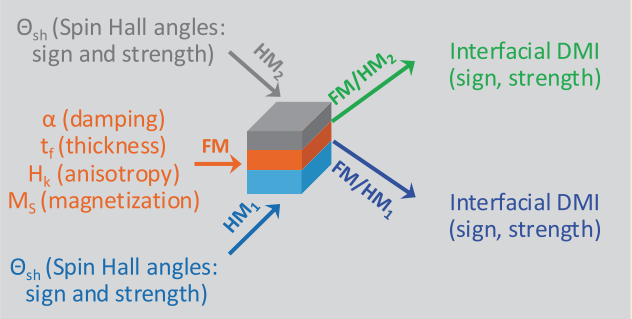


W. Jiang, et al.,
Physics Reports, 704, 1(2017).


W. Jiang, et al., Science 349, 6245 (2015).
W. Jiang, et al., Phys. Rev. B, 99, 104402 (2019).
W. Jiang, et al., Physics Reports 704, 1-49 (2017).
Z. Wang., et al., Nature Electronics 3, 672 (2020).
H. Zhou, et al., Adv. Funct. Mater., 31, 2104426 (2021).
T. Xu, et al., Phys. Rev. Materials 5, 084406 (2021).
J. Liu, et al., Chin. Phys. Lett., 39, 017501 (2022).
Q. Zhang, et al., Phys. Rev. Lett. 128, 167202 (2022).
T. Xu, et al., ACS Nano 17, 7920 (2023).
Y. Dong, et al., Appl. Phys. Lett. 124, 162407 (2024).


**Interface optimization:**

**material, thickness, stacking**

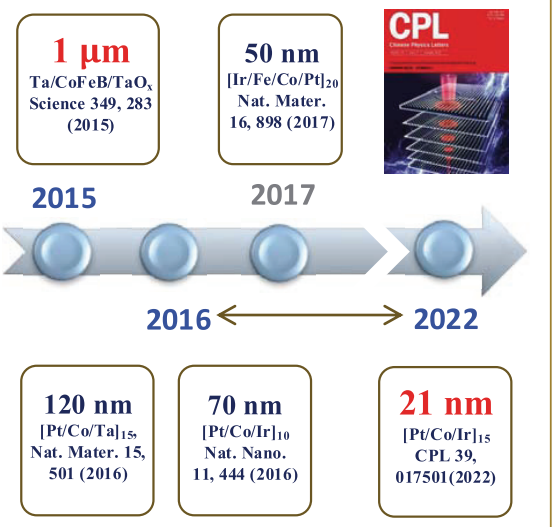




# Emerging topological physics

**topological charge**

$$Q = \frac{1}{4\pi}\int \mathbf{m}\cdot\left(\partial_x\mathbf{m}\times\partial_y\mathbf{m}\right)dxdy$$

**electric charge $q_e$**
**Lorentz force**
$F_l = q_e\,(v \times B_z)$

**topological charge Q**
**Magnus force**
$f_m = Q\,(v \times e_z)$

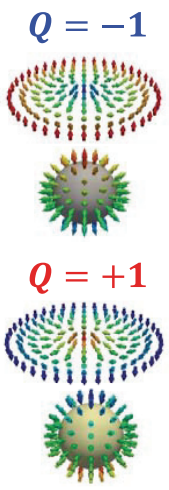


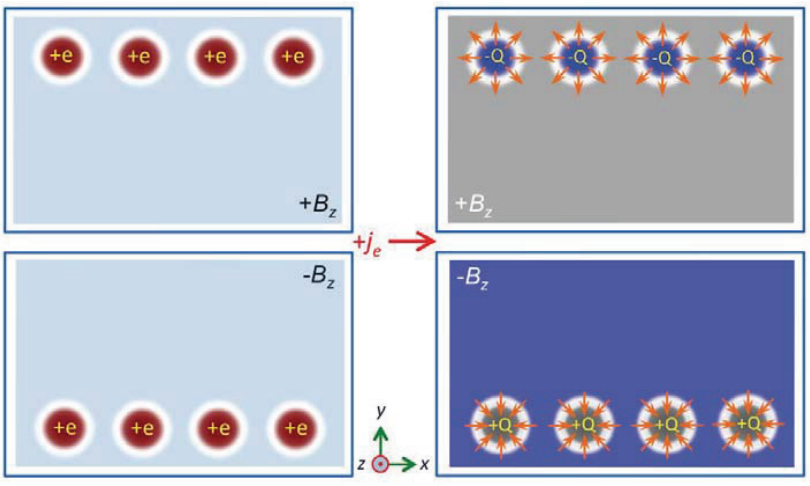


**Quasiparticles bring new flavors into the Hall family!**

# Skyrmion Hall effect and thermodynamics

## Skyrmion Hall effect: New member in the Hall Trio

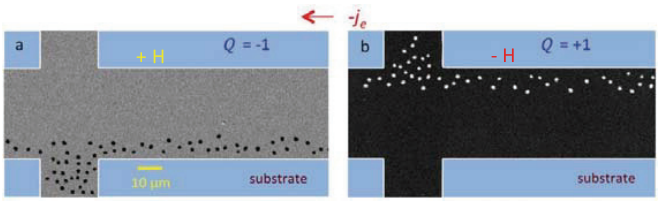


## Nonlinear topological thermodynamics of skyrmions

**Linear diffusion**

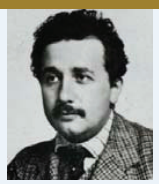

**Experiment**

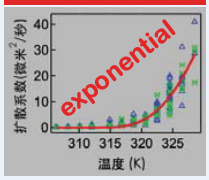


**Clockwise**

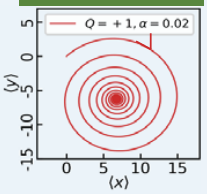


**Counterclockwise**

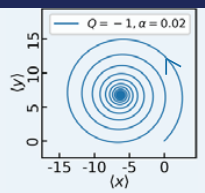



W. Jiang, et al., Nature Physics 13, 162 (2017).
Z. Wang, et al., Phys. Rev. B, 100, 184426 (2019).
L. Zhao, et al., Phys. Rev. Letts. 125, 027206 (2020).
C. Song, et al., Nano Letters, 22, 9368 (2022).
J. Liu, et al., Nano Letters, 23, 4931 (2023).
Y. Yang, et al., Nature Communications 15, 1018 (2024).




# Outline


1: Background

2: Emerging materials and Topological physics

**3: Deterministic generation and long-distance transportation of skyrmions**

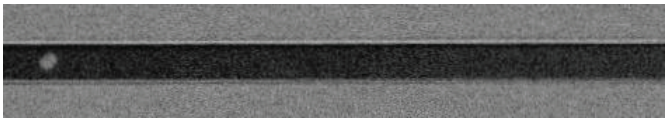

4: Optimization of skyrmionic MTJ

5: Conclusion and outlook

# Skyrmions on the racetrack

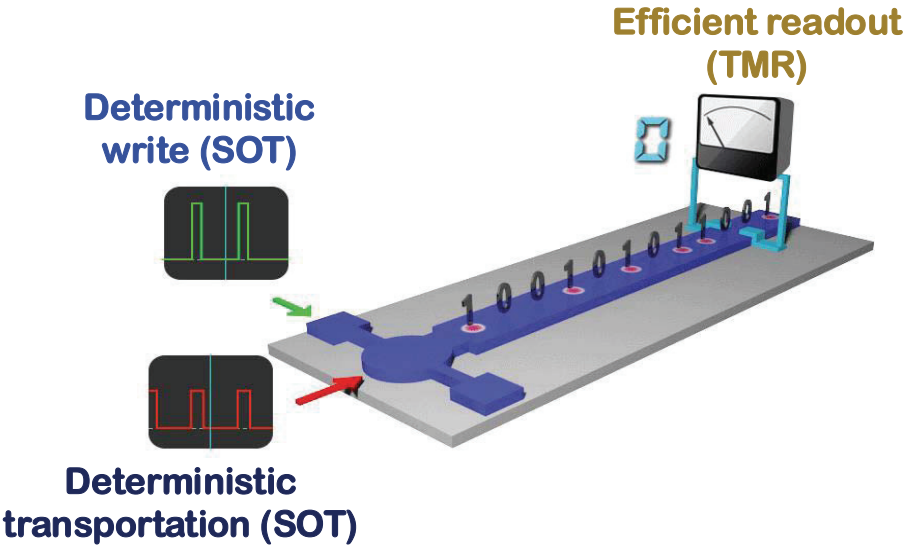


**Three key challenges:**

**bottleneck of device applications**



# Multiphysics simulation

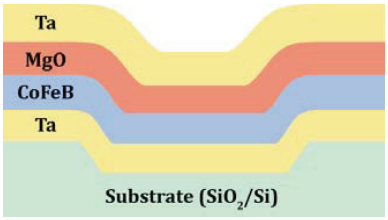


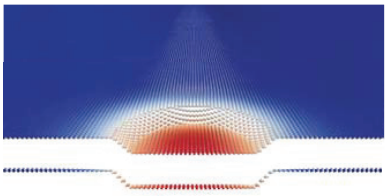

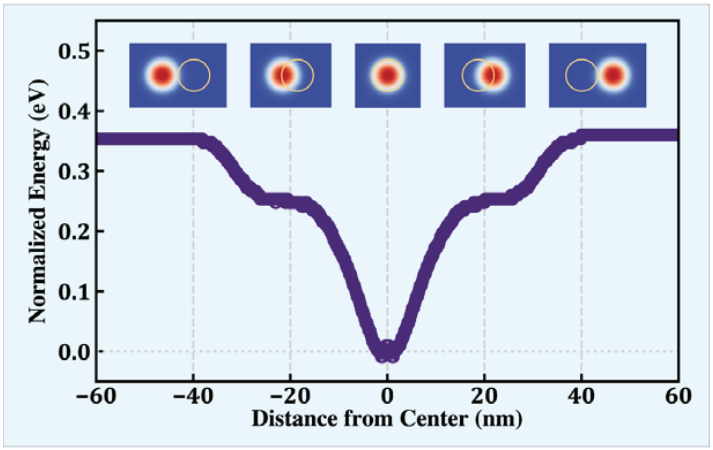


- Introduce concaved surface with nm-thick indentations
- Subsequent grow magnetic films on these substrate
- concaved surface generates unflat energy landscape
- Local energy minima traps skyrmions

# Patterning of skyrmion lattice

$B_z = +0.12\text{mT}$ After $J \sim 5\ \text{MA/cm}^2$

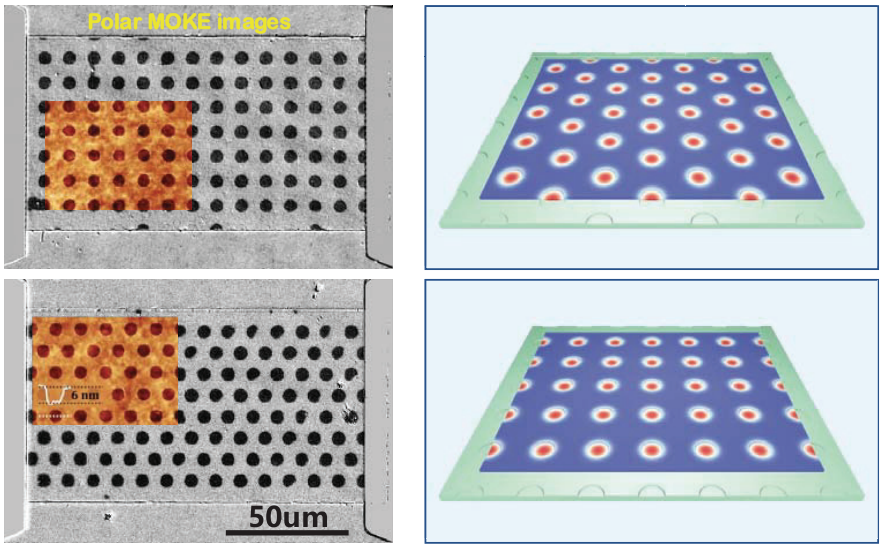


- 6nm-thick, 4um-diameter periodic indentations
- Designed skyrmions by the geometry of indentations



# 1D skyrmion racetrack

- Deterministic generation of skyrmions — write
- Precisely controlled transportation — move
- Electric detection of skyrmions by TMR — read

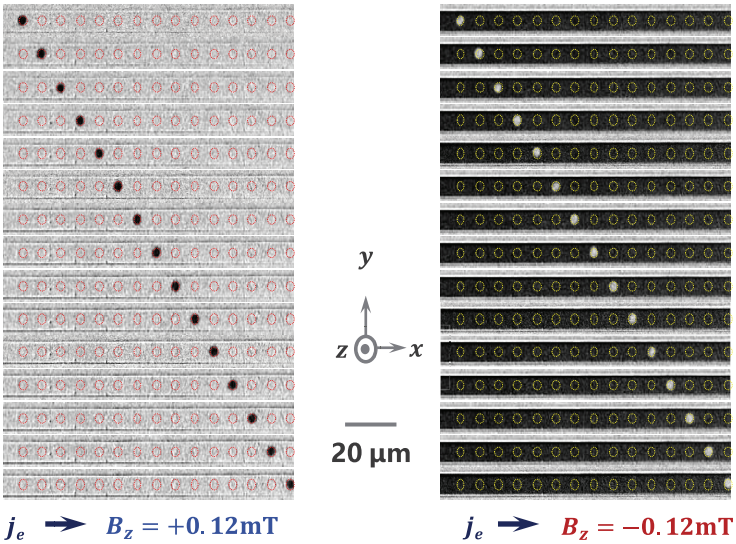

# Skyrmion shift register

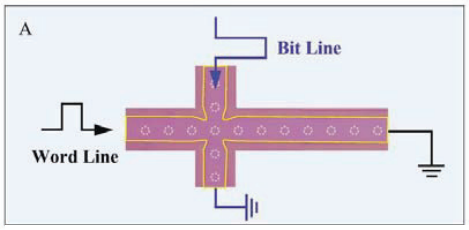


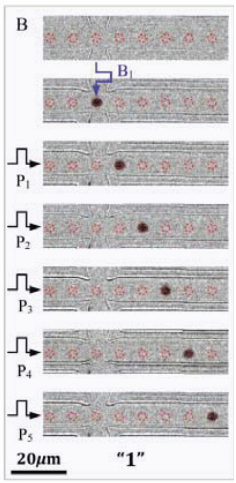




# Outline

1: Background

2: Emerging materials and Topological physics

3: Deterministic generation and long-distance transportation of skyrmions

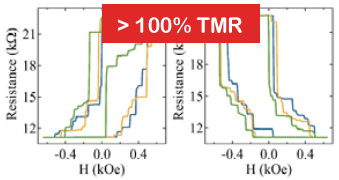


**4: Optimization of skyrmionic MTJ**

5: Conclusion and outlook

# Concept of skyrmion racetrack memory

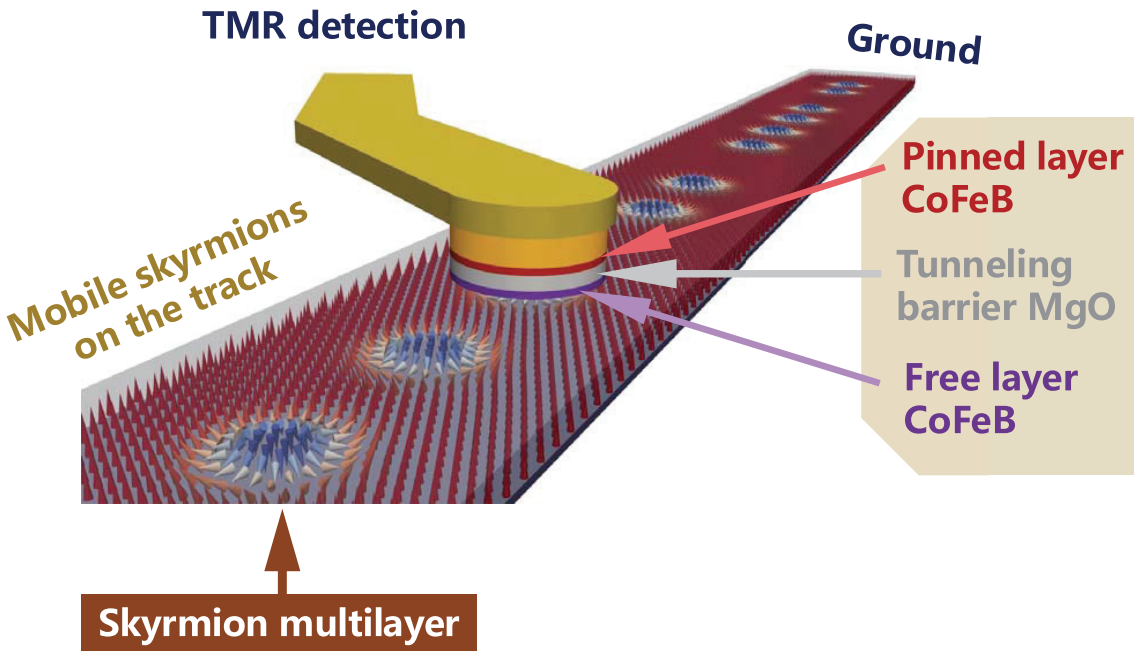




# Typical Skyrmion MTJ

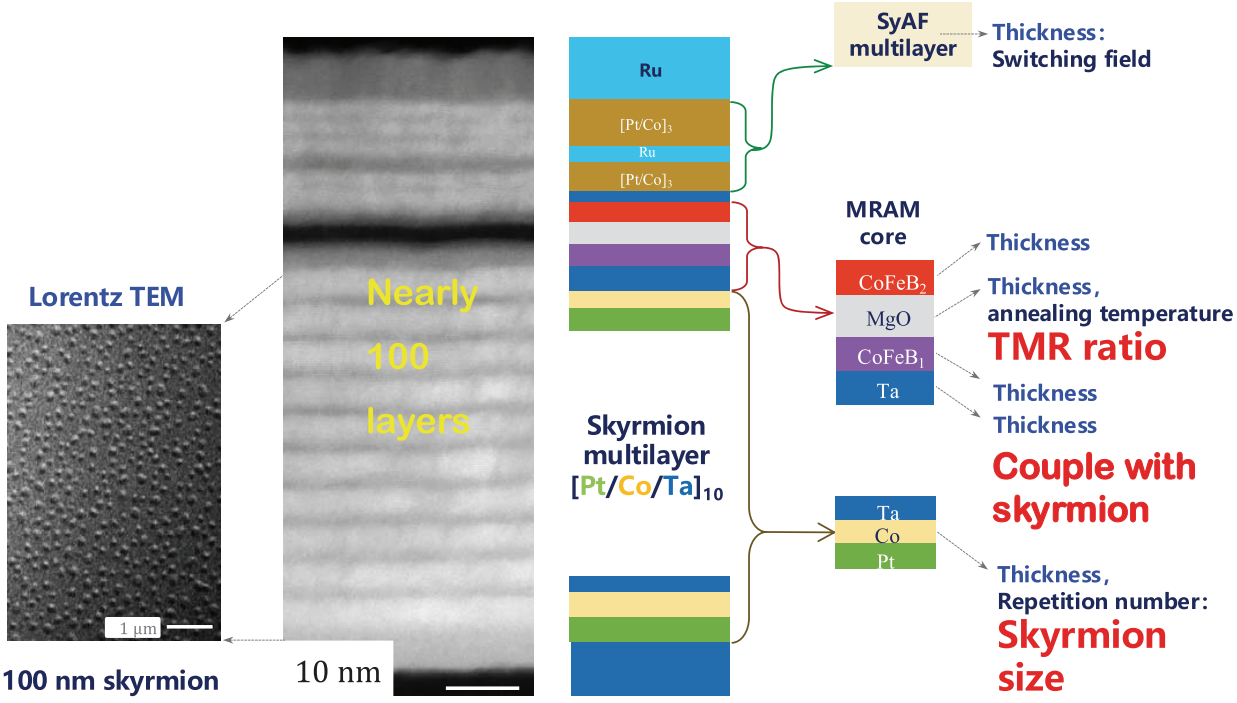


◆ Complex stack, many parameters, challenging to optimize

# Optimization of skyrmion MTJ

### Thickness of bottom CoFeB

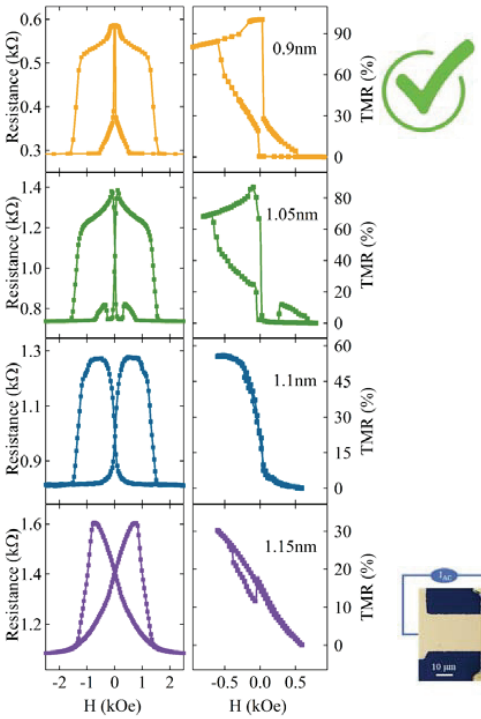


### Effect of annealing temperature

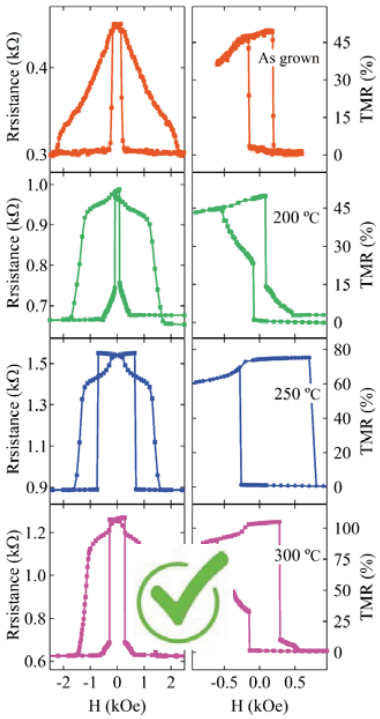




# Performance of skyrmion MTJ

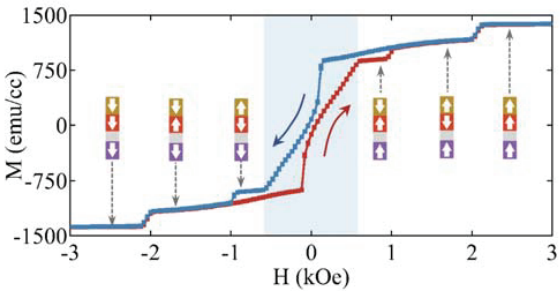


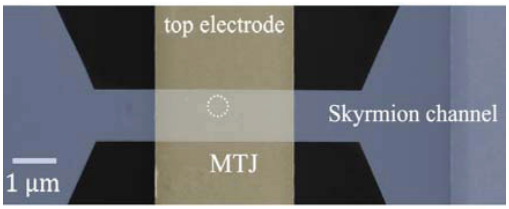


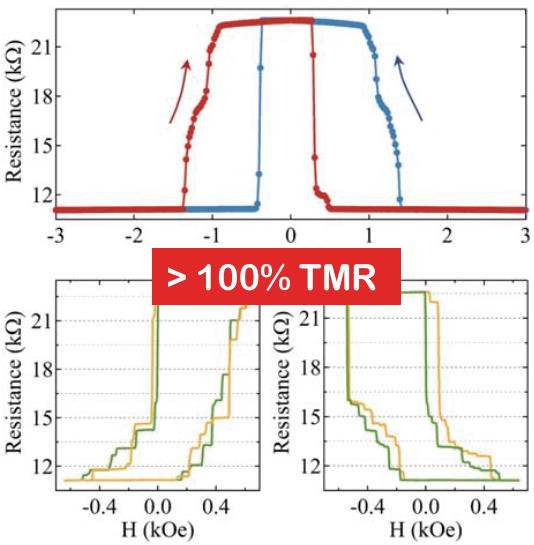


**> 100% TMR**

- **Fabricated 500 nm skyrmion MTJ**
- **Efficient detection of skyrmions with 100% TMR**
- **TMR steps may suggest the existence of skyrmions**

# Conclusions

- Optimized materials and topological physics
- Deterministic generation and transportation of skyrmions
- Efficient detection of skyrmions with 100% TMR

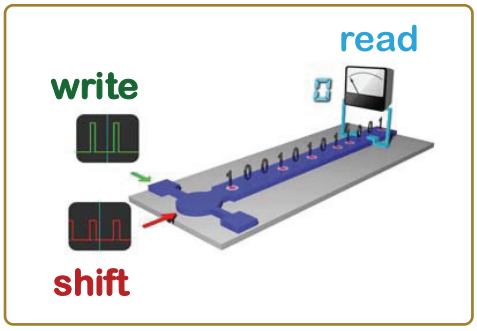


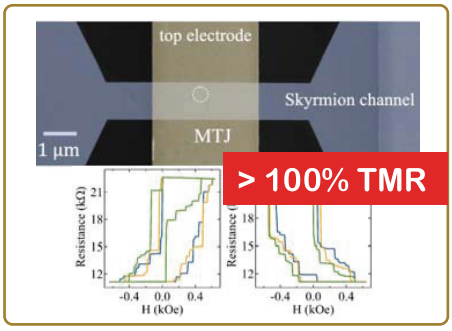


## Thank you for your attention!

## Students and postdocs wanted!

MEMO

# Dissociative Oxygen Adsorption and Incorporation in $Co_3O_4$-Dispersed $BaZr_{0.9}Sc_{0.1}O_{2.95}$ for PCFC Cathode

Hitoshi Takamura

S. Kamohara, Akihiro Ishii, Itaru Oikawa

Department of Materials Science, Graduate School of Engineering,
Tohoku University, Sendai, Japan

E-IMR workshop, Nov 26, 2024, Sendai Japan

## Solid Oxide Cells (SOCs)

$$H_2 + \frac{1}{2}O_2 = H_2O$$

SOC：Highest efficiency・Reversible operation

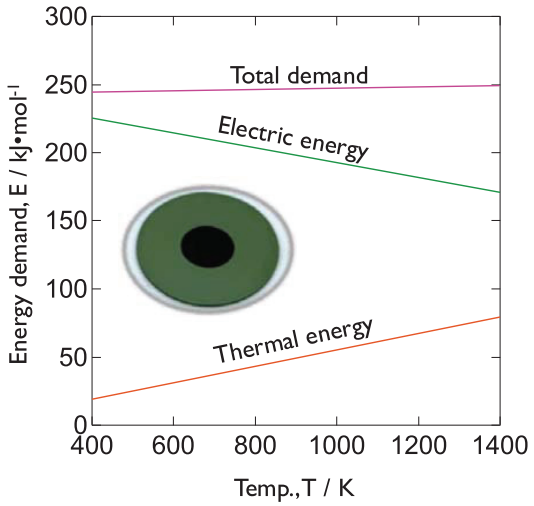


**Funding**

USA： Department of Energy (DOE)
FY2021 Hydrogen Shot "1 1 1"
(1$/1kg in 1 decade)
FY2022 PEM electrolyzer > 620 MW
EU：Clean Hydrogen JU (€150 M)

Target efficiency：≈ 3.0 – 3.5 kWh/Nm$^3$
Target cost：300 $/kW, 400—500 €/kW

**Industries**

USA：Bloom Energy, Fuel Cell Energy, etc.
EU：Sunfire, Topsoe, Ceres Power, etc.

## Surface Oxygen Exchange Reaction

1. $O_2 \overset{\Re_a}{\leftrightarrow} 2O^*_{ad}$ Dissociative adsorption reaction

2. $O^*_{ad} + 2e^- + 2H^+ \rightarrow H_2O$ Water generation reaction

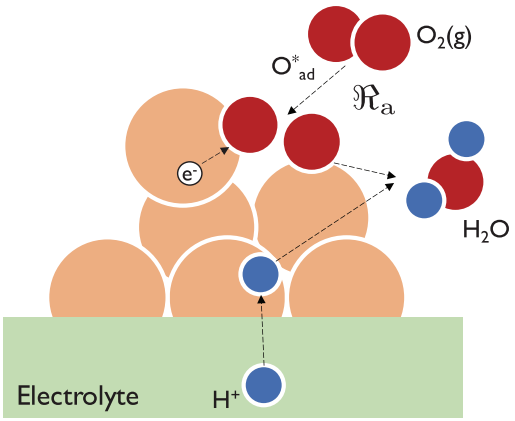


Most oxide cathode materials

→ $\Re_a$ becomes rate-limiting step[1]

→ Raising $\Re_a$ enhances the total surface exchange reaction.

Protonic conductor (PC)

[1] G. Mather *et al.*, *Appl. Sci.*, 2021, **11**, 5363.



## Dissociative adsorption rate of Co-containing oxides

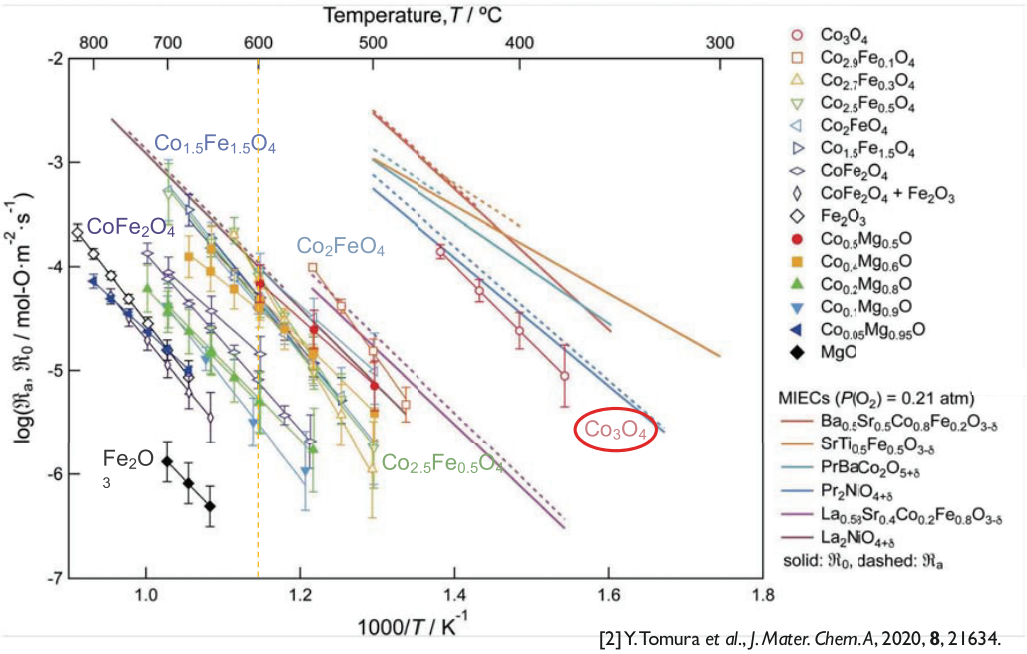


[2] Y. Tomura *et al.*, *J. Mater. Chem. A*, 2020, **8**, 21634.

# $R_a$ vs. [Co] for Co-based oxides

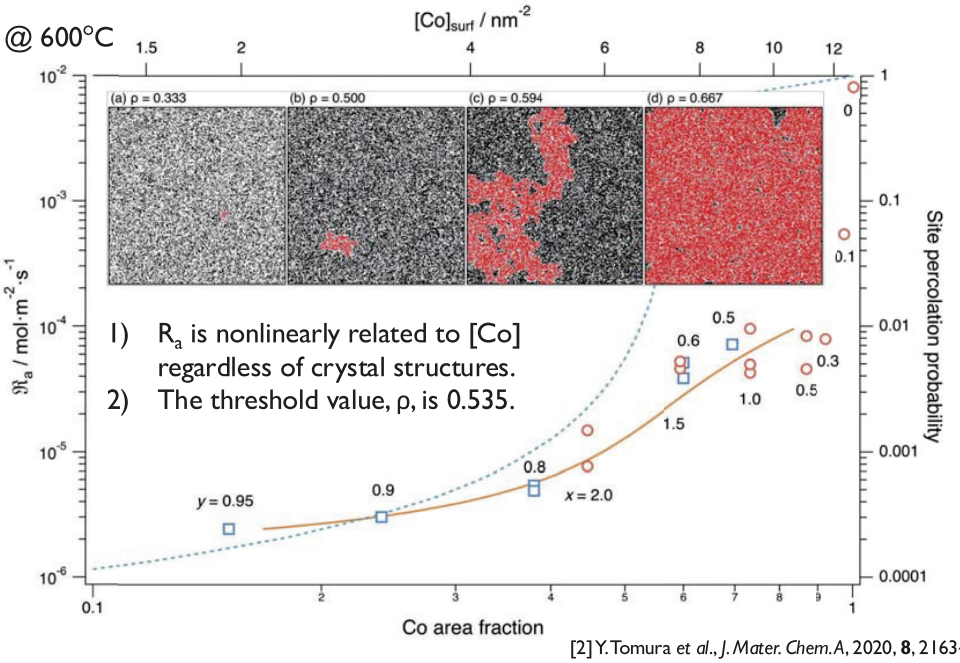


[2] Y. Tomura *et al.*, *J. Mater. Chem. A*, 2020, **8**, 21634.



# Surface Oxygen Exchange Reaction

$$1.\ O_2 \overset{\Re_a}{\leftrightarrow} 2O^*_{ad}$$

$$2.\ O^*_{ad} + 2e^- + 2H^+ \rightarrow H_2O$$

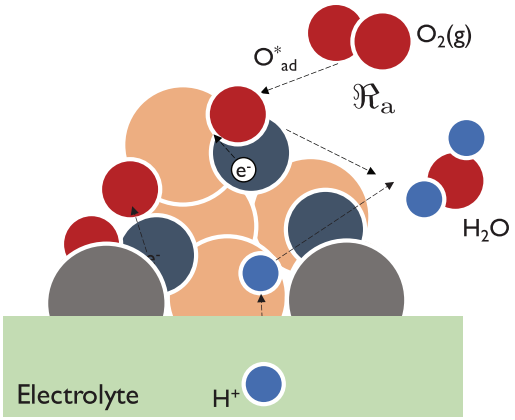


The focus of this study:

Adding $Co_3O_4$ with high $\Re_a$ to enhance the cathode property.

⇨ Works as a catalyst to promote surface exchange rate

⇨ What amount of Co is required?

⇨ Dispersed or solid solution?

Protonic conductor (PC)

Dissociation catalyst ($Co_3O_4$)

Solid solution (Co-doped BZ)

# Objective

To quantify the effect of $Co_3O_4$ addition to protonic conductor $BaZr_{0.9}Sc_{0.1}O_{3-\delta}$ (BZS10) on its surface exchange reaction

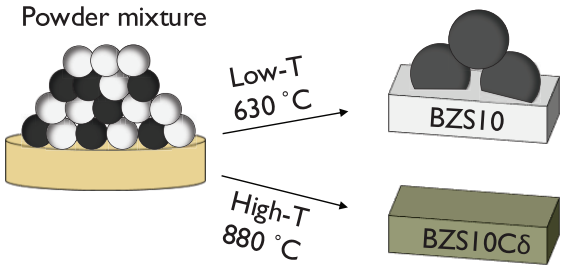


Dispersed (two phases)

Solid solution (single phase)



# Sample preparation

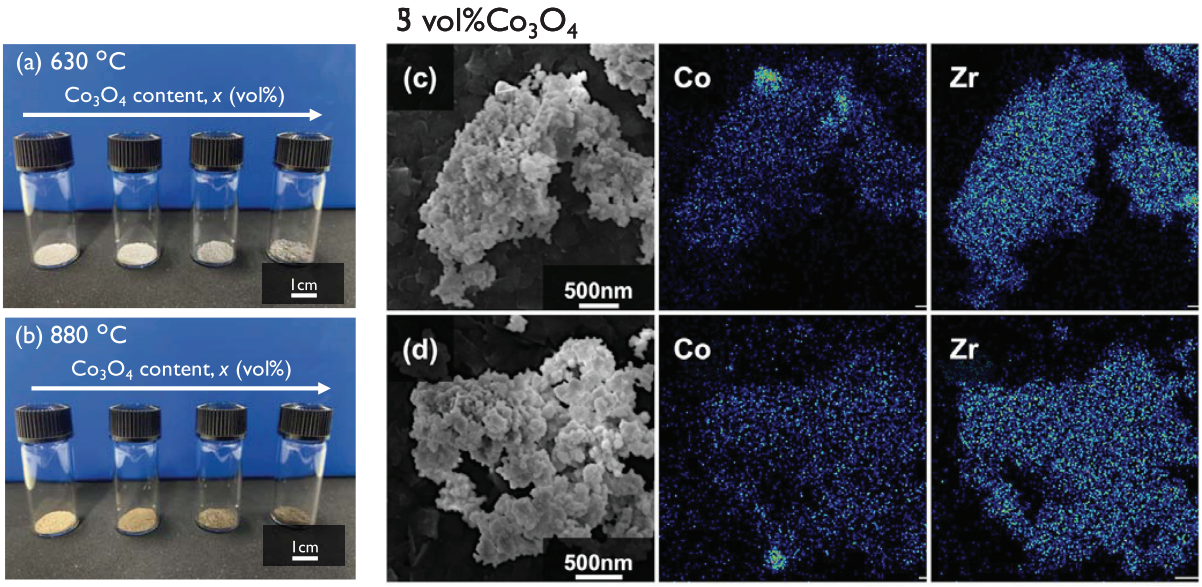

# Magnetic analysis for phase determination

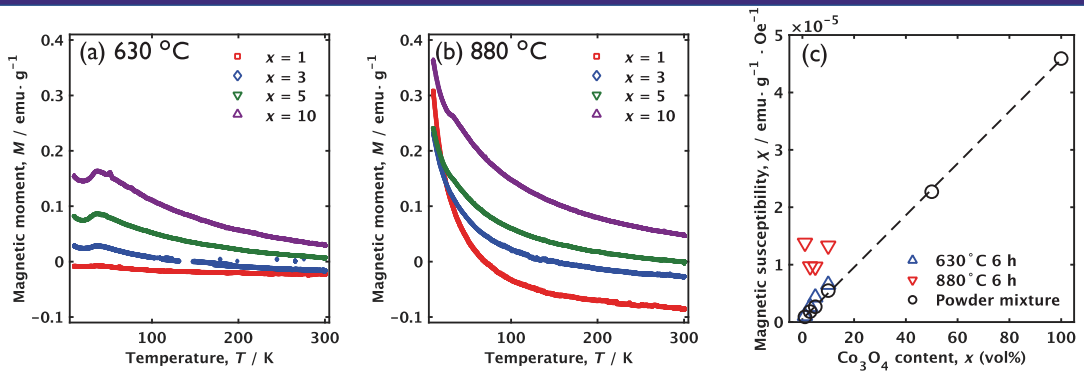


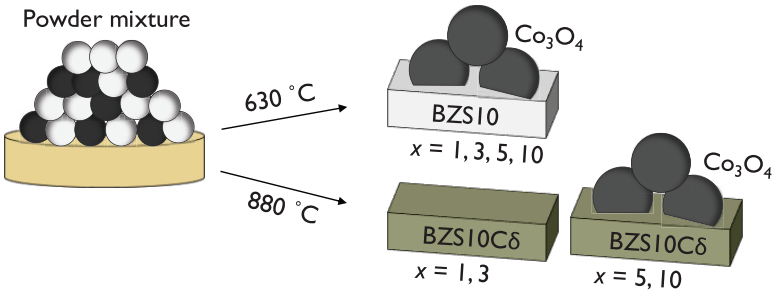




# Pulse Isotope Exchange (PIE) [4]

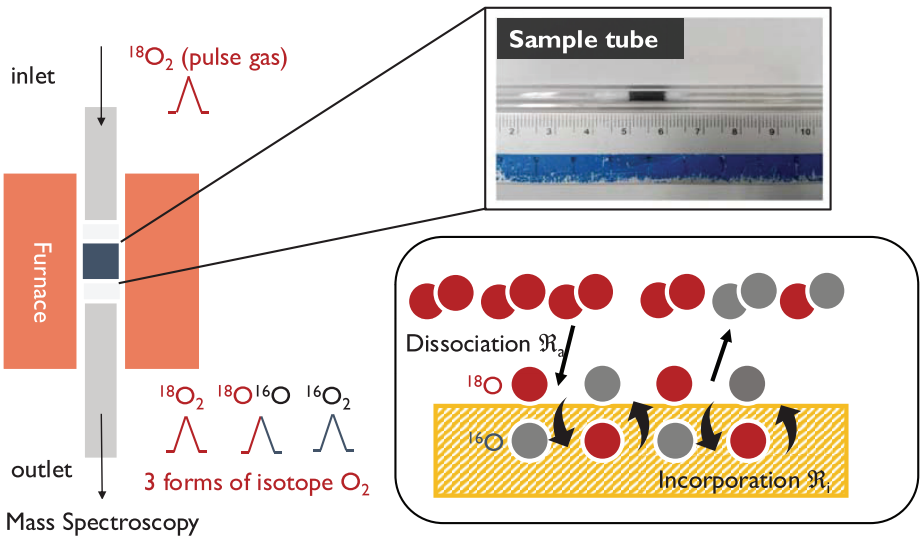


[4] H.J.M. Bouwmeester, *et al.*, *Phys. Chem. Chem. Phys.*, 2009, **11**, 9640. 

# PIE Analysis Procedure (e.g. $BaZr_{0.9}Sc_{0.1}O_{3-\delta}$)

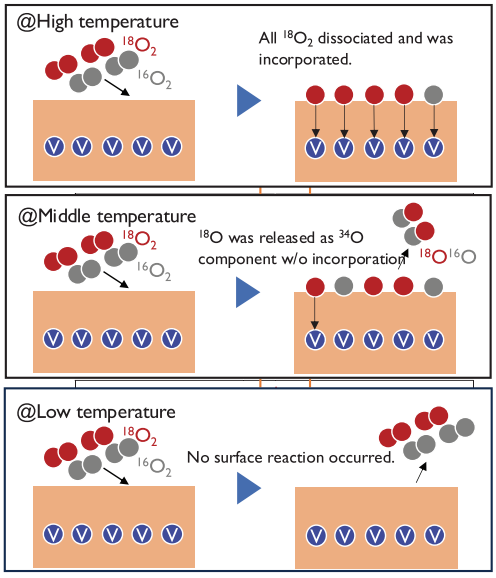


The ratio of peak area ⇨ Isotope fraction, $f$

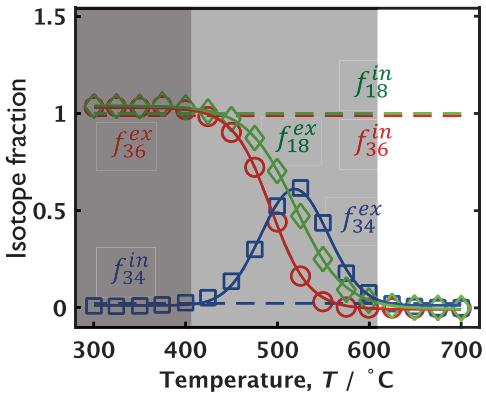


$$f_{18}^{ex} = f_{36}^{ex} + \frac{1}{2} f_{34}^{ex} \quad f_{18}^{in} = f_{36}^{in} + \frac{1}{2} f_{34}^{in}$$

Exchange reaction rate, $\Re_0 = \frac{n}{\tau_r S} \ln\left(\frac{f_{18}^{in}}{f_{18}^{ex}}\right)$



# PIE Analysis : $Co_3O_4$ addition

$BaZr_{0.9}Sc_{0.1}O_{3-\delta}$

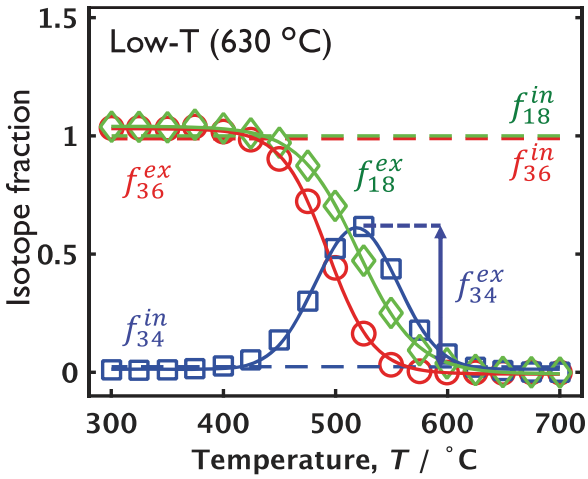


$BaZr_{0.9}Sc_{0.1}O_{3-\delta}$–3 vol%$Co_3O_4$

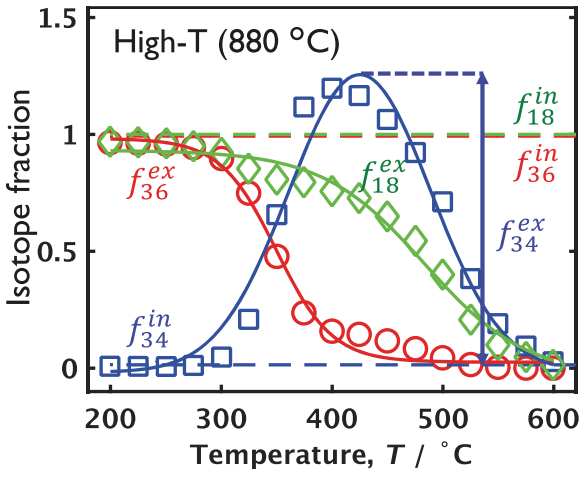


$f^{ex}_{34}$ becomes higher by adding $Co_3O_4$ by approx. a factor of 2

▶ Oxygen dissociation was enhanced by $Co_3O_4$ addition

# Arrhenius plot of the exchange reaction rate, ℜ0

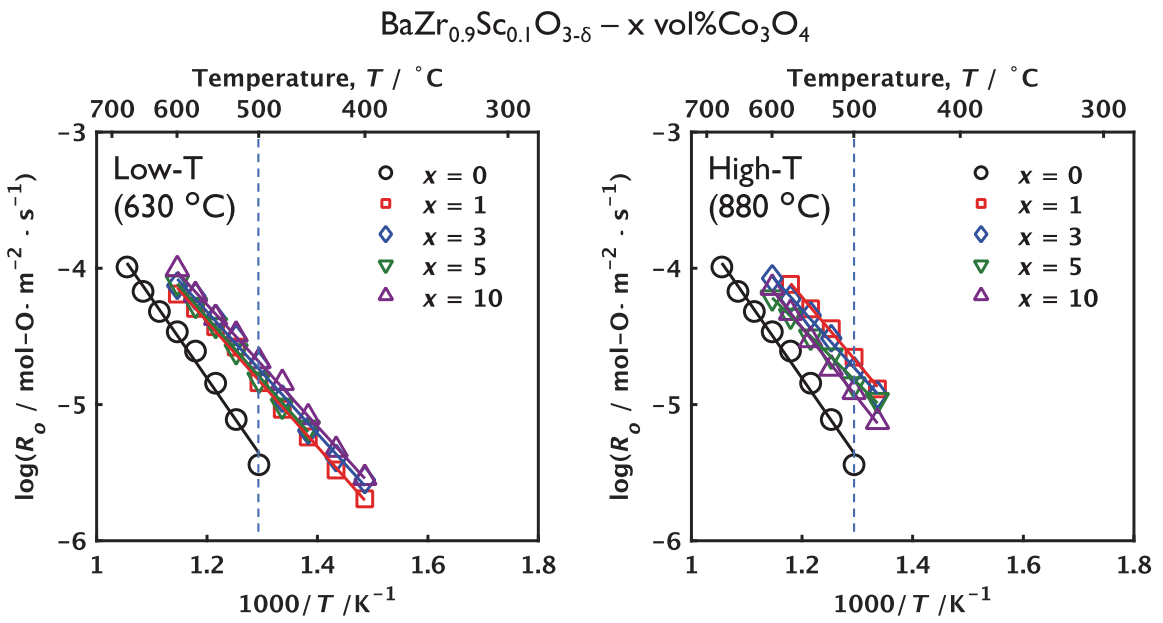




# ℜ0@500 °C as a function of $Co_3O_4$ amount

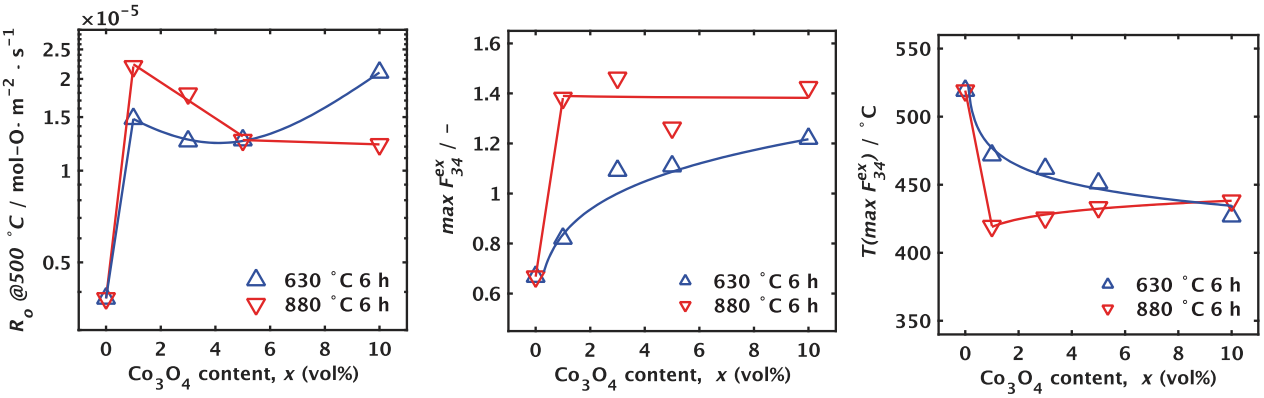


- BZS10Cδ solid solution significantly enhanced R0 at x = 1. However, this enhancement was reduced above x = 3. The two-phase composites increased the oxygen dissociation activity as $Co_3O_4$ content increased.
- Changes in $F_{34}$ as a function of $Co_3O_4$ content also supported these trends.

# Expected surface exchange process for $Co_3O_4$-added BZS

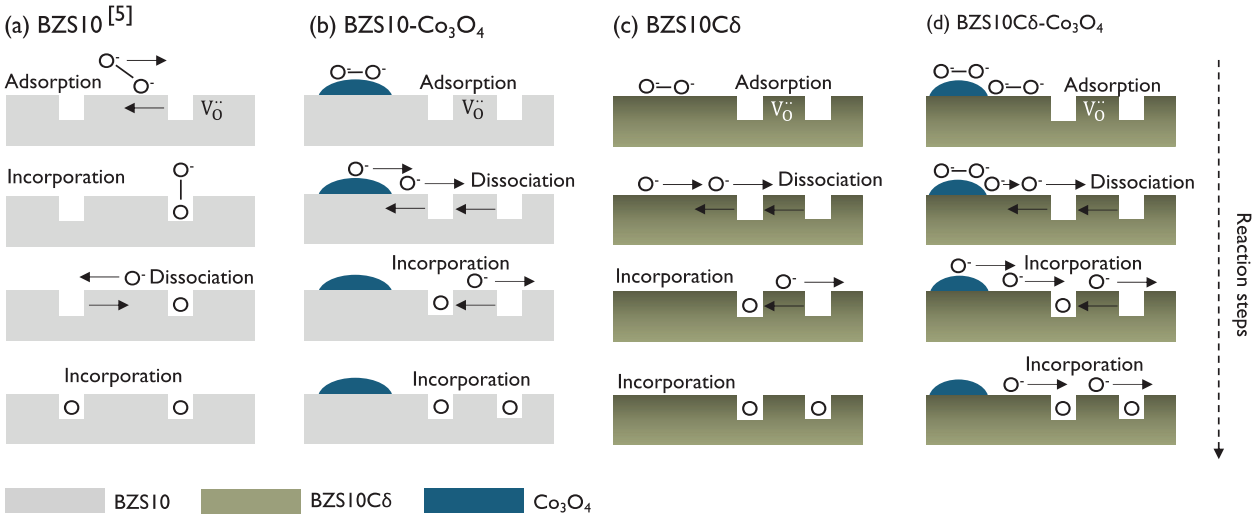


[5] M. Schaube *et al.*, *J. Mater. Chem. A*, 2019, **7**, 21854.



# Conclusions

The surface exchange properties of a protonic conductor mixed with a dissociative adsorption catalyst, BZS10-x vol%$Co_3O_4$, were investigated.

- Co-containing solid solutions, BZS10Cδ, were formed by high-temperature heat treatment (880 °C); meanwhile, $Co_3O_4$ existed as separated particles when heat-treated at a lower temperature (630 °C) regardless of x.
- The formation of the BZS10Cδ solid solution significantly enhanced $R_0$ at x = 1. However, this enhancement was reduced above x = 3. This decrease in $R_0$ was attributed to reduced oxygen vacancies associated with hole compensation by further Co dissolution. The two-phase composites increased the oxygen dissociation activity as $Co_3O_4$ content increased.
- Doping a large amount of Co is unnecessary to promote the surface exchange reaction itself. Meanwhile, other factors, including electronic conductivity, are also crucial for the cathode to work.

S. Kamohara, A. Ishii, I. Oikawa, H. Takamura, "Dissociative Oxygen Adsorption and Incorporation in $Co_3O_4$-Dispersed $BaZr_{0.9}Sc_{0.1}O_{2.95}$ for PCFC Cathode", *ACS Appl. Mater. Interfaces* 2024, **16**, 52339.

# Acknowledgements


- Prof. N. Tezuka (VSM)
- Ms. Y. Nakano (ICP-MS)

This work was supported in part by JSPS KAKENHI (22H04914) and the 3rd period of SIP "Smart energy management system" by CSTI (JPJ012207).


JSPS SIP Cross-ministerial Strategic Innovation Promotion Program

Thank you for your kind attention!

MEMO

# Atomically precise layer-by-layer modification of perovskite oxides

**Di Chen**[1,2]

[1]The Future Laboratory, Tsinghua University

[2]School of Materials Science and Engineering, Tsinghua University

Email: dichen@tsinghua.edu.cn

**2024-11-26, E-IMR**

## Challenge: structure control at atomic scale

- **Missing surface structure leads to conflict structure-activity relationship**

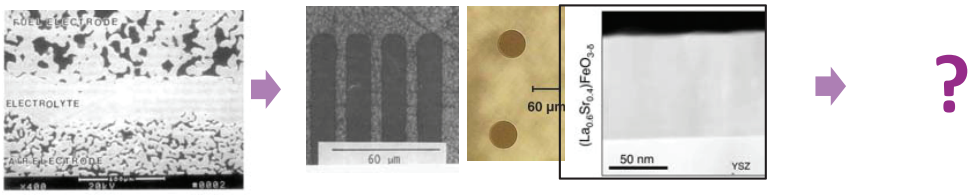


Porous electrode

Patterned metal electrode/Thin film oxide electrode

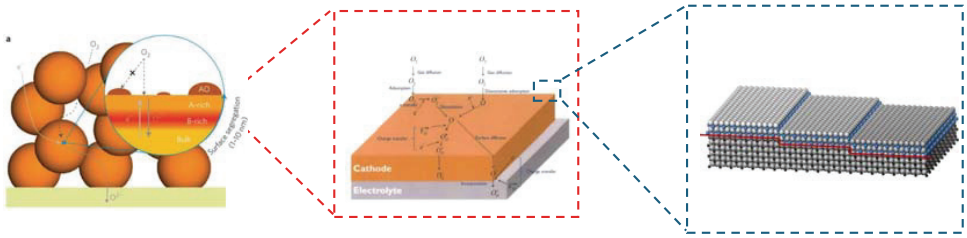

# New model system: fully epitaxial thin films

清華大學 Tsinghua University

- **Polycrystalline** thin films

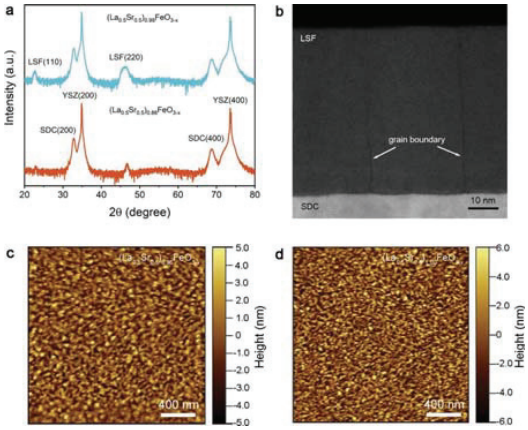


- Multiple grain boundaries;
- Complicated surface terminations;

- **Epitaxial single crystalline** thin films

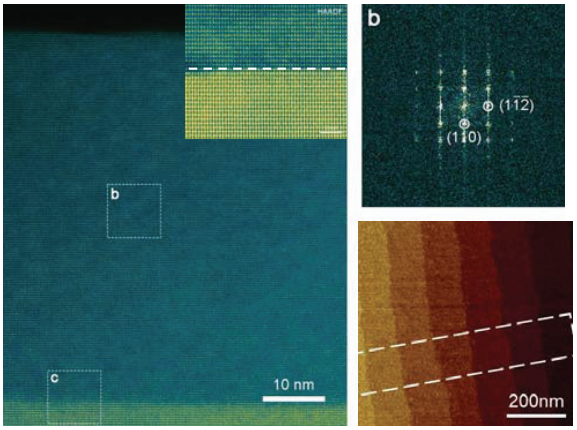


- NO grain boundaries;
- UNIFORM surface terminations;

# Mobility and clustering of O and anion vacancies in $ABX_3$ perovskites as energy materials

Francesco Cordero
CNR-ISM, Roma-Tor Vergata, Italy

$BX_2$ plane | with freely dispersed $V_X$ | clustered $V_X$

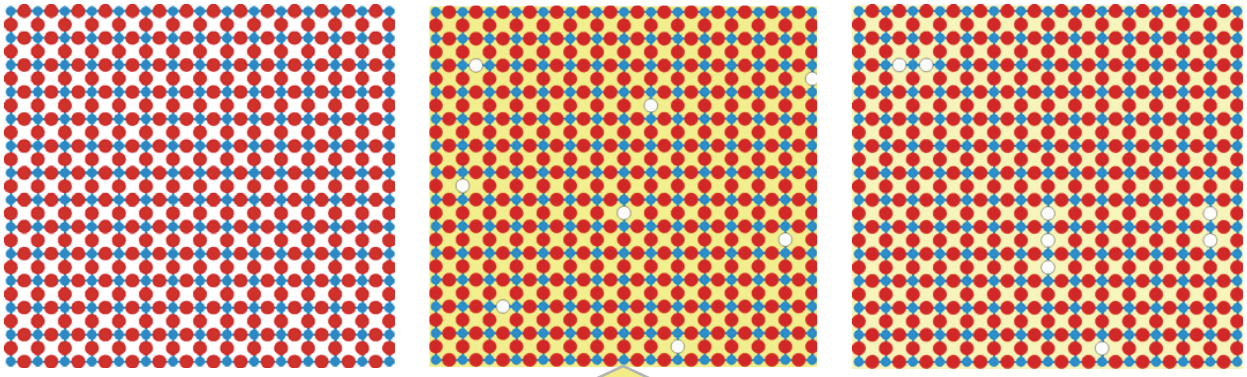

mobile electrons doped by $V_X$

slower mobility
smaller doping

Francesco Cordero — anelastic spectroscopy
CNR-ISM, Area della Ricerca di Roma-Tor Vergata, Roma, Italy
Floriana Craciun — dielectric spectroscopy
Francesco Trequattrini Physics Dept., Univ. "La Sapienza", Roma

Paulo Sergio da Silva Jr., Michel Venet
Dep. Fisica, Universidade Federal de São Carlos, Brazil — $(Ba/Sr)TiO_3$

Pietro Galizia, Elisa Mercadelli
CNR-ISSMC, Faenza, Italy — $(Ba/Ca)(Ti/Zr)O_3$
SELWA Project
Next Generation EU n. 20229PNWM7

Hans Theo Langhammer
Martin Luther University of Halle-Wittenberg, Germany — $BaTiO_3$

Gloria Zanotti, Venanzio Raglione, ...
CNR-ISM, Montelibretti, Roma, Italy — $(MDABCO)(NH_3)I_3$

Victor Fruth, Simona Ionita, ...
Inst. Physical Chemistry, Romanian Academy, Bucharest — $(TMCM)MnCl_3$

## Perovskite $ABX_3$ structure

A,B cations  X anion

network of $BX_6$ octahedra

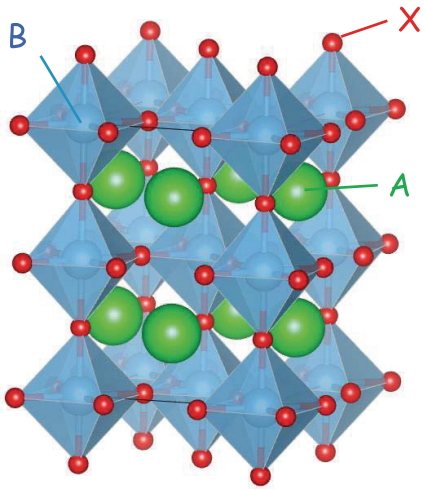


3D

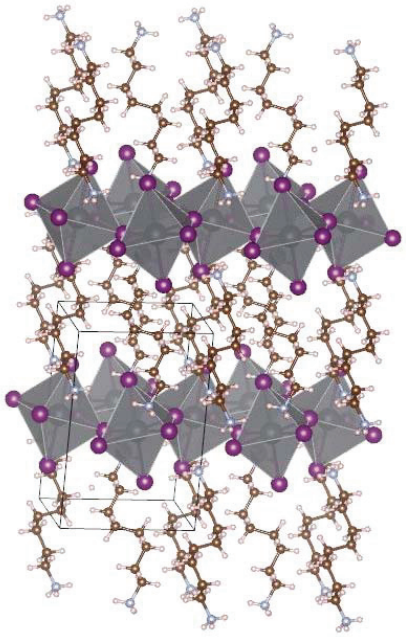

2D

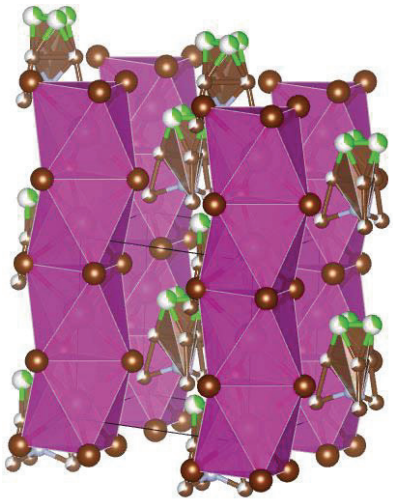

1D

too large A (especially organic)

## $ABX_3$ perovskites as energy materials

| | oxides X = O | metal-organic halides X = Cl,Br,I |
|---|---|---|
| supercapacitors | electrode<br>A = La,Sr,Ce, …<br>B = Ni,Fe,Co,Mn, …<br>$LaMnO_{3-\delta}$ (anionic) | electrode<br>A = MA,FA,Cs, …<br>B = Pb, … [LYS21] |
| batteries | electrode<br>$AgNbO_3$ for $Na^+$,$K^+$ [OKC24] | electrode esp. 2D/1D perovsk<br>A = MA,FA,Cs, …<br>B = Pb,Bi,Cu, … [TLL22] |
| fuel cells | electrolyte/electrode<br>A = Ba,Sr,La, …<br>B = Zr,Ce,Y, … | |
| mechanical energy harvesting | piezoelectric<br>A = Ba,Pb,Bi,Na, …<br>B = Ti,Zr,Mg,Nb, … | piezoelectric<br>A = organic molecule<br>B = o.m.,Pb,Mn,… |
| solar cells | | power conversion eff >25%<br>A = MA,FA,Cs, …<br>B = Pb, … [LYS21] |
| thermoelectrics | | |

## $ABO_{3-\delta}$ perovskite electrodes/electrolytes for anion exchange

Solid Oxide Fuel Cells

electrolyte/electrode
A = Ba,Sr,La, …
B = Zr,Ce,Y, …

J. Tyler Mefford *et al.*, Nature Mater. 13, 726 (2014)
**Anion charge storage through oxygen intercalation in $LaMnO_3$** perovskite pseudocapacitor electrodes

Qian *et al.*, J. Energy Chem. 89, 41 (2024)
Emerging **perovskite materials for supercapacitors**

He *et al.*, Inorg. Chem. 63, 13755 (2024)
Cr-Substituted **$SrCoO_{3-\delta}$** Perovskite with Abundant Oxygen Vacancies for High-Energy and Durable Low-Temperature **Antifreezing Flexible Supercapacitor**

## $ABO_{3-\delta}$ perovskite electrodes for alkali intercalation

Pérez-Vicente et al., ACS Appl. Energy Mater. 5, 15749 (2022)
A Comparative View of **Alkaline and Alkaline-Earth Element Intercalation into Perovskite-Type $A_xLa_yTiO_3$** (A = Li, Na, or Mg) Based on Theoretical Calculations and Experiments

Li *et al.*, Adv Mater. e2107262 (2022)
Perovskite-Type **$SrVO_3$ as High-Performance Anode Materials for Lithium-Ion Batteries**

Orbay *et al.*, Batteries & Supercaps e202400602 (2024)
**Sodium and Potassium storage behaviour in $AgNbO_3$** Perovskite

## Role of $V_O$ in oxide electrodes for alkali intercalation

- $V_O$ may be created during the extraction of the alkali metals from the cathode and degrade it
- modify the electronic properties, enhance the electric conductivity
- expand the lattice → enhance the $Li^+/Na^+$ mobility

$TiO_2$ plane of perovskite

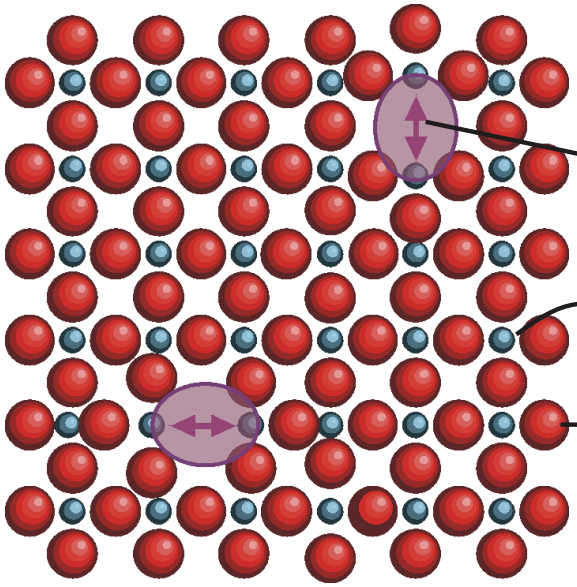

positively charged $V_O$ with elastic dipole

mainly repulsion with nn cations

$Ti^{4+}$ $r$ = 0.605 Å

$O^{2-}$


## Role of $V_O$ in oxide electrodes for alkali intercalation

- $V_O$ may be created during the extraction of the alkali metals from the cathode and degrade it
- modify the electronic properties, enhance the electric conductivity
- expand the lattice → enhance the $Li^+/Na^+$ mobility

$TiO_2$ plane of perovskite


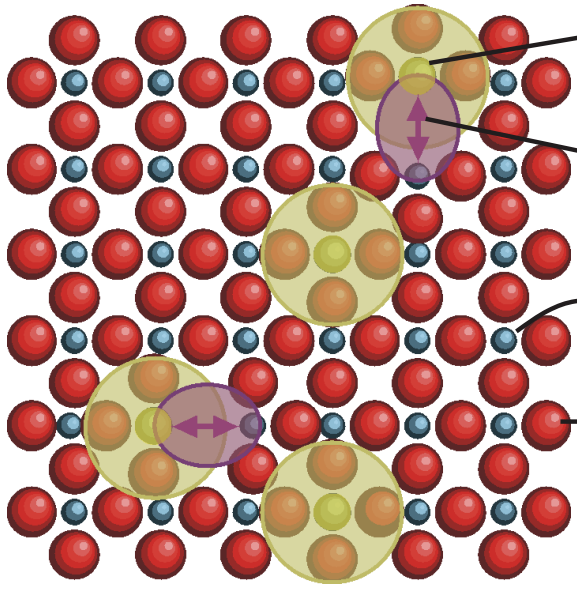

$e^-$ on $Ti^{3+}$ $r$ = 0.67 Å
30% larger volume

small polaron / band state


positively charged $V_O$ with elastic dipole

mainly repulsion with nn cations

$Ti^{4+}$ $r$ = 0.605 Å

$O^{2-}$


pairing, clustering, ordering of $V_O$
- reduce the amount of doped mobile electrons
- affect the volume expansion

# Dynamic Young's modulus / mechanical spectroscopy

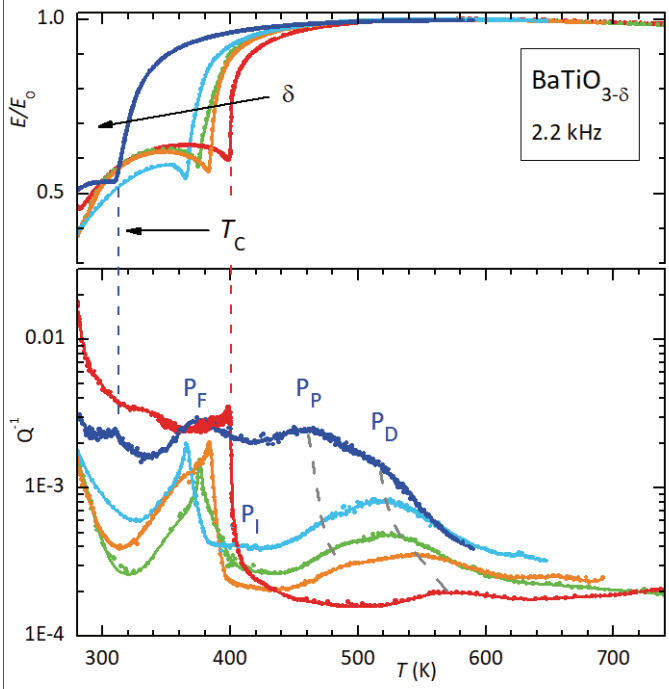


Young's modulus $E = E' + iE''$

| anelastic | | dielectric/impedance |
|---|---|---|
| $E$ | $\leftrightarrow$ | electric modulus = $1/\varepsilon$ |
| $Q^{-1}$ | $\leftrightarrow$ | $\tan(\delta)$ |

elastic energy loss coefficient
$Q^{-1} = E''/E'$

free flexural resonance

electrostatic 0.1-100 kHz

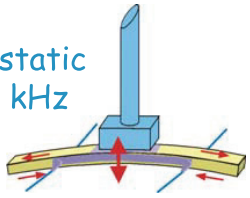

thermocouple wires

elastic anomalies → phase transitions
peaks in the losses → mobility of defects

# Debye anelastic relaxation from reorienting elastic dipoles

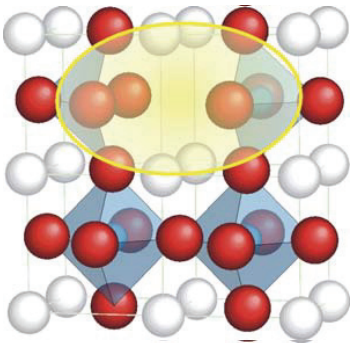

$V_O$ in perovskite

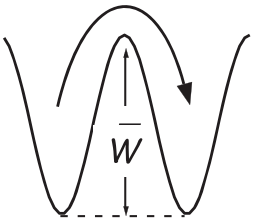


Arrhenius law for the hopping/reorientation time:

$\tau = \tau_0 \exp(W/kT)$

$$\lambda^{(\gamma)} = \begin{pmatrix} \lambda_1 & 0 & 0 \\ 0 & \lambda_2 & 0 \\ 0 & 0 & \lambda_1 \end{pmatrix}$$

$$\Delta\lambda = \lambda_2 - \lambda_1$$

elastic dipole $\lambda$ = strain per unit concentration

$$Q^{-1} = \frac{M''}{M'} \propto \frac{(\Delta\lambda)^2}{T} \frac{\omega\tau}{1+(\omega\tau)^2}$$

Debye peak

maximum at $\omega\tau = 1$

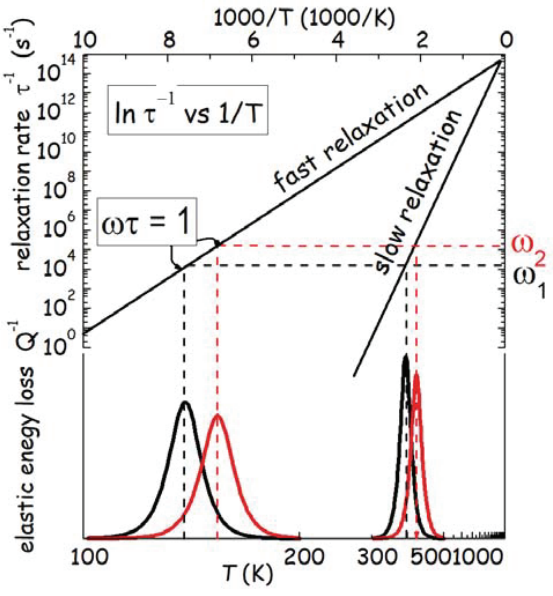

## $A^{2+}B^{4+}O^{2-}_{3-\delta}$ with A = Ba,Sr,Ca and B = Ti,Zr

Stable cationic valences → negligible O deficiency $\delta$ unless
- acceptor impurities/dopants with charge compensating $V_O$
- reducing treatment in CO or $H_2$ atmosphere

## Samples reduction/oxygenation

Induction heating at 900-1250 °C for 0.5-3 h in $CO/O_2$ flow
+ homogeneization 800 °C for 1 h

sample on alumina or YSZ plates and inserted in Pt holder

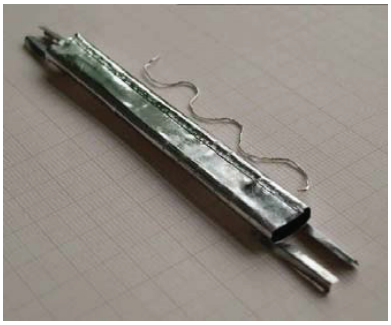

flow of ~1000 mbar
0.1CO + 0.9Ar or $O_2$

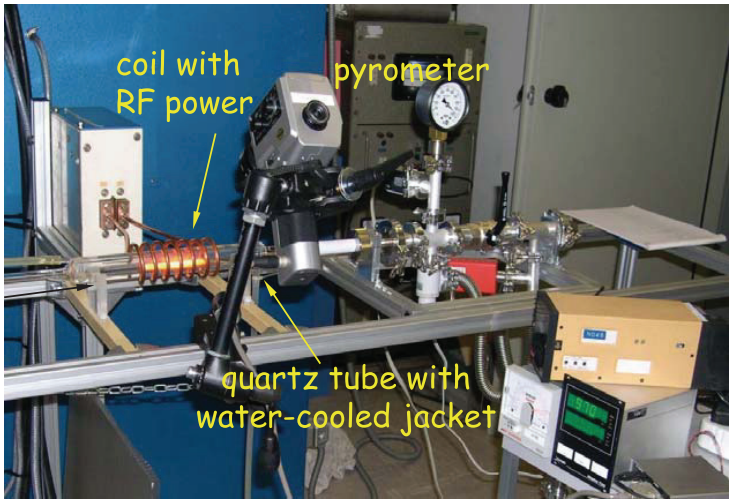


O stoichiometry:
- mass change after reduction and reoxygenation
- temperature of the structural phase transition

## Expected behaviour of $A^{2+}TiO_{3-\delta}$ with $\delta < 0.02$

$BaTiO_{3-\delta}$ becomes hexagonal if $\delta \geq 0.02$

Common belief: with $\delta$ ~ few % the $V_O$ in perovskite titanates are randomly dispersed and diffuse over a barrier of ~1 eV

↓

expected anelastic spectrum →

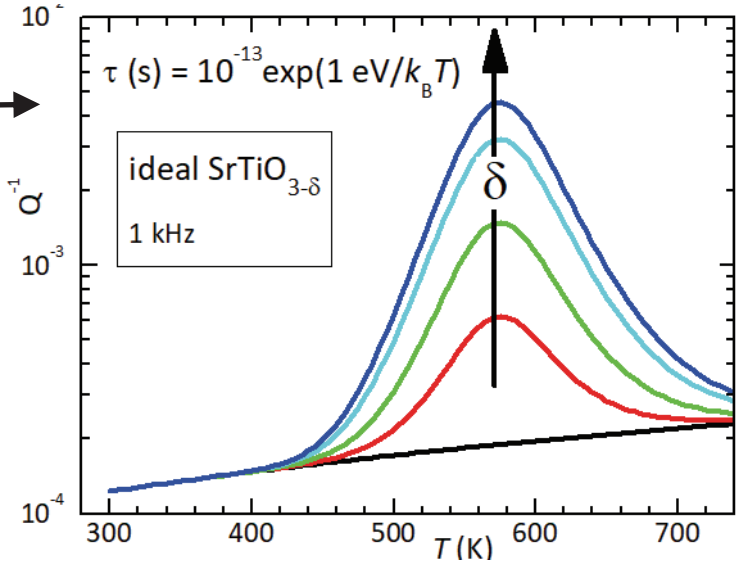


## Anelastic spectrum of $SrTiO_{3-\delta}$

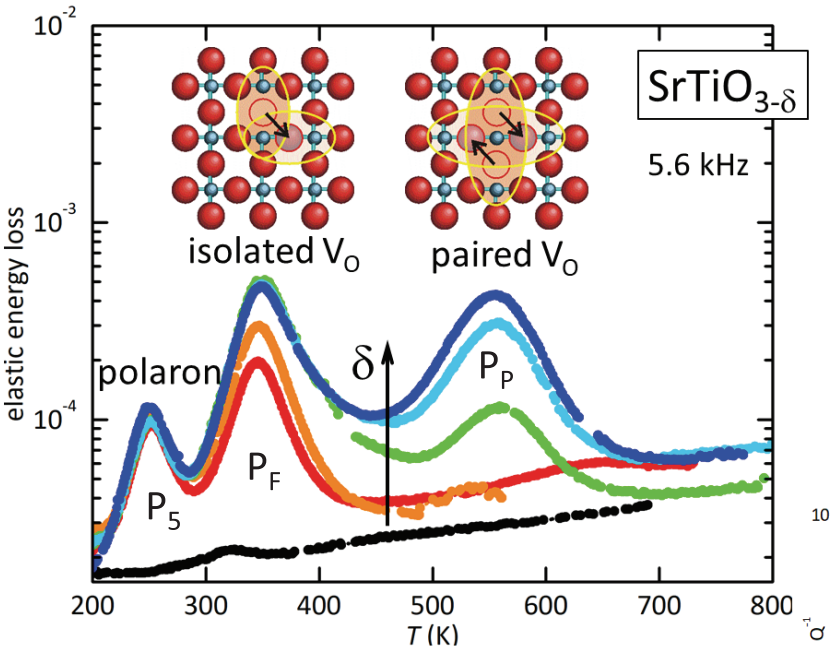


The creation of $V_O$ introduces several peaks:

$P_F$-$P_P$ grow considerably with increasing $\delta$ and therefore are due to $V_O$

$P_5$ saturates already at $\delta$ = 0.001 and has a low activation energy: polarons?

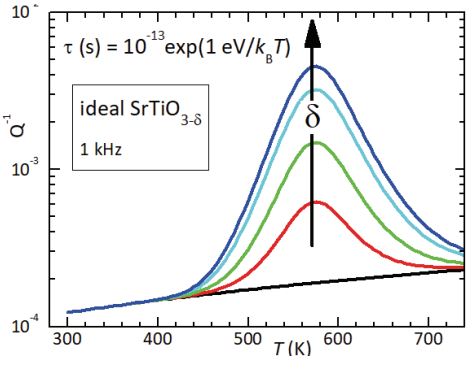


F. Cordero, Phys. Rev. B 76, 172106 (2007)

## Explanation of $P_F$ and $P_P$ in terms of free and paired $V_O$

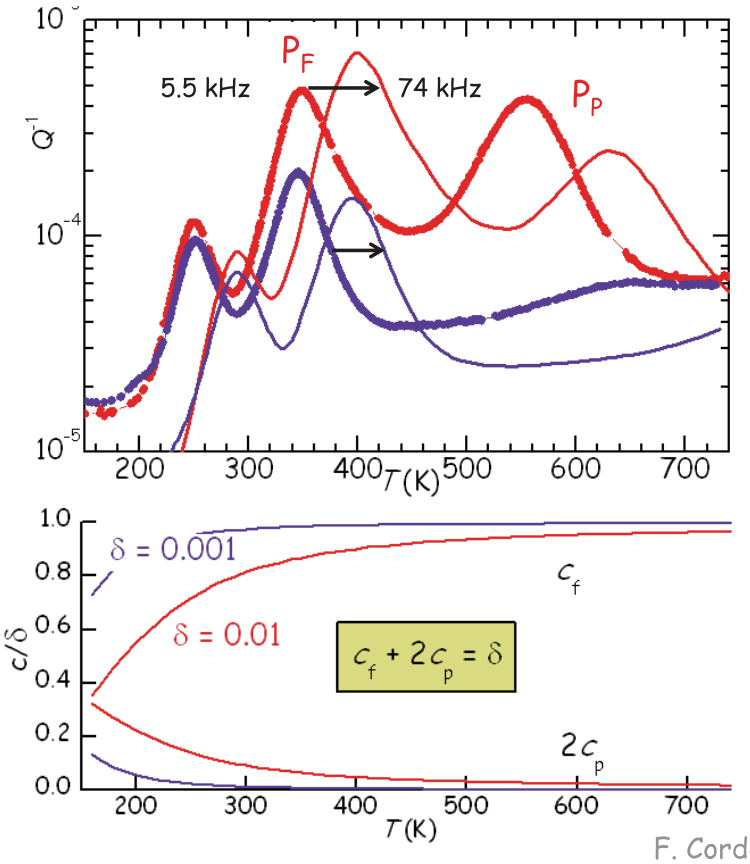


**$P_F$: free $V_O$** $\Delta(T) \propto c_f/T$

at low $\delta$ only $c_f \sim \delta$

$P_P$ is absent

$P_F$ decreases as $1/T$

at high $\delta$ $c_f = \delta - 2c_p$

pairs dissociation →

$c_p(T)$ is a decreasing function

$c_f(T)$ is an increasing function

**$P_P$: paired $V_O$** $\Delta(T) \propto c_p/T$

$c_p(T)$ is a decreasing function

the intensity decreases faster than $1/T$

F. Cordero, Phys. Rev. B 76, 172106 (2007)

## Statistical model for aggregated $V_O$

Subdivide the crystal into clusters of cells that are small enough to write their grandpartition function Z with all the possible configurations of $V_O$

(1) $Z = \sum_\alpha w_\alpha = \sum_\alpha m_\alpha \exp\left(\frac{n_\alpha \mu - E_\alpha}{kT}\right)$ (2) $\mu$ : $\frac{kT}{Z}\frac{\partial Z}{\partial \mu} = \frac{\sum_\alpha n_\alpha w_\alpha}{\sum_\alpha w_\alpha} = \sum_\alpha \bar{n}_\alpha = \delta$

$n_\alpha$ occupation number of $\alpha$-th configuration
$m_\alpha$ multiplicity
$E_\alpha$ energy
$w_\alpha$ statistical weight
$\mu$ chemical potential from the implicit equation (2)

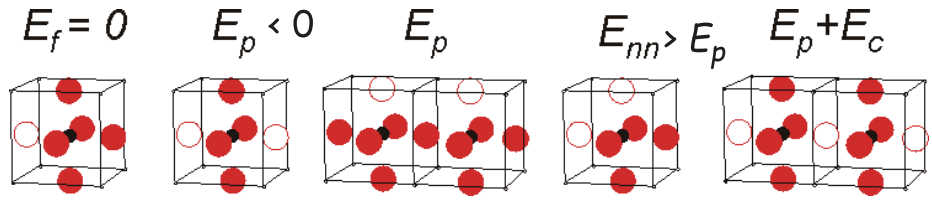


isolated (free)

stable pairs

nearest neighbours pair

chain

F. Cordero, Phys. Rev. B 76, 172106 (2007) + Phys. Rev. B 47, 7674 (1993)

## Anelastic relaxation

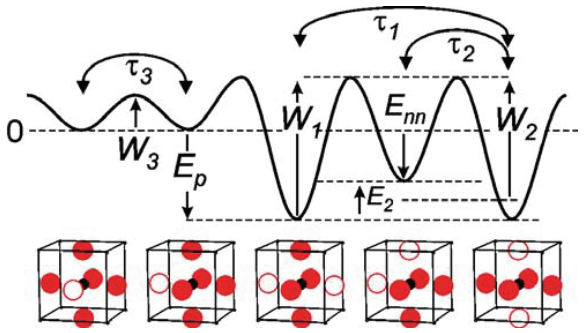


Three relaxations corresponding to $P_F$, $P_P$ and $P_I$:

$$Q^{-1} = \frac{2}{9}\frac{cv_0}{s_{11}k_BT}(\Delta\lambda)^2\frac{\alpha(\omega\tau)^\alpha}{1+(\omega\tau)^{2\alpha}}$$

parameters:
$W_1$ = barrier for free hopping
$W_3$ = barrier for pair reorientation
$W_2$ = barrier for intermediate step
$E_p$ = pair binding energy
$E_c$ = binding of additional V into a chain
$\tau_0$ = preexponential factors
$\alpha$ = Fuoss-Kirkwood broadening
$\Delta\lambda$ = change of elastic dipole for isolated V
$(\Delta\lambda)_1 \approx 2\Delta\lambda =$ " for pair reorientation

$P_I$ between states differing by $E_2 = W_1 - W_2$:

$$\Delta(T) \propto \frac{c_p}{T\cosh^2(E_2/2kT)}$$

$$\tau^{-1} = \tau_0^{-1}\exp(-W_2/kT)\cosh(E_2/2kT)$$

scripts for calculating μ, concentrations, and $Q^{-1}$ peaks written in Origin C and integrated in the non linear fitting tool

F. Cordero, Phys. Rev. B 76, 172106 (2007)

## Fit

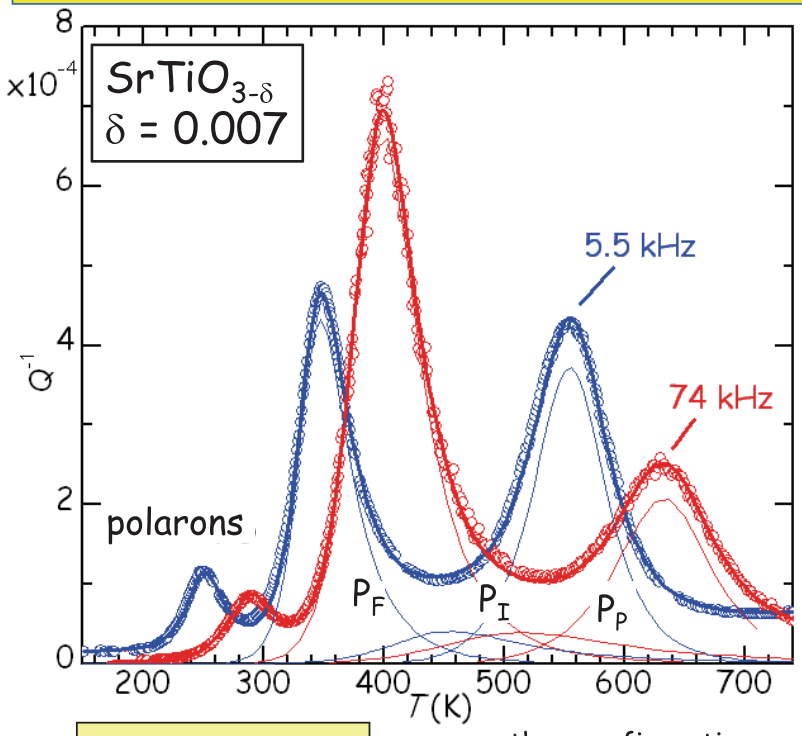


same parameters for all δ > 0.001 !

other configurations contribute to P2:
$c > c_P$ and $(\Delta\lambda)_P \sim (\Delta\lambda)_F$

**binding energies**
**$E_P$ = 0.184 eV**
**$E_C$ = 0.26 eV**

**free isolated $V_O$ ($P_F$)**
$c = c_F$
**$W_F$ = 0.60 ± 0.007 eV**
$\tau_{0F} = (5 \pm 1)\times10^{-14}$ s
$\alpha \geq 0.95$
$(\Delta\lambda)_F = 0.026$

**pair reorientation ($P_P$)**
$c = c_P$
**$W_P$ = 0.97 ± 0.04 eV**
$\tau_{0P} = (7 \pm 4)\times10^{-14}$ s
$\alpha \geq 0.95$
$(\Delta\lambda)_P = 1.87\times(\Delta\lambda)_F$

**intermediate ($P_I$)**
$c = c_P$
$W_P \sim 0.86$ eV
$\alpha \sim 0.35$
$(\Delta\lambda)_P = 5\times(\Delta\lambda)_F$

F. Cordero, Phys. Rev. B 76, 172106 (2007)

## The electrostatic repulsion between $V_O$ hinders the formation of pairs

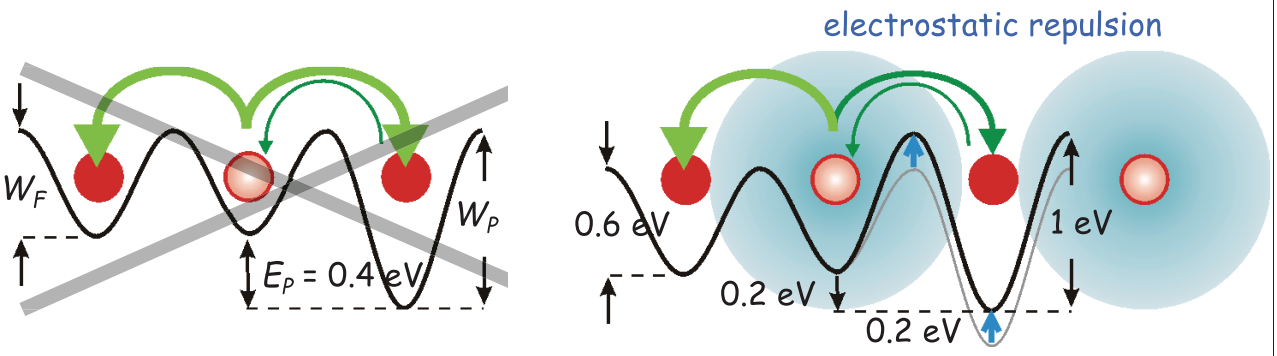


pair binding energy $E_P$

$E_P \sim 0.2$ eV < $W_P - W_F = 0.4$ eV

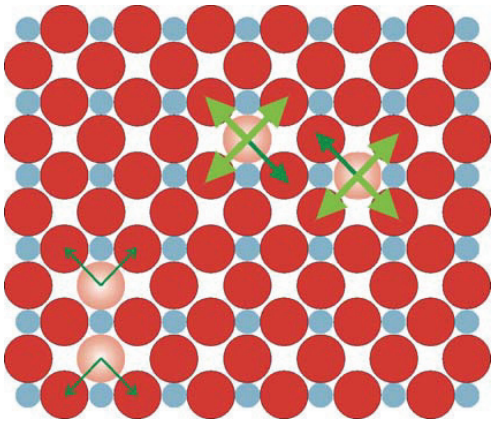

the free $V_O$ hop very fast, but avoid the jumps next to another $V_O$ to form a pair

slower approach to equilibrium for the concentrations of pairs and chains

## $V_O$ pairs confirmed by DXRS and PES in $SrTiO_{3-\delta}$

Highly O deficient $SrTiO_3$ films obtained by PLD at low $p_{O2}$

$V_O$-$Ti^{2+}$-$V_O$ pairs and chains

diffuse X-ray scattering: linear defects

Photoemission spectroscopy : $Ti^{2+}$

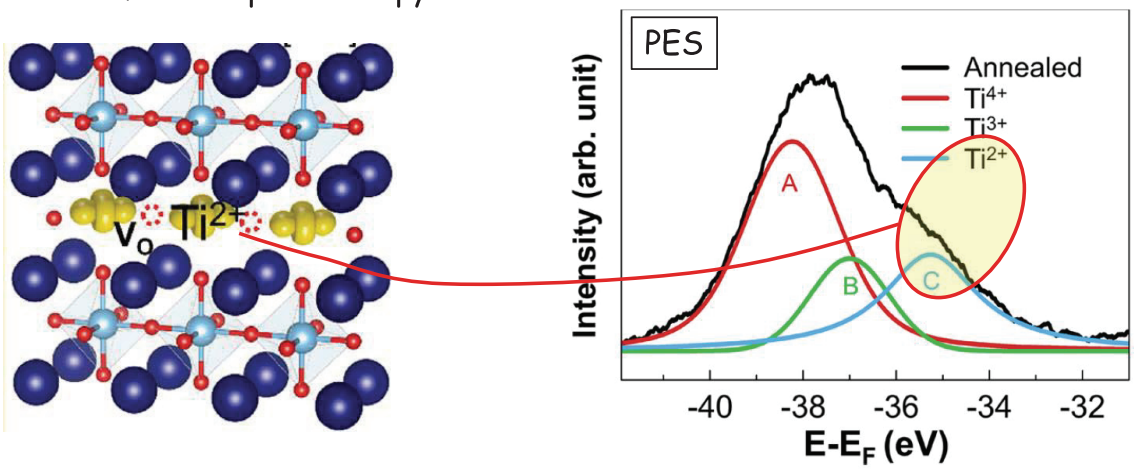


Eom *et al.* "Oxygen Vacancy Linear Clustering in a Perovskite Oxide"
J. Phys. Chem. Lett. 8, 3500 (2017)

## Electron doping depends on the $V_O$ aggregation

isolated $V_O$: $Ti^{3+}$-$V_O$-$Ti^{3+}$

$Ti^{3+}$ mobile as polaron or band state
→ electrical conductivity

pairs/chains of $V_O$: $Ti^{3+}$-$V_O$-$Ti^{2+}$-$V_O$-$Ti^{3+}$

$Ti^{2+}$ is only between two $V_O$
→ each pair or chain segment subtracts two electrons from conduction

the $V_O$ aggregation reduces doping

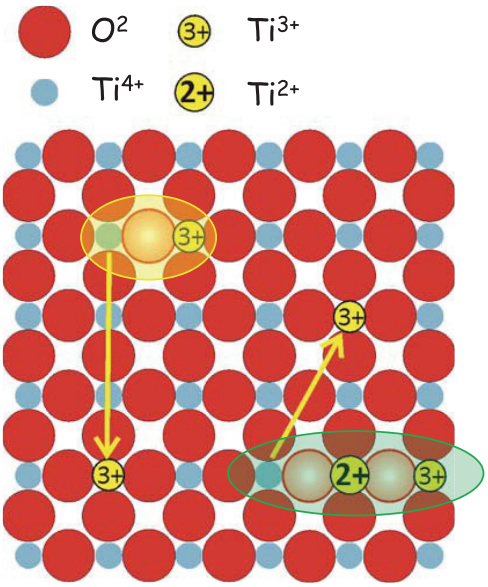


## Comparison between ST, BT and BCTZ

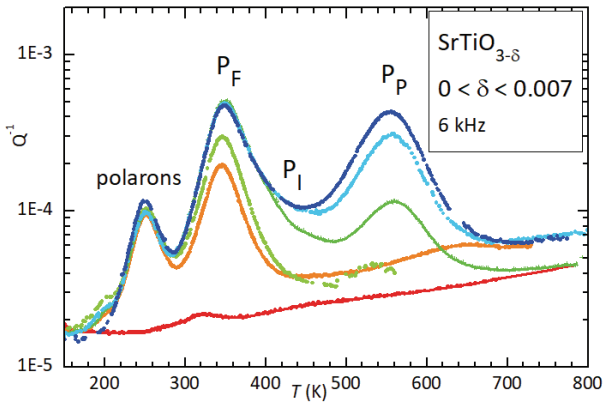


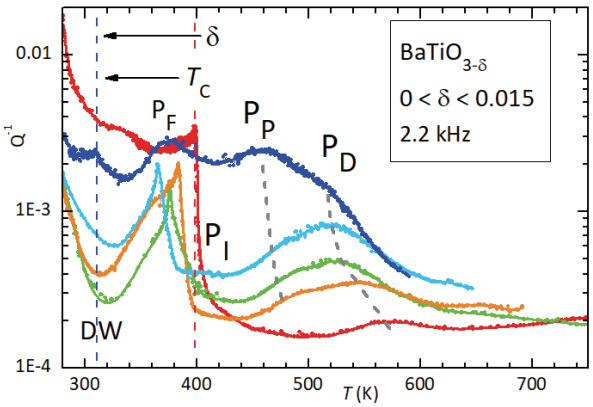


F = hopping of free/isolated $V_O$
P = reorientation of paired $V_O$
I = intermediate stage for pair reorientation
D = native defect-$V_O$ pair, e.g. $V_{Ba}$-$V_O$
DW = domain walls below $T_C$

ceramic BT vs crystal ST:
- peaks ~10% broader
- the activation energies decrease increasing δ
- $(\Delta\lambda)_{BT}$ ~ 3×$(\Delta\lambda)_{ST}$ → larger intensities

ceramic BCTZ
much broader peaks, larger activation energies

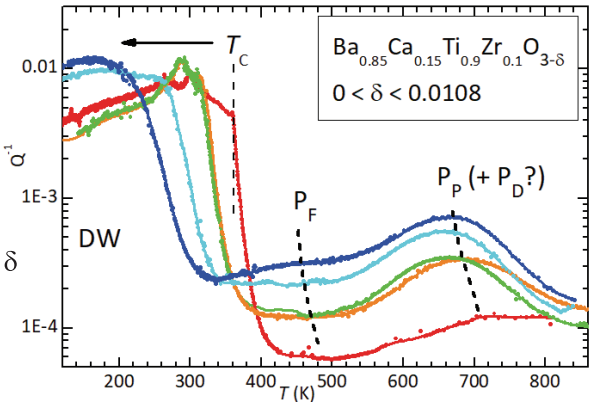


BT: F. Cordero, F. Trequattrini, D.A.B. Quiroga, P.S. Silva Jr., J. Alloys Compd. 874, 159753 (2021)

## Magnitude of the elastic dipole of $V_O$

Major contribution to the anisotropy $\Delta\lambda$: the positively charged $V_O$ pushes outwards the nn $Ti^{4+}$ atoms. Easier in $BaTiO_3$

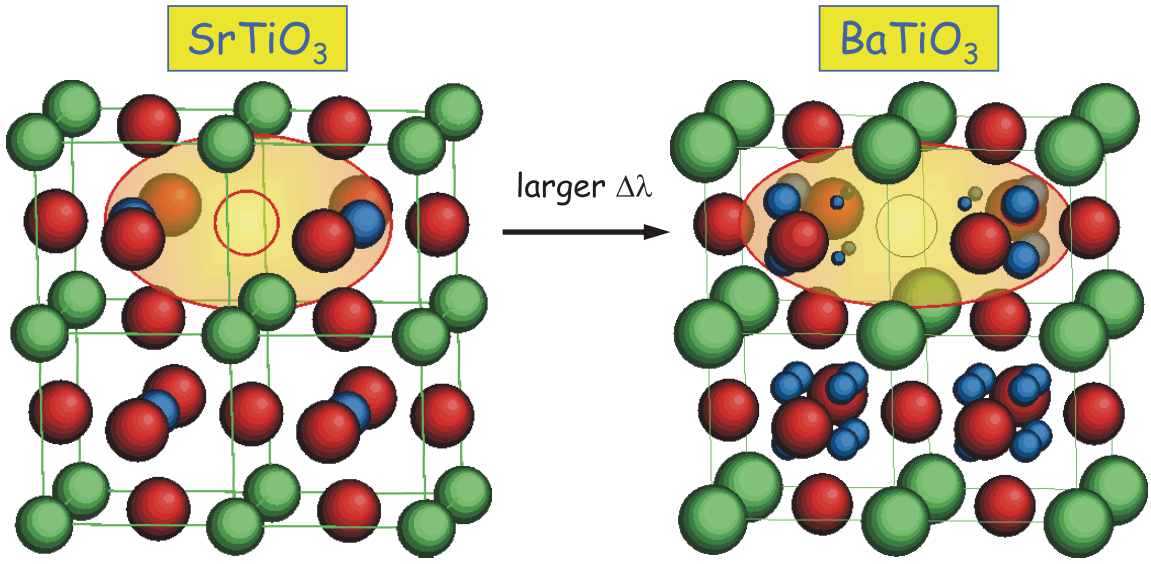


In $BaTiO_3$ the nn Ti atoms may populate only the outward off-centre sites, increasing their outward displacement

BT: F. Cordero, F. Trequattrini, D.A.B. Quiroga, P.S. Silva Jr., J. Alloys Compd. 874, 159753 (2021)

## Decrease of activation energies with doping

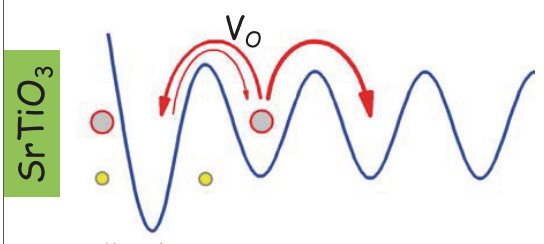


small polaron

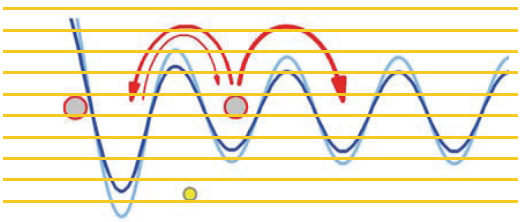

small polaron + band

higher doping →

the potential is washed out by screening → smaller barriers (minor effect in $SrTiO_3$)

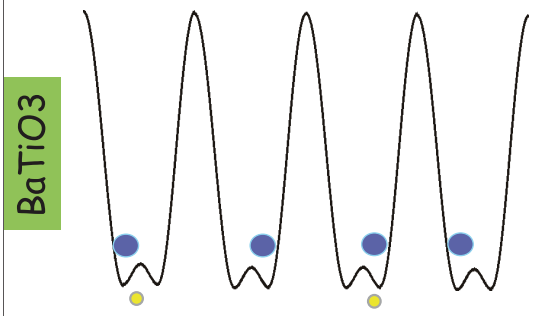


8 site potential for Ti

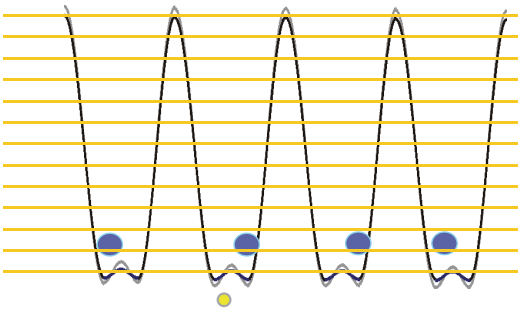

larger effect on the small barriers of off-centre Ti, responsible for the lowering of $T_C$

- Ti off-centering in undoped $BaTiO_3$ → larger relaxation around $V_O$ → larger barrier and $\Delta\lambda$
- doping reduces off-centering and all these effects

## The $V_O$ introduce a strong dependence of $T_C$ on history

## The doping of mobile electrons depends on $V_O$ clustering

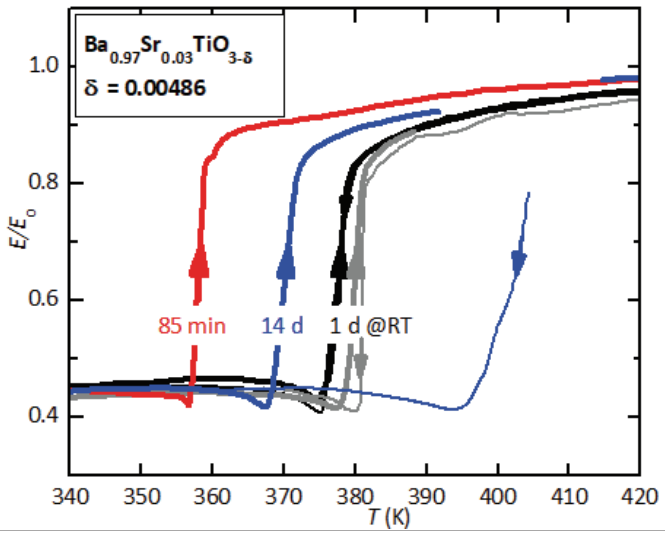


Here $T_C$ spans a range >40 K with up to 30 K of reverse thermal hysteresis (blu)

## No dependence of $T_C$ on history when $\delta = 0$

heatings after different aging times in the FE phase

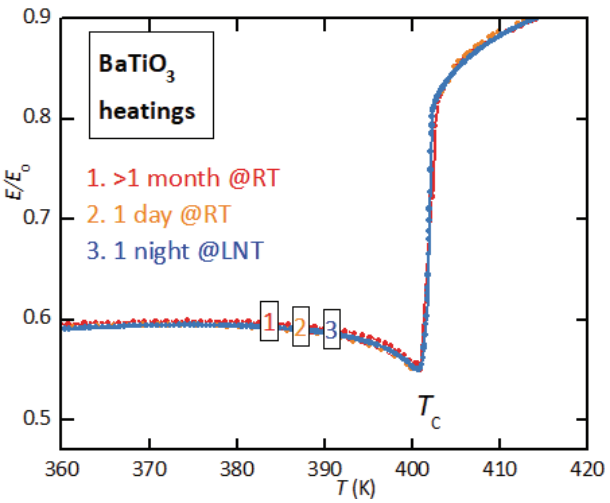


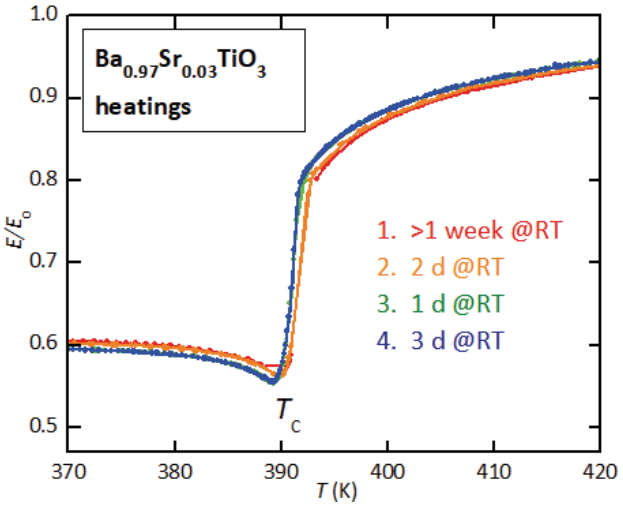


>1 month at RT
<1 day at RT
1 night at LNT

$T_C$ changes of <1 K (<2.5 K in BST)

## Increase of $T_C$ with the permanence in the FE phase

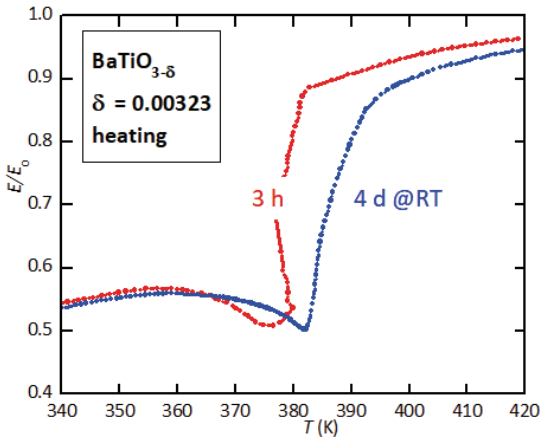


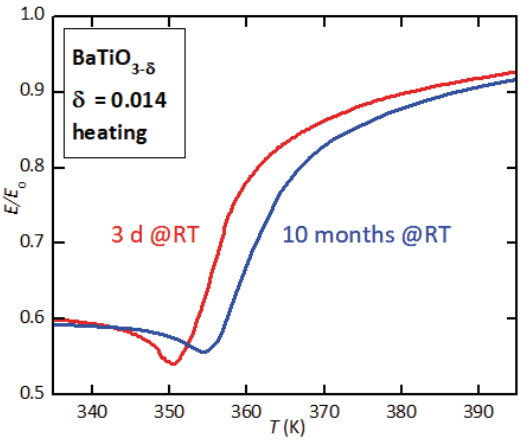


- ~0.3% $V_O$ sufficient to introduce history dependence of $T_C$
- over hours to days (months?) $T_C$ increases with the permanence at room temperature in the FE state

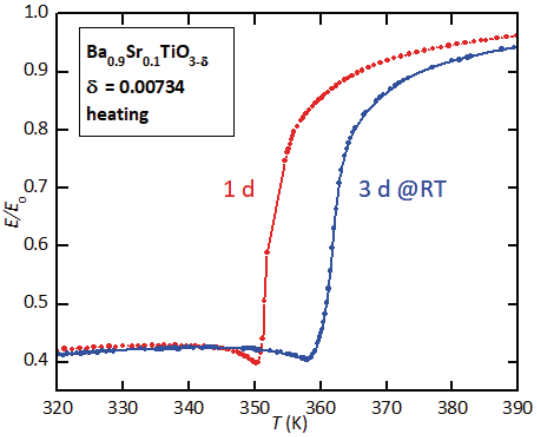


## Smallest $T_C$ after long permanence in the FE phase

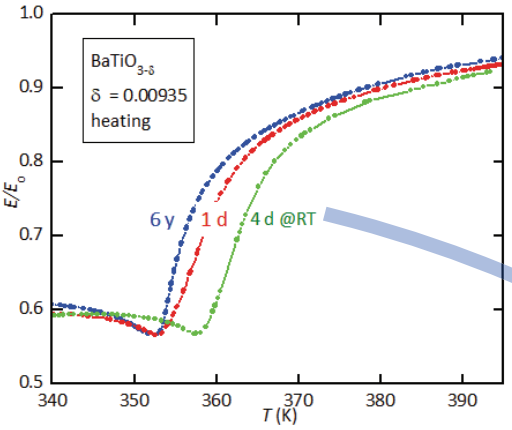


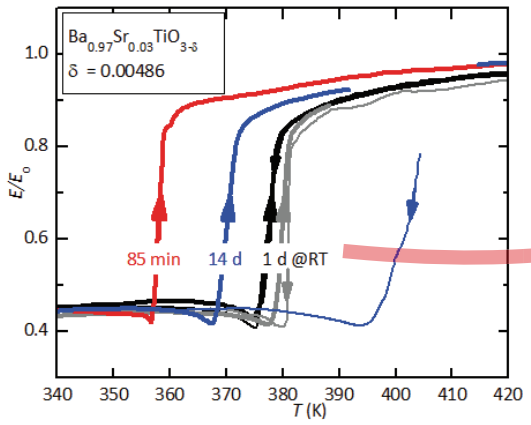


$T_C$ increases with aging in the FE state for days or months, beyond which it decreases

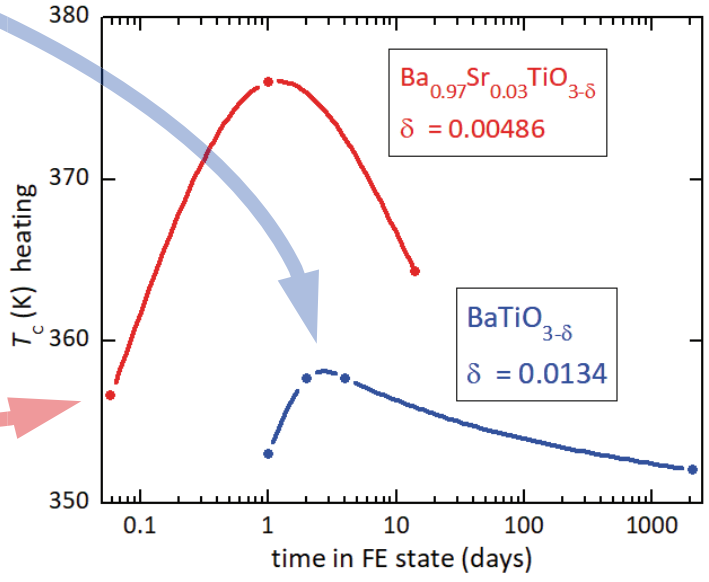

## Mobile dipolar defects stabilize the FE state → enhance $T_C$

**"Stabilization effect in ferroelectric materials during aging in ferroelectric state"**
Dazhi Sun, Xiaobing Ren, Kazuhiro Otsuka
*Appl. Phys. Lett.* 87, 142903 (2005)

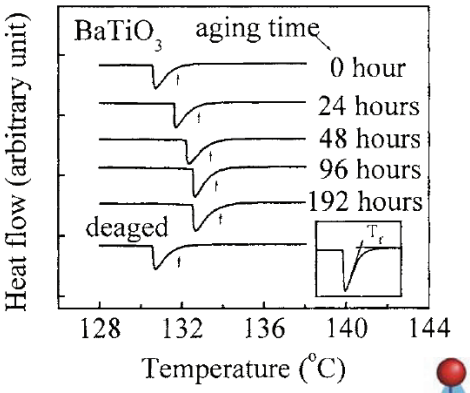


aging a $BaTiO_3$ crystal with $Fe'_{Ti} - V^{\bullet\bullet}_O$ defects increases $T_C$ of 2.5 K

the $V_O$ slowly jump around $Fe^{3+}$ reorienting the electric dipoles of the defect pairs parallel to the internal field of the domains

⇩

additional bias field that stabilizes the domains

⇩

enhancement of $T_C$

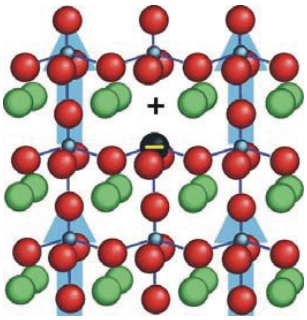

## Stabilization of the FE state: acceptor-$V_O$ vs $V_O$

$Fe'_{Ti} - V^{\bullet\bullet}_O$ pairs: electric dipoles orient parallel to the polarization

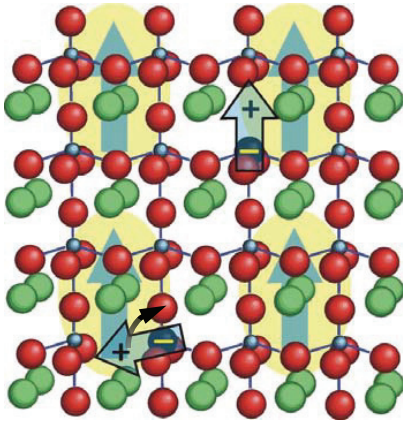

lowering of the electric energy
stabilization of the FE-T domains
increase $T_C$
$\Delta T_C \leq 2.5$ K

only $V_O$: elastic dipoles orient parallel to the tetragonal strain

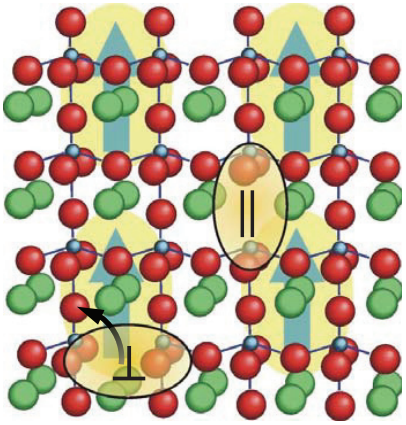

lowering of the elastic energy
stabilization of the FE-T domains
weaker than electric
$\Delta T_C \leq 20$ K

there must be another mechanism for the increase of $T_C$ with only $V_O$

## Doping and $T_C$ depend on the $V_O$ aggregation

| | | |
|---|---|---|
| isolated $V_O$: | $Ti^{3+}$-$V_O$-$Ti^{3+}$ | $Ti^{3+}$ is mobile as polaron or band state → electrical conductivity |
| pairs/chains of $V_O$: | $Ti^{3+}$-$V_O$-$Ti^{2+}$-$V_O$-$Ti^{3+}$ | $Ti^{2+}$ is only between two $V_O$ → each pair or chain segment subtracts two electrons from conduction |

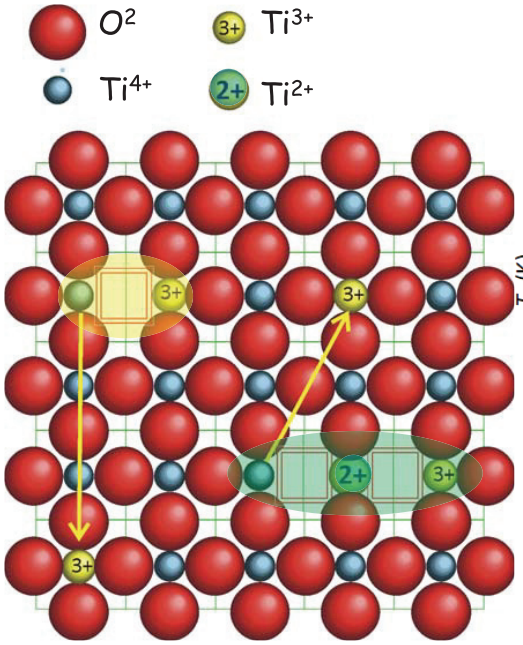


$T_C$ is mainly reduced by the free charges, which screen the FE dipoles, rather than by $V_O$ themselves

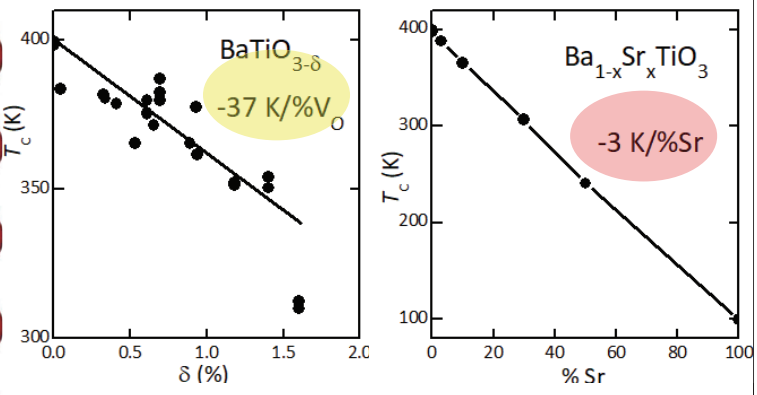


$V_O$ aggregation enhances $T_C$

## Initial slow aggregation of $V_O$ → rise of $T_C$

- when cooling through $T_C$, the kinetics for the aggregation of the charged $V_O$ is slowed by their electrostatic repulsion
- at RT the aggregation into pairs and chains proceeds for hours and days
- mobile charges are removed
- $T_C$ rises

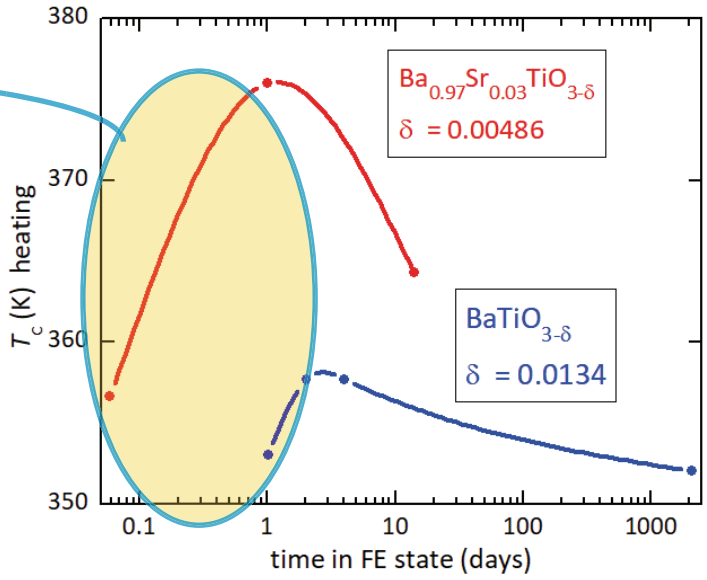

## What mechanism for lowering $T_C$ after long aging?

We need a slower mechanism that dissociates the pairs

Hypothesis: the lowest energy for $V_O$ in the FE state is not aggregated in pairs within the domains but isolated at domain walls

- after the DWs have settled down, the $V_O$ migrate from within the domains to decorate the DW
- slow process through multiple dissociations of pairs
- final $V_O$ dissociation at the DW releases mobile electrons
- $T_C$ decreases

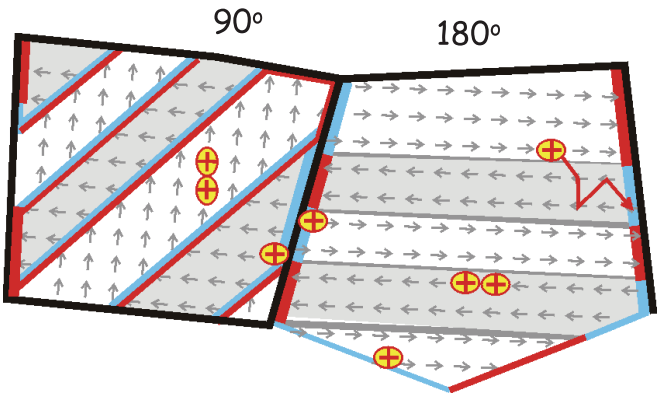


First-principles calculations:
- $V_O$ mainly attracted by 90° DWs
- binding energy comparable or larger than that of pairs.

Chandrasekaran *et al.*,
Phys. Rev. B 93, 144102 (2016)

## The $V_O$ pin the 90° domain walls

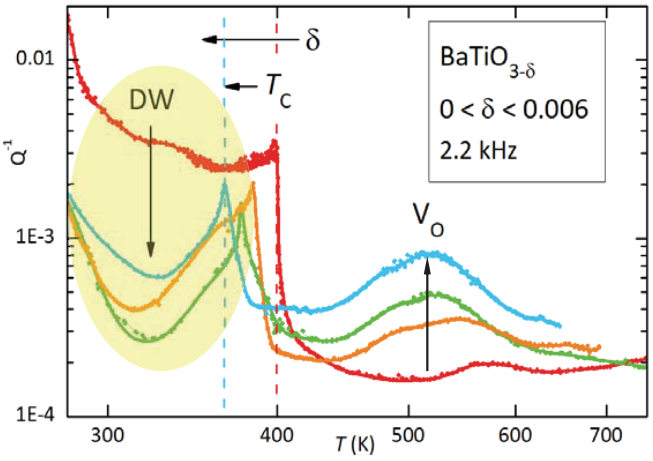


pinning of 90° domain walls
(drop of DW relaxation)

why should $V_O$ at 90° DW prefer to be isolated rather paired ?

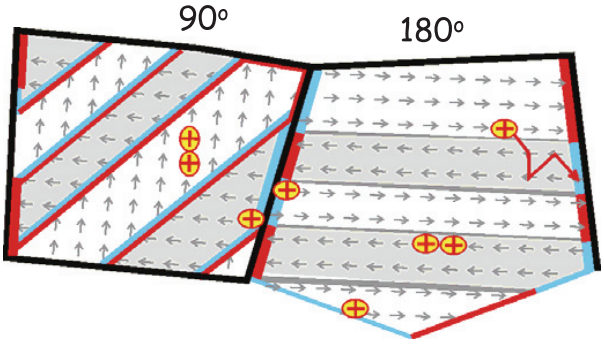

## 90° domain walls are optimally decorated by isolated $V_O$

Pairs are along <100> do not match 90° DW along <110> and split

↓

insulating $Ti^{2+} \rightarrow$ 2 conducting $Ti^{3+}$

↓

$T_C$ decreases

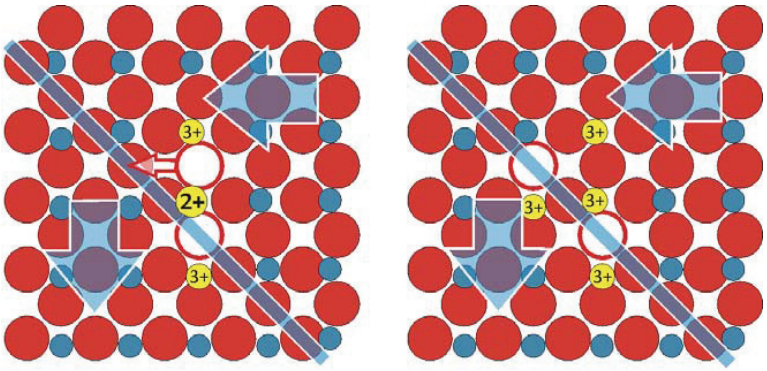


## Slow mechanism that lowers $T_C$: $V_O$ pair splitting for decorating DWs

When cooling through $T_C$, most of the $V_O$ are aggregated in pairs and chains

Pairs are along <100> do not match 90° DW along <110> and split

↓

insulating $Ti^{2+} \rightarrow$ 2 conducting $Ti^{3+}$

↓

$T_C$ decreases

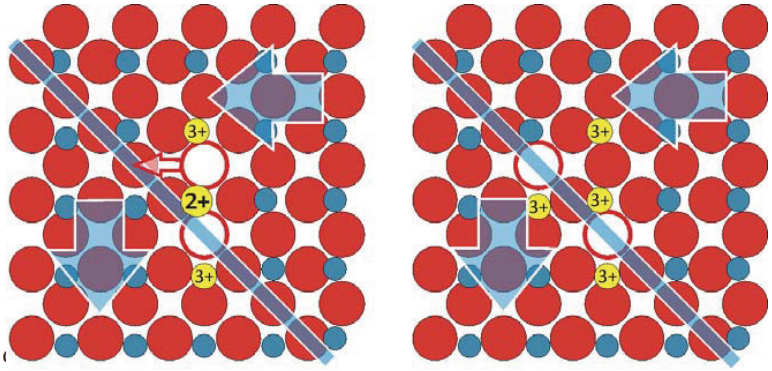


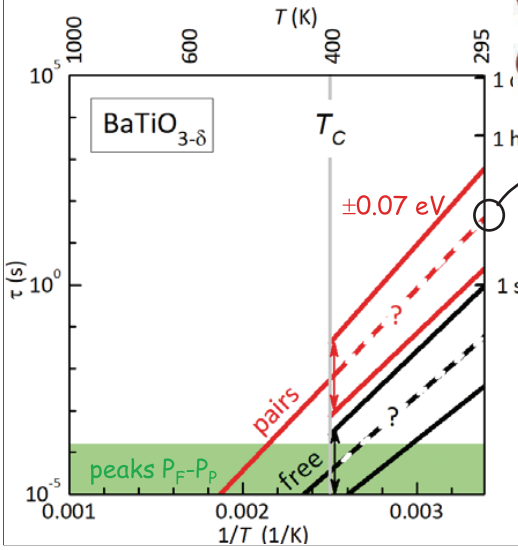


The mean splitting time extrapolated from the PE phase is one minute, but many steps are required for all the pairs to reach the DW.

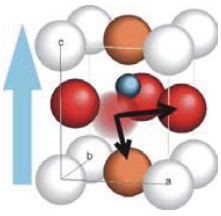

in the FE phase jumps within and out of planes perpendicular to the polarization are different splitting of the activation energies

## No anomalies in $T_C$ of BCTZ

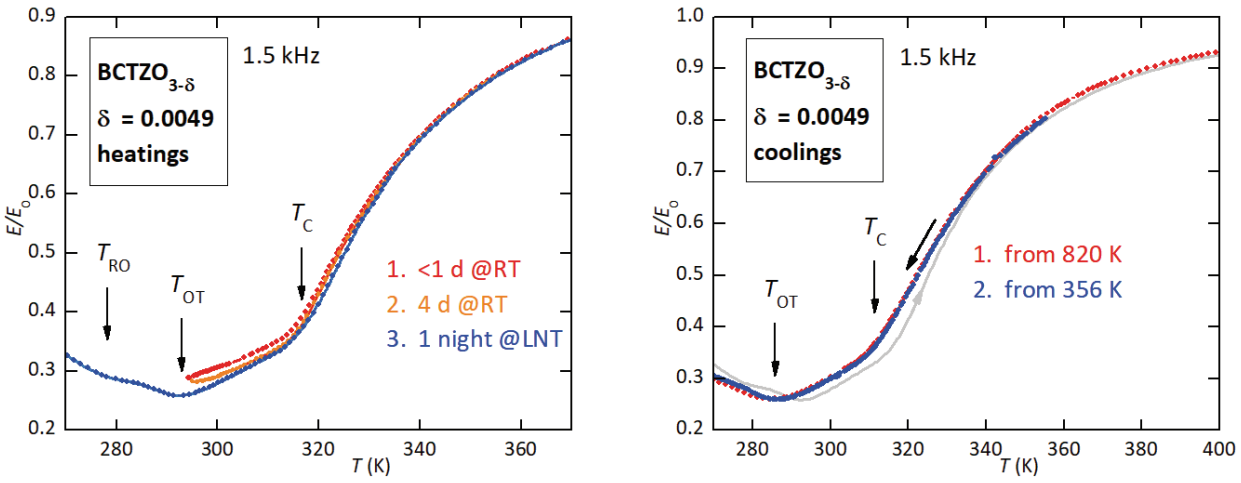


$(Ba_{0.85}Ca_{0.15})(Zr_{0.1}Ti_{0.9})O_3$

no anomalies in $T_C$ : the $V_O$ pairs are static at RT

## Hopping rates: aging in BT but not in BCTZ

When cooling through $T_C$ most $V_O$ are aggregated

↓

the rate determining process for diffusion of $V_O$ to DWs is pair splitting:
minutes for $BaTiO_3$
$10^2$ years for BCTZ

DWs may adapt fast to nearly static $V_O$ but they are not flexible enough to pass through all of them

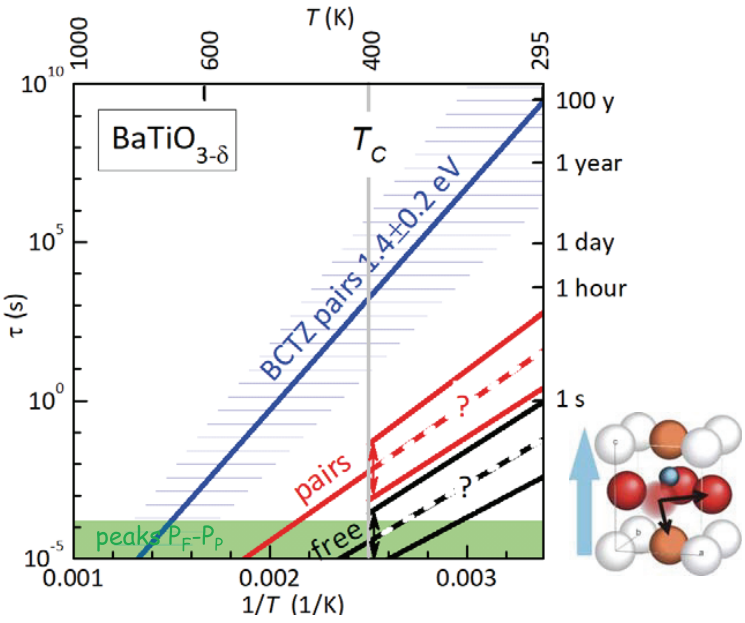


| $V_O$ jumps in the PE phase | | activation energy (eV) | mean time @RT |
|---|---|---|---|
| BT | free hopping | 0.72 eV | ms |
| BT | pair reorientation/splitting | 0.86 eV | min |
| BCTZ | " | 1.4 eV | 100 years |

# Conclusions

The anelastic spectra of O deficient $SrTiO_{3-\delta}$, $BaTiO_{3-\delta}$ and BCTZ contain the same peaks due to isolated and paired $V_O$, In FE BT there is an additional dependence of the activation energies on $\delta$ (off-centre Ti).

$V_O$ pairing occurs also at $\delta < 0.01$ and slows the kinetics for O diffusion and for reaching equilibrium even in the asbence of trapping dopants

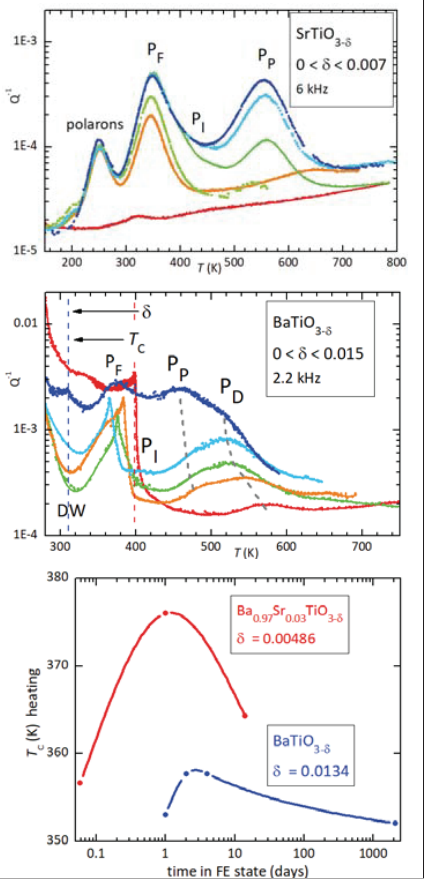


$T_C$ of O deficient BT has a peculiar dependence on the aging time in the FE state, which is explained in terms clustering of $V_O$ in the PE phase and slow dissociation to decorate the 90° DWs in the FE phase.

$V_O$ pairing reduces the doping of mobile electrons from $2\delta$ (all $V_O$ isolated) to $\delta$ (all paired).
→ electric conductivity, cell volume, hopping barriers

E-IMR International Workshop 2024 @IMR Tohoku Univ., 26th November 2024

# *Nanostructure and chemical state imaging of energy materials by coherent X-ray diffraction*

**Yukio TAKAHASHI**

Materials Evaluation and Analysis Research Unit /
International Center for Synchrotron Radiation Innovation Smart

## *Multi-scale Structures of Energy Materials*

**Atomic-scale (Å)**
**Model structure system**
***Bottom-up approach***

*Model systems* are not fully applicable to *practical materials*

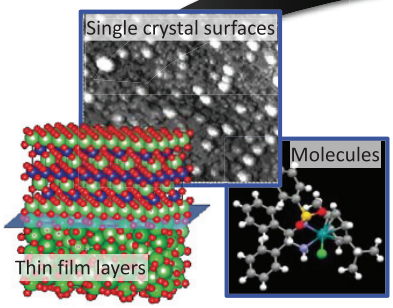


- Simple phase/structure, well discussed by SPM, TEM, theoretical calculations, etc…

**Nano-mesoscale (nm-μm)**

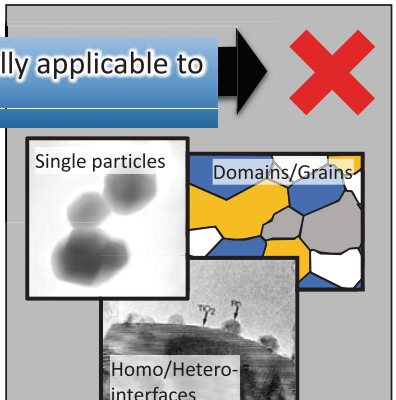


A. D. Logan, et al, *Langmuir* **4**, 827 (1998).

- **Non-uniform structures →Non-uniform functionalities**

**Macroscale (>mm)**
**Macroscopic system**

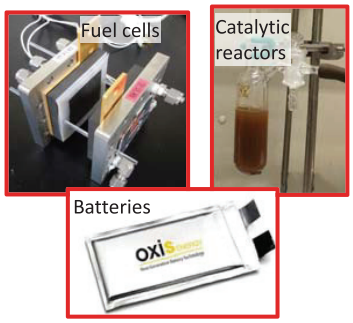


- Maximizing functions
- Non-uniform and complex
- Averaged structure analysis by XRD, XAFS, etc…

***Top-down approach***

Only *apparent structural parameters* can be incorporated into *models*

***Required measurement/analyzing methods to understand physics/chemistry in nano-mesoscale***

- **High-resolution, large field-of-view observation in three dimension**
- **Identification of hidden correlations between structural factors and material functions using big-data analysis**

## *Coherent X-ray Diffraction Imaging: Breakthrough of Spatial Resolution of X-ray Microscopy*

*Scanning Coherent X-ray Diffraction Imaging (X-ray Ptychography)*

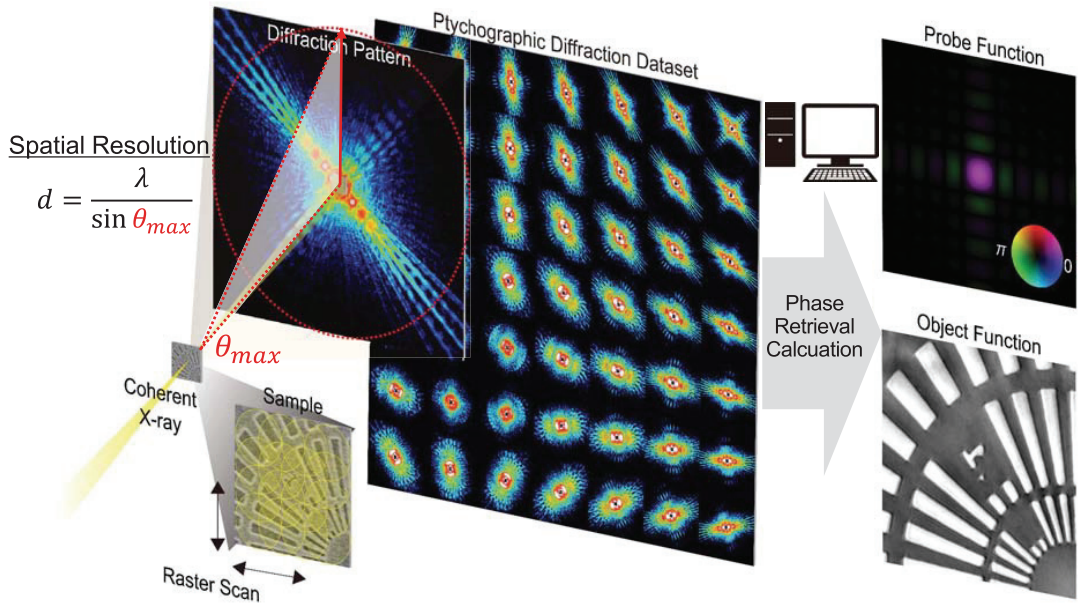


- **Computation substitutes for X-ray imaging lens**
- **Spatial resolution does not depend on accuracy of X-ray lens fabrication**
- **High-intensity coherent X-ray beam to achieve high-spatial resolution**

## *High-resolution X-ray ptychography apparatus at SPring-8*

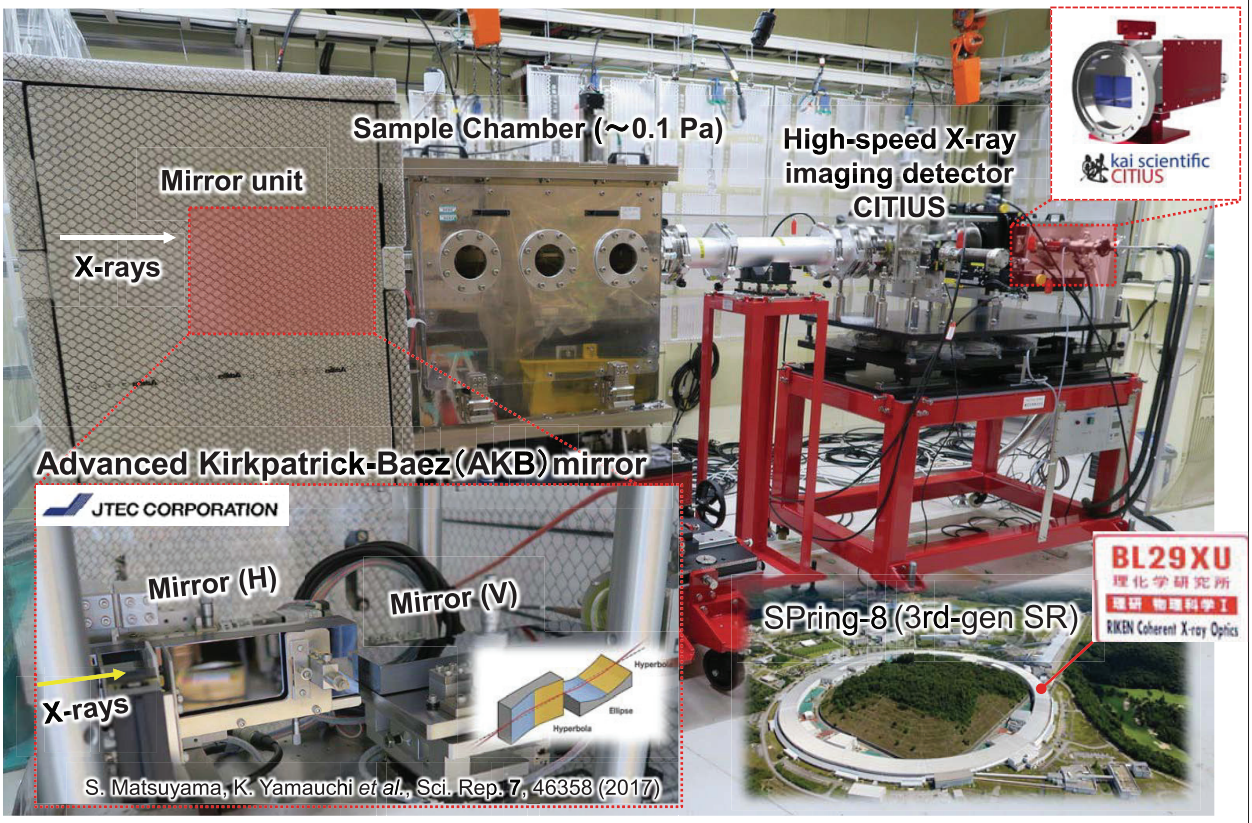



M. Hirose, N. Ishiguro, Y. Takahashi *et al.*, *J. Synchrotron Rad.* **27**, 455-461 (2020).
Y. Takahashi, M. Abe, T. Hatsui *et al.*, *J. Synchrotron Rad.* **30**, 989-994 (2023).

# Catalyst material: $Ce_2Zr_2O_x$ Solution Oxide (CZ-x)

- Stoichiometric oxygen storage/release in the crystal bulk structure (efficiency: ~90%)
- Used as co-catalyst of automobile exhaust purification three-way catalyst

### Expanding operation window

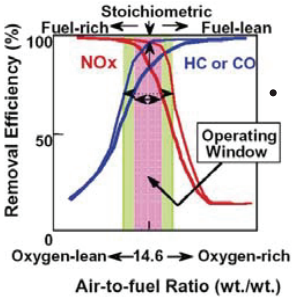


- Control the oxygen concentration in catalyst system

A. Suda, *el al. J. Ceram. Soc. Jpn.* 110, 126 (2002.

### Framework of crystal structure

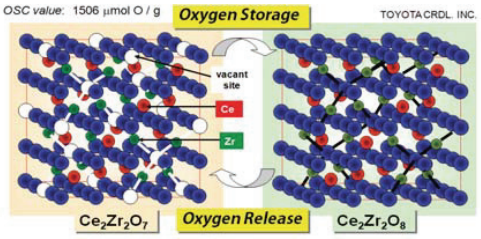


Pyrochlore-type $Ce^{3+}$ ⇄ κ-phase (fluorite-type) $Ce^{4+}$

### 3D Spectroscopic ptychography

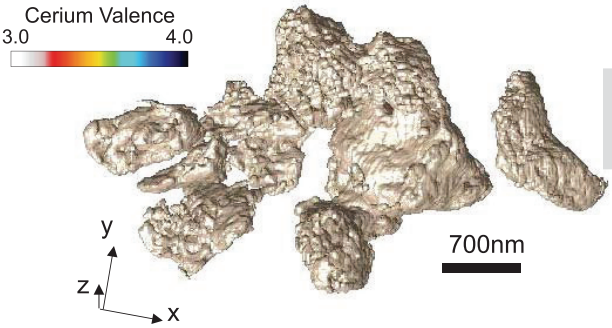


Data mining

### Visualization of reaction pathway

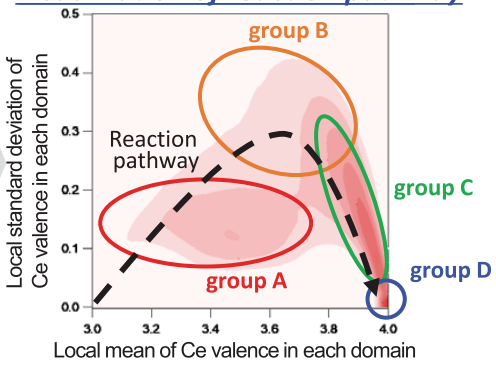


M. Hirose, N. Ishiguro, H. Dam, M. Tada, Y. Takahashi *et al.*, *Communs. Chem.* **2**:50 (2019)

# Battery material: Spinel-type $LiNi_{0.5}Mn_{1.5}O_4$ (LNMO)

- Rechargeable battery using the reversible reduction of lithium ions to store energy
- Development of cathode materials for higher capacitance, higher voltage, and higher energy density

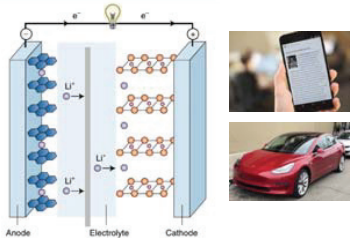




John B. Goodenough, *Nat. Electronics* **1**, 204 (2018)

### Spinel-type $LiNi_{0.5}Mn_{1.5}O_4$ (LNMO)

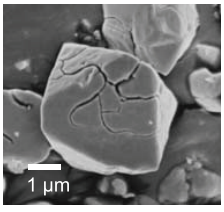


- ✓ High energy density, high working voltage ~5 V
- ✓ Rapid capacity fade during charge/discharge cycling
- ✓ Cracks, Dissolution of $Mn^{3+}$ in electrolyte

S. Kuppan *et al.*, *Nat. Commun.* **8**, 14309 (2017)

### Spectroscopic ptychography

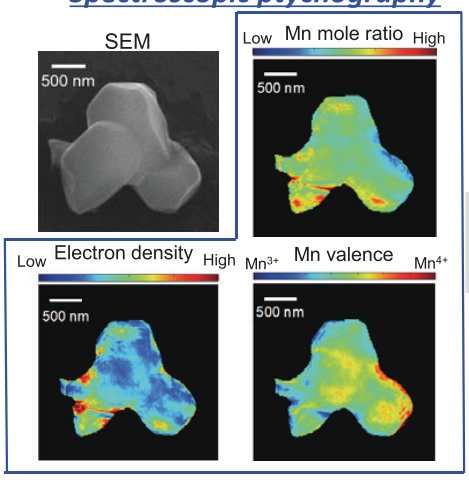


Data mining

### Visualization of Degradation Factor

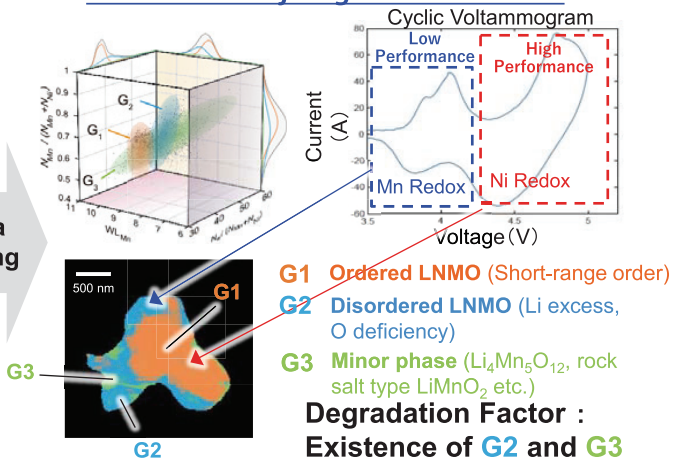


- **G1** Ordered LNMO (Short-range order)
- **G2** Disordered LNMO (Li excess, O deficiency)
- **G3** Minor phase ($Li_4Mn_5O_{12}$, rock salt type $LiMnO_2$ etc.)

**Degradation Factor : Existence of G2 and G3**

H. Uematsu, N. Ishiguro, Y. Takahashi *et al.*, *J. Phys. Chem. Lett.* **12**, 5781–5788 (2021)

# From SPring-8 to NanoTerasu

**SPring-8**(3rd-gen SR)


**NanoTerasu**(4th-gen SR)


First Beam: December 2023
User Operation: April 2024

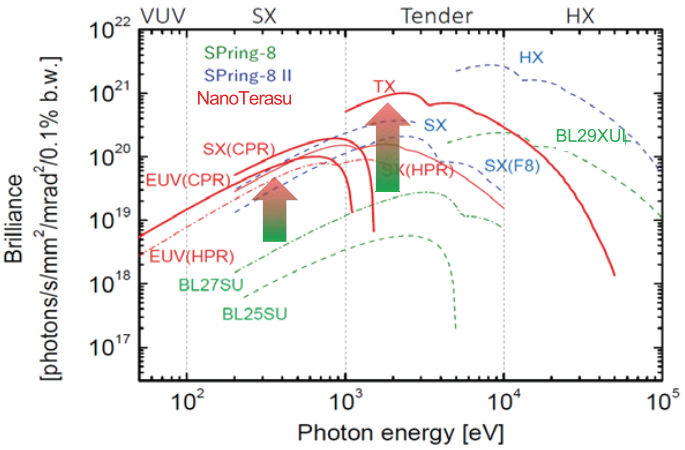


- Soft and tender X-rays at NanoTerasu are significantly brighter than SPring-8
- Tender X-ray at NanoTerasu would be still brighter than SPring-8-Ⅱ

# BL10U: X-ray Coherent Imaging BL in NanoTerasu

- In-Vacuum Undulator
- Energy range: **2.1keV～15keV**
- Fixed-exit harmonic rejection plane triple mirrors and Si111 double crystal monochromator
- Differential pumping system: **No Be windows**
- **Advanced KB focusing mirrors** (Sep. 2024)
- **CITIUS detector** (Jan.2025)

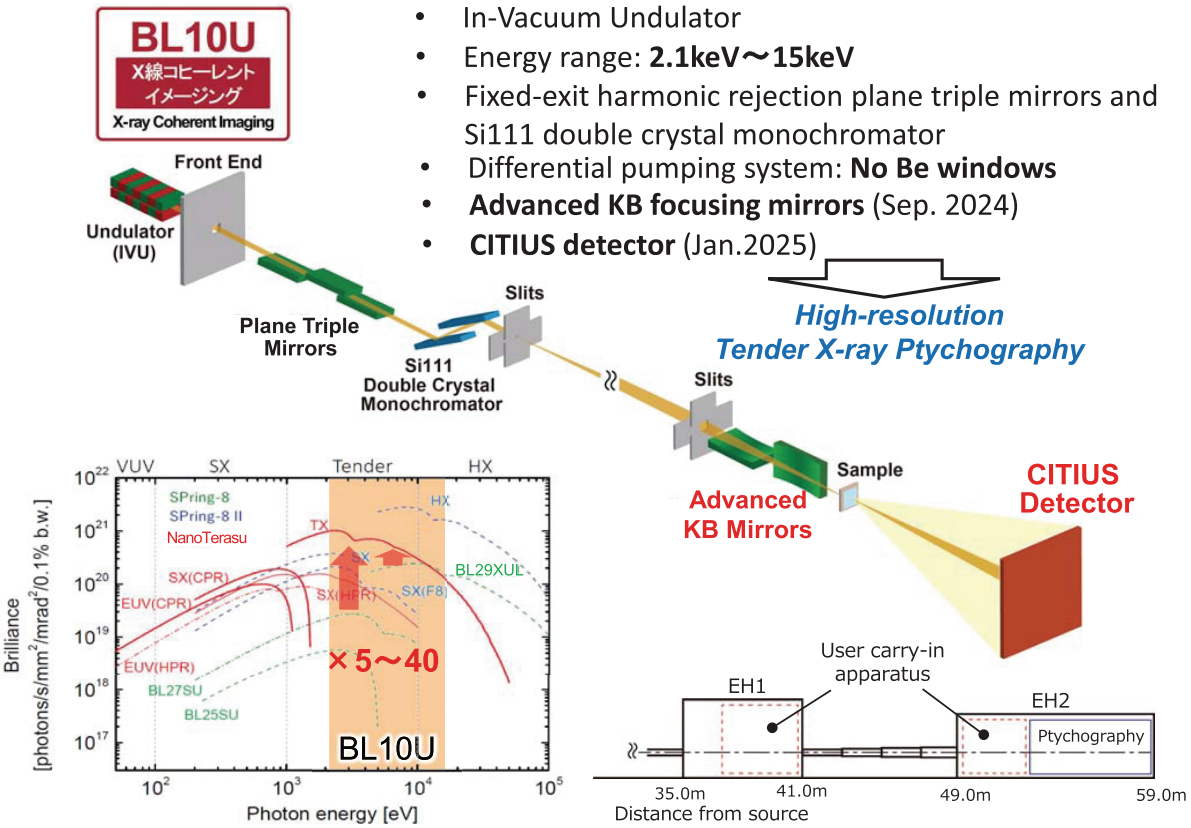

## *First Experiment of Tender X-ray Ptychography at NanoTerasu BL10U*

**April 9th-11th, 2024**

- X-ray energy: 3.5 keV
- Sample: sulfurized polymer

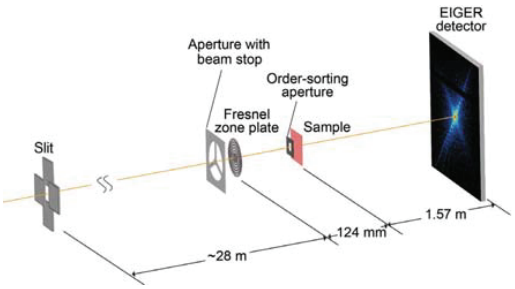


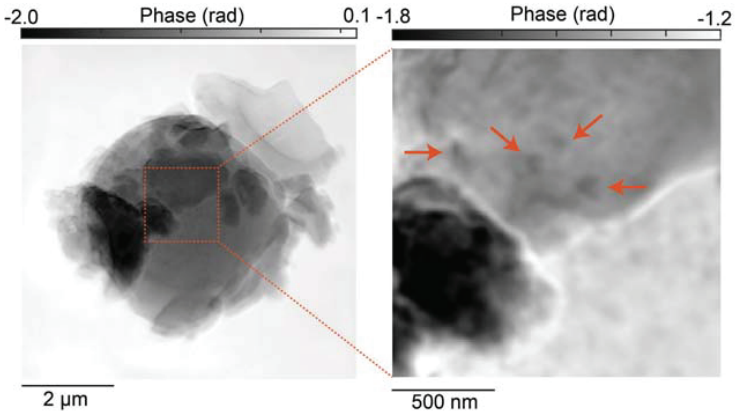


⇒ **49.3 nm resolution**

| | April 2024 | | Near Future |
|---|---|---|---|
| Ring Current | 160 mA | ×2.5 | 400 mA |
| Focusing optics (Effective Focusing Efficiency) | FZP (~0.2% ) | ×303 | AKB mirrors (~66% ) |
| Detector (Measurement Efficiency) | EIGER 1M (~33%) | ×2.9 | CITIUS 840k (~97%) |
| Effective flux (photons/s) | 2.8 × $10^7$ photons/s | ×2200 | 6.1 × $10^{10}$ photons/s |

Diffraction intensity decays at $q^{-4}$ ⇒ 49.3 nm /$(2200)^{1/4}$ = **7.2 nm !!**

N. Ishiguro, F. Kaneko, M. Abe, Y. Takahashi *et al.*, Appl. Phys. Express **17**, 052006 (2024)

## *First Paper on Experiments Using Synchrotron Radiation at NanoTerasu*


OPEN ACCESS

Applied Physics Express **17**, 052006 (2024) **LETTER**

https://doi.org/10.35848/1882-0786/ad4846


Check for updates

### Towards sub-10 nm spatial resolution by tender X-ray ptychographic coherent diffraction imaging


Nozomu Ishiguro[1,2], Fusae Kaneko[3,4], Masaki Abe[1,2], Yuki Takayama[1,2,5,6], Junya Yoshida[1], Taiki Hoshino[1,2,4,6], Shuntaro Takazawa[1,7], Hideshi Uematsu[1,7], Yuhei Sasaki[1,7], Naru Okawa[1,7], Keichi Takahashi[8], Hiroyuki Takizawa[8], Hiroyuki Kishimoto[3], and Yukio Takahashi[1,2,4,9*]

[1]*International Center for Synchrotron Radiation Innovation Smart (SRIS), Tohoku University, 468-1 Aramaki-Aza-Aoba, Aoba-ku, Sendai, 980-8572, Japan*
[2]*RIKEN SPring-8 Center, 1-1-1 Kouto, Sayo-cho, Sayo-gun, Hyogo 679-5148, Japan*
[3]*Sumitomo Rubber Industries, Ltd. 2-1-1 Tsutsui, Chuo, Kobe, Hyogo 651-0071, Japan*
[4]*Institute of Multidisciplinary Research for Advanced Materials (IMRAM), Tohoku University, 2-1-1 Katahira, Aoba-ku, Sendai 980-8577, Japan*
[5]*Graduate School of Agricultural Science, Tohoku University, 468-1, Aoba-ku, Sendai 980-0845, Japan*
[6]*Research Center for Green X-Tech, Green Goals Initiative, Tohoku University, 6-6, Aoba-ku, Sendai 980-8579, Japan*
[7]*Department of Metallurgy, Graduate School of Engineering, Tohoku University, Aoba-yama 02, Aoba-ku, Sendai 980-8579, Japan*
[8]*Cyberscience Center, Tohoku University, 6-3, Aramaki Aza Aoba, Aoba-ku, Sendai 980-8578, Japan*
[9]*Institute for Materials Research, Tohoku University, 2-1-1 Katahira, Aoba-ku, Sendai 980-8577, Japan*

*E-mail: ytakahashi@tohoku.ac.jp



Received April 20, 2024; accepted May 6, 2024; published online May 27, 2024


**Paper Accepted within One Month after Beamtime !!**
**Selected as Spotlights 2024**

## *Future perspectives:*
## *Visualization of unexplored areas using tender X-ray ptychography*

### Visualization of reactions in lithium-sulfur battery materials

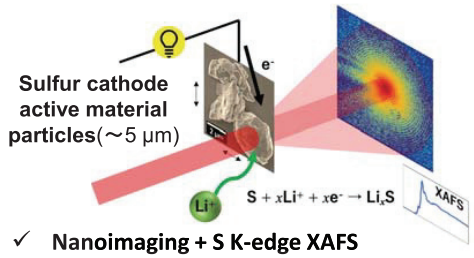


- ✓ **Nanoimaging + S K-edge XAFS**
- ✓ **Use of data mining**
- ✓ **Electrochemical operando measurement**

### Non-destructive internal inspection of advanced semiconductor devices

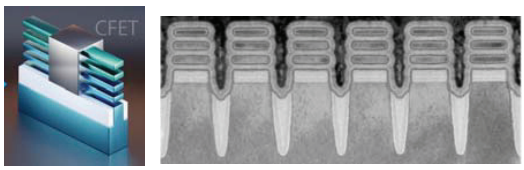


https://www.tel.co.jp/museum/magazine/report/202407_02/?section=1

- ✓ **Three-dimensional visualization by computed tomography/multi-slice method**
- ✓ **Visualization of device internal structure without cross-sectional processing**

### Nanoscale structural and elemental analysis in vivo

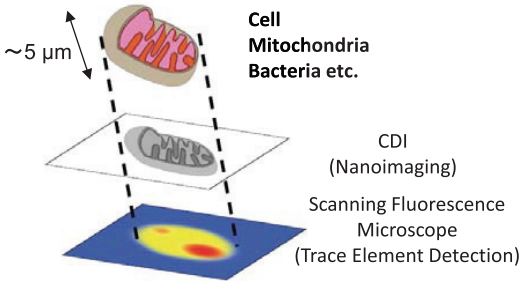


- ✓ **Visualization of distribution and transport of phosphorus, sulfur, etc.**

### Observation of filler diffusion and aggregation within tire rubber

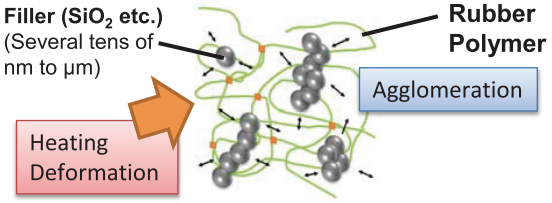


- ✓ **sub-sec to msec temporal resolution + nanoscale resolution imaging**
- ✓ **Nanostructure-mechanical property correlations**

# Layered Manganese Dioxide as a Heat-Storage Material Utilizing Environmental Water Vapor

**Norihiko L. OKAMOTO, and Tetsu ICHITSUBO**

**Institute for Materials Research, Tohoku University**

***E-IMR International Workshop 2024***
**IMR, Tohoku Univ., Sendai, Japan**
**November 26th, 2024**

# Harvesting Energy from Waste Heat

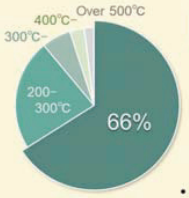


## Low-grade waste heat (100–200℃)

needs to be **recovered & reused**
for achieving a sustainable society.

C. Haddad *et al.*, *Energy Procedia*, **50**, 1056–1069 (2014).

- **Thermoelectricity** Conversion from temperature difference to electricity
  Limited by Carnot efficiency & no storage
- **Thermal energy (heat) storage** Without conversion
  On-demand spatially & temporally

➢ **Potential applications**

**Waste heat from factories**
can be used as an auxiliary heat source in other manufacturing sites.

**Natural thermal energy**
The heat stored during the day or in summer can be reused at night or in winter.

**Automobile engines/batteries**
The stored waste heat can be used to preheat the engine. Due to the limited space available, a high-density heat storage material is desirable (> 1000 MJ/m$^3$).

# Basic Concept of Heat Storage

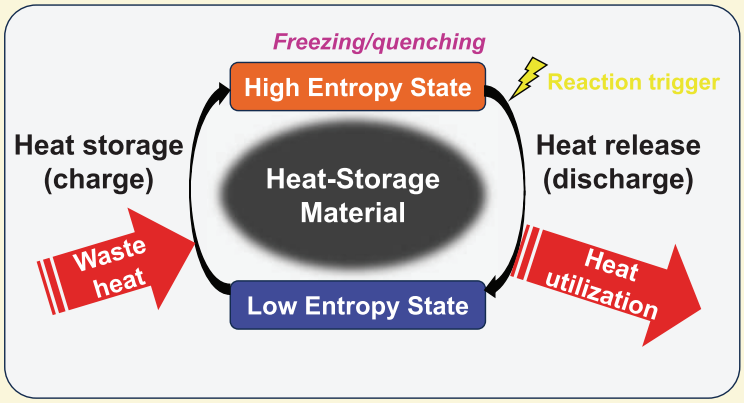


Enthalpy-Temperature relationship

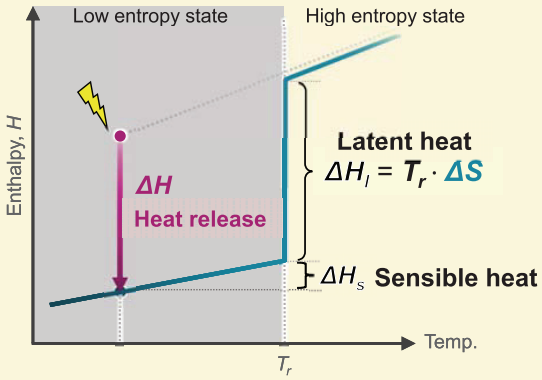


**The KEY for long-term heat storage is how to freeze the high entropy (enthalpy) state, and how to trigger the exothermic reaction on demand.**

**Good heat-storage materials require:**

- ❖ **High energy density**
  Utilizing reaction with **large** $\Delta S$ : **Solid** ⟷ **Gas**
- ❖ **High reaction rate & reversibility**
- ❖ **Material's stability, safety & abundance**

# Classification of Heat-Storage Materials by Reaction Mechanisms

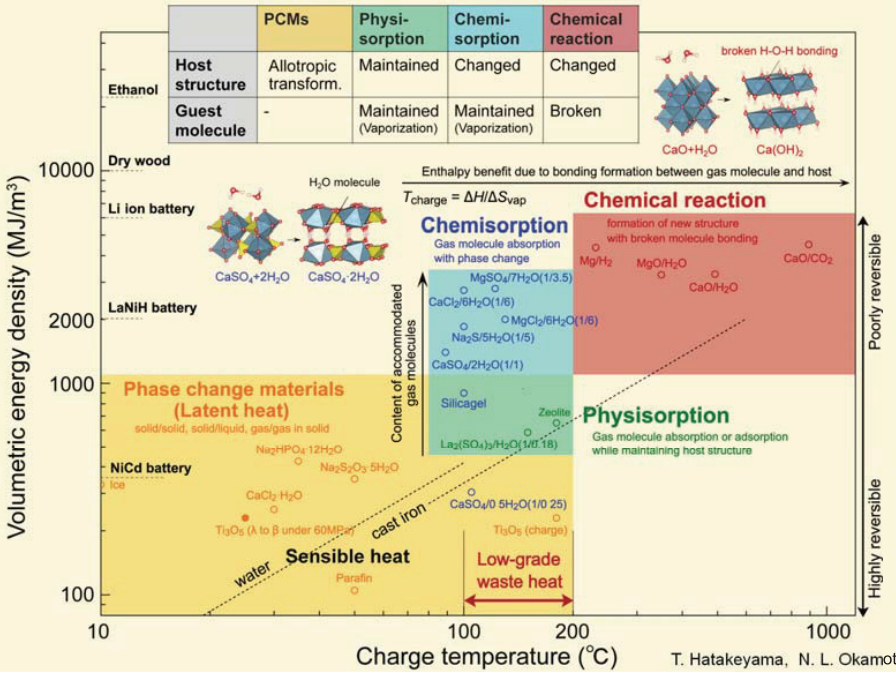


**Chemical reaction type**
- Poor reversibility
- High energy density
- High charge temperature

**Chemisorption type**
- Poor reversibility
- Middle energy density
- Middle charge temperature

**Physisorption type**
- Good reversibility
- Low energy density
- Middle charge temperature

**TCMs** (thermo-chemical materials)

**Phase change (latent heat) type**
- Good reversibility
- Low energy density
- Charge temperature: melting temp., etc.

**Sensible heat type**
- Good reversibility
- Low energy density
- Charge temperature: not defined

T. Hatakeyama, N. L. Okamoto, H. Li, T. Ichitsubo et al., *Nat. Commun.*, **13**, 1452 (2022).

# Phase Change (Latent Heat) Type

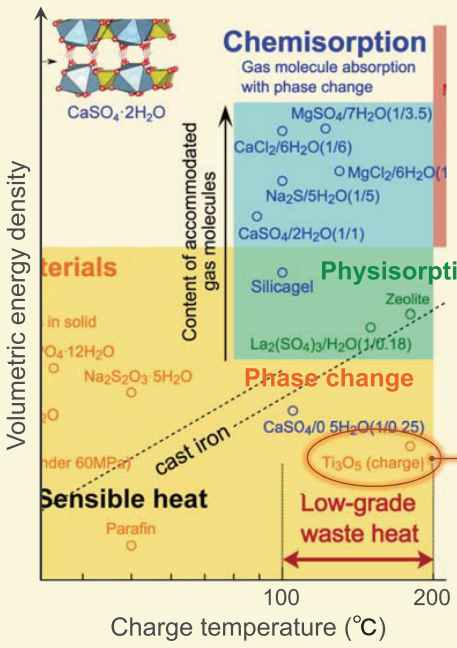


Latent heat between solid/liquid or liquid/gas: **good reversibility**
However, maintaining the supercooled (high entropy) state is difficult.

Solid-solid allotropic transformation

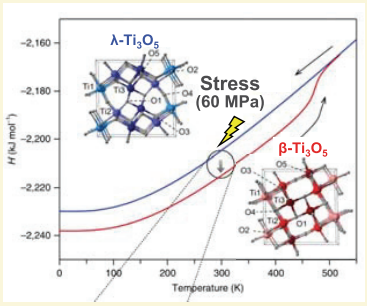


H. Tokoro, S. Ohkoshi *et al.*, *Nat. Commun.*, **6**, 7037 (2015).

**Reaction triggered by applying stress**
- **On-demand use of released heat**

**Solid/solid structural transformation**
- **Fast reaction**

⇒ **High heat-release rate is expected.**

**Entropy gap (*ΔS*) between solid states is usually small.**

⇒ ***δQ* (~ *ΔH*) is inevitably small.**

$\lambda\text{-}Ti_3O_5$ (quasi-stable) → $\beta\text{-}Ti_3O_5$

$$\Delta H = T_{charge}\Delta S_{\beta\rightarrow\lambda} = 460\ \mathrm{K} \times 25\ \mathrm{J/K\cdot mol\text{-}Ti_3O_5}$$

cf. Ice's melting entropy: 22 J/K·mol-$H_2O$
Energy density: 320 MJ/m$^3$

**Utilization of gas phase (large *ΔS*) is desired!**

# Chemisorption Type

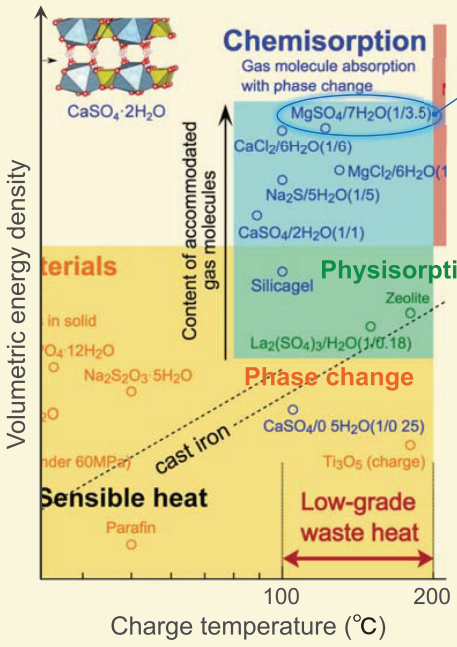


Example of water absorption

$MgSO_4\cdot H_2O + 5H_2O\ (g) \rightarrow MgSO_4\cdot 6H_2O\ (s)$

$$\Delta H = T_{discharge}\Delta S_{vap} = 300\ \mathrm{K} \times \underbrace{\sim 145\ \mathrm{J/K\cdot mol\text{-}H_2O}}_{\text{Sublimation entropy (gas ↔ solid)}} \times 5$$

【Merit】
- Sublimation entropy for water absorption is large.
- Large amount of **$H_2O$ (5 mol)** absorbed per mol-$MgSO_4$

⇒ **High energy density**

【Demerit】
- Highly deliquescent
- Large structural/volumetric changes upon water absorption/release

⇒ **Sluggish & irreversible**

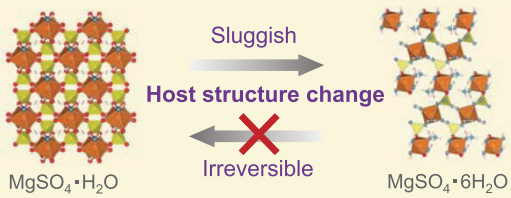


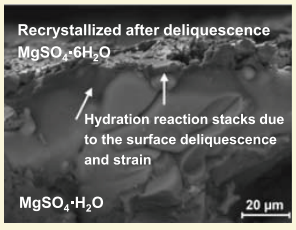


M. Steiger *et al.*, *Crystal Growth & Design*, **8**, 1 (2008).

# Physisorption Type

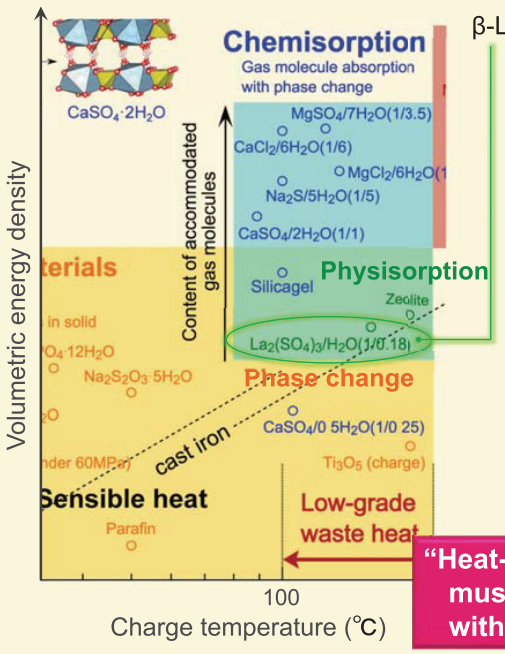


$\beta$-$La_2(SO_4)_3$ + $H_2O$ (g) → $La_2(SO_4)_3 \cdot H_2O$ (s)

N. Hatada, K. Shizume, and T. Uda, *Adv. Mater.*, **29**, 1606569 (2017).

*In-situ* HTXRD @3%$H_2O$ in $O_2$

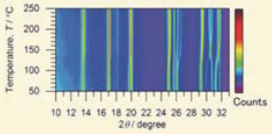

Host structure maintained

TG @1.2%$H_2O$ in Ar

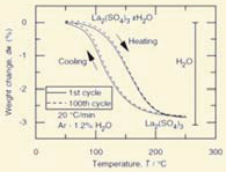

Single phase reaction

【Merit】

- Small structural/volumetric changes upon water absorption/release

  ➡ **High reaction rate & reversibility**

【Demerit】

- Small amount of **$H_2O$ (<1 mol)** absorbed per $La_2(SO_4)_3$ (17 atoms/u.f.)

  Ratio of number of atoms, host : guest = 17 : 3 = **1 : 0.18**

  ➡ **Low energy density**

**"Heat-storage material with reversibility and large energy density" must be capable of absorbing/releasing a large amount of water with minimal structural/volumetric changes.**

# Layered Manganese Dioxide (δ-$K_{0.33}MnO_2$)

Pyrolysis of $KMnO_4$ at 700℃

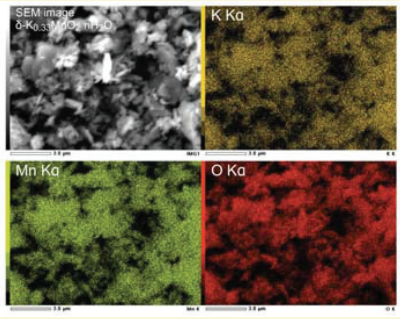


**"Crystal water" has been known to exist in δ-$MnO_2$, but is it released *without* structural change (intercalation)? Water release temperature? Hydration enthalpy?**

STEM-HAADF Image

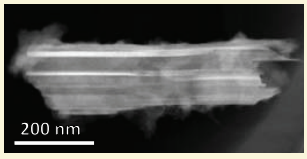


Atomic resolution STEM-HAADF

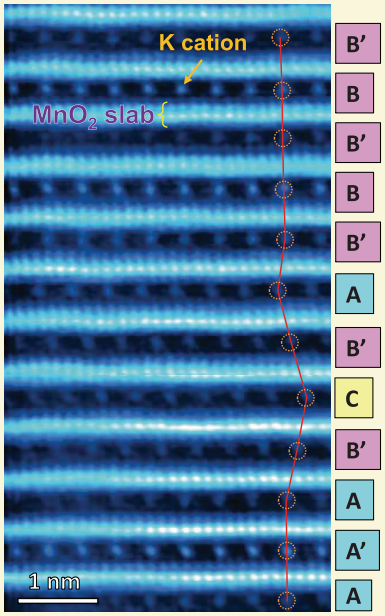


Reported structure ($K_{0.33}MnO_2$)

Space group: $P6_3/mmc$ (#194)

Lattice constants: $a$ = 2.84 Å, $c$ = 14.03 Å

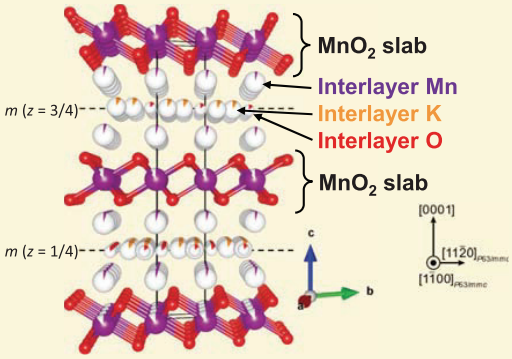


A.C. Gaillot et al., *Chem. Mater.*, **15**, 4666 (2003).

N.L. Okamoto et al., *Energy Storage Mater.*, **61**, 102912 (2023).

# Structural Changes during Hydration/Dehydration: In-Situ XRD

**In ambient atmosphere** (R.H.60%@25℃ =1.8%$H_2O$)

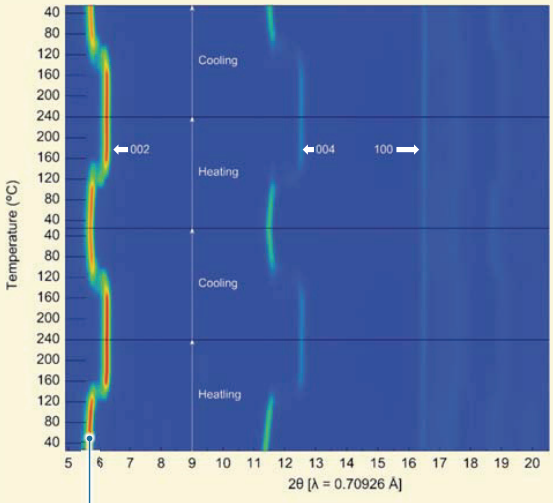


Interlayer distance shrinks/expands by 9% upon hydration/dehydration.
The layered structure is maintained.

**"Water intercalation"**

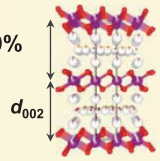


**In dry $N_2$**

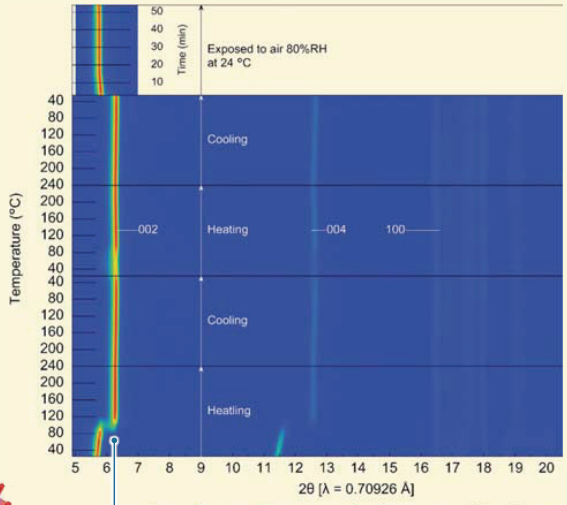


Interlayer distance is irreversible due to the absence of water molecules.

# Water Absorption/Release Behavior under Controlled Humidity

**TG-DTA** (R.H.70%@25℃ = 2.2%$H_2O$ in $N_2$)

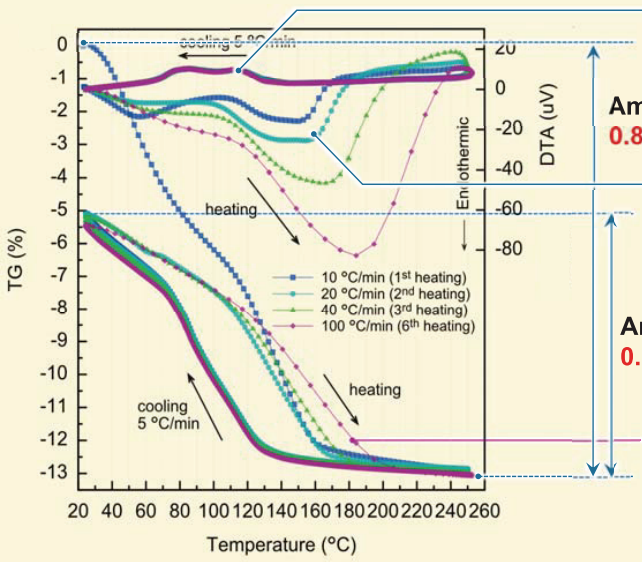


Heat release upon water absorption

Amount of initial $H_2O$ release
0.83 $H_2O$ / $K_{0.33}MnO_2$

Heat absorption upon water release

Amount of reversible $H_2O$ absorption/release
0.5 $H_2O$ / $K_{0.33}MnO_2$

Heating rate: 100℃/min
Charge completed within 3 min.

**High rate property**

# Amount of Heat Storing/Release Upon Water Release/Absorption

**Heat storage** (DSC in dry Ar)

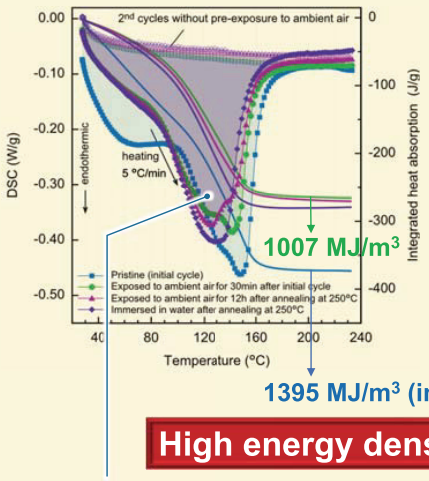


1395 MJ/m$^3$ (initial)

**High energy density**

The amount of absorbed heat: **61.7 kJ/mol-$H_2O$**

(corresponding to the reversibly released/absorbed water = 0.50 mol-$H_2O$)

**Heat release** (exposed to humidified Ar @28℃ in DSC)

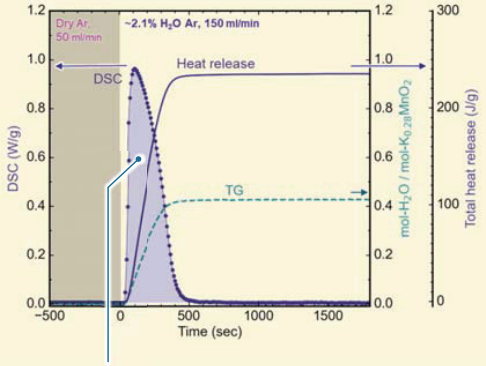


The amount of released heat: **59.4 kJ/mol-$H_2O$**

⇒ $\Delta S$ = 145.0 J/K/mol-$H_2O$

≒ Sublimation entropy of ice (0℃): 140.5 J/K/mol

State of the interlayer water molecules in $K_{0.33}MnO_2$ is: **"Solid-like"**

*c.f.* Evaporation entropy of water (100℃): 109 J/K/mol

Melting entropy of ice (0℃): 22 J/K/mol

# Heat Storage/Release Mechanism Utilizing $H_2O$ Molecules in Air

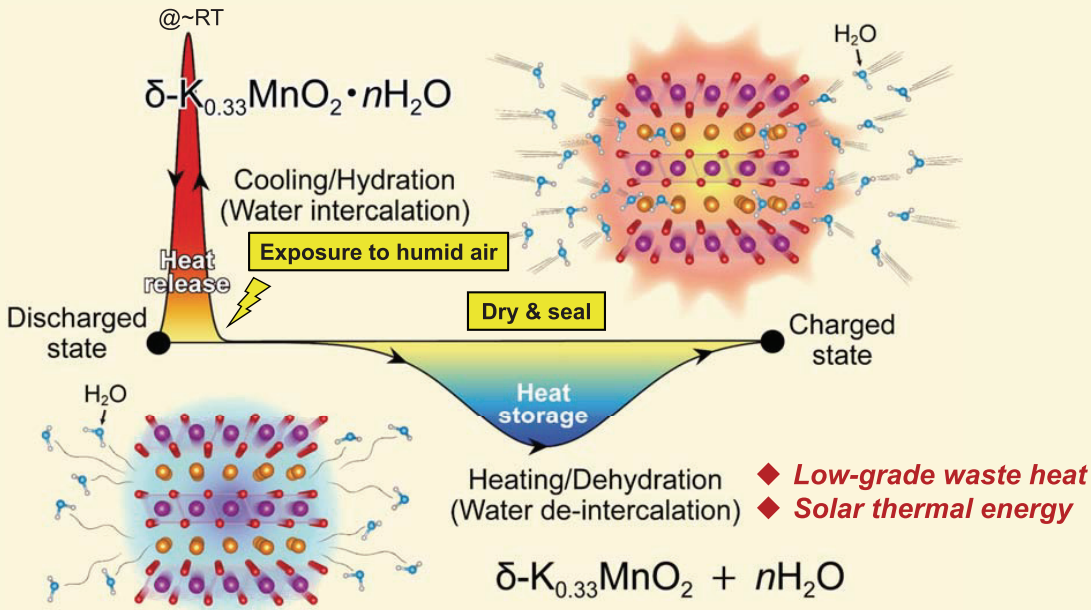


- ***Low-grade waste heat***
- ***Solar thermal energy***

**Container ($MnO_2$) + water vapor (high entropy state)**

# Comparison with Existing Materials

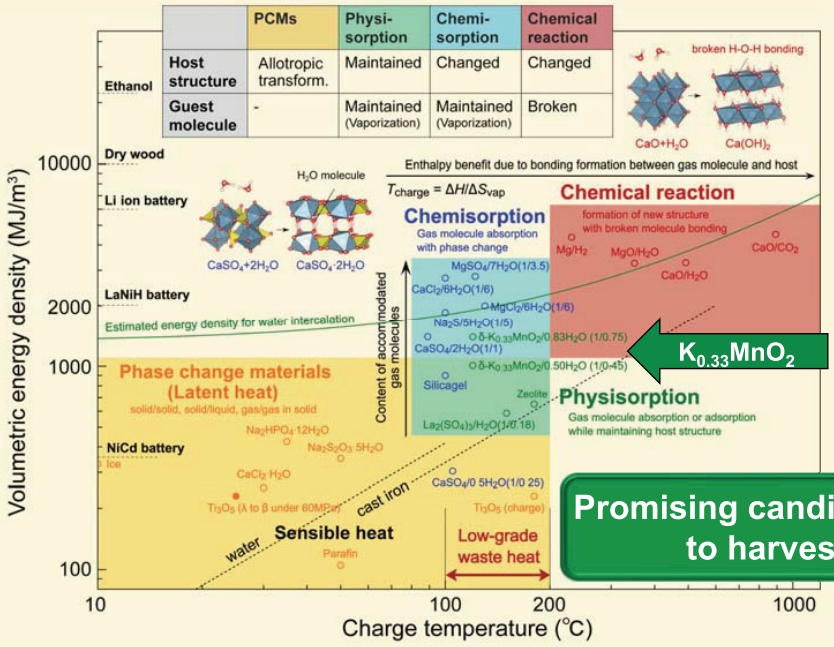


$K_{0.33}MnO_2$

**Versatile properties of $MnO_2$**

- ❖ High energy density
- ❖ Low charge temperature
- ❖ High rate
- ❖ High cyclability
- ❖ Environment friendliness
- ❖ Resourcefulness

**Promising candidate for heat-storage material to harvest low-grade waste heat**

T. Hatakeyama, N. L. Okamoto, H. Li, T. Ichitsubo et al., *Nat. Commun.*, **13**, 1452 (2022).

# Summary

Layered $MnO_2$ is a promising candidate for heat-storage material to harvest low-grade waste heat.

The salient features of the K-containing layered $MnO_2$ are:

❑ It can store/release heat via the **water intercalation mechanism**, in which water molecules in a moist atmosphere are inserted into and removed from the interlayers.

❑ It exhibits an **excellent balance** of various properties required for heat-storage materials:

- ❖ **High energy density: 1000 MJ/m³**
  - ➡ Large entropy gap between water vapor and "ice"
- ❖ **Low charge temperature: 100-160℃**
  - ➡ Suitable for harvesting low-grade waste (solar) heat
- ❖ **High rate & cyclability**
  - ➡ Subtle structural change upon water intercalation
- ❖ **Excellent environmentality & resourcefulness**
  - ➡ Water, oxide & abundant Mn

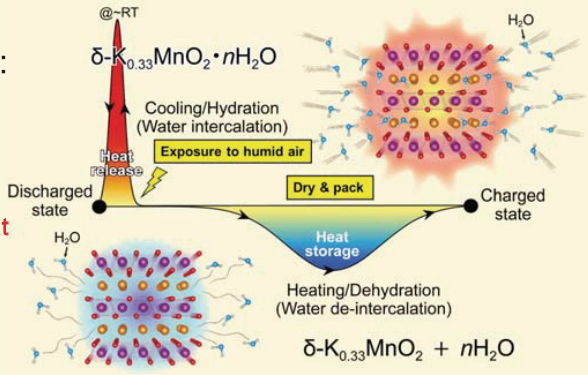

MEMO

# A new AB3-based alloy with reversible hydrogen absorption/desorption reactions and less degradation

T. SATO[1], H. SAITOH[2], R. UTSUMI[2], J. ITO[3], K. OBANA[3], Y. NAKAHIRA[2], D. SHEPTYAKOV[4], T. Honda[5, 6], H. SAGAYAMA[6], S. TAKAGI[1], T. KONO[1], H. YANG[7,8], W. LUO[9], L. LOMBARDO[10], A. ZÜTTEL[7,8], S. ORIMO[6, 11]

[1]Institute for Materials Research, Tohoku University, Japan,
[2]National Institutes for Quantum Science and Technology (QST), Japan
[3]Shibaura Institute of Technology, Japan
[4]Paul Scherrer Institut, Switzerland
[5]J-PARC Center, High Energy Accelerator Research Organization (KEK), Japan
[6]Institute of Materials Structure Science, High Energy Accelerator Research Organization (KEK), Japan
[7]École Polytechnique Fédérale de Lausanne (EPFL) Valais/Wallis, Switzerland
[8]Empa Materials Science and Technology, Switzerland
[9]School of Environmental and Chemical Engineering, Shanghai University, China
[10]Department of Chemistry, Graduate School of Science, Kyoto University, Japan
[11]Advanced Institute for Materials Research (WPI-AIMR), Tohoku University, Japan

E-IMR International Workshop 2024, Nov. 26, 2024

## Today's contents

- Hydrogen storage materials
- Research backgrounds
  (Y, Mg)$Co_3$:
  Reversible hydrogen absorption and desorption reactions
  Narrow hysteresis
  Less degradation up to 100 cycles
  Gravimetric hydrogen density: 1.68 mass% (< 10 MPa)
- Results
  Syntheses
  Hydrogen storage properties (< 10 MPa)
  Crystal structure
- Conclusions

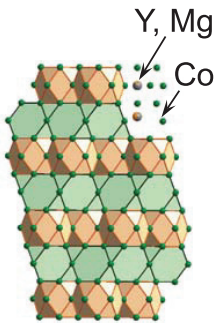


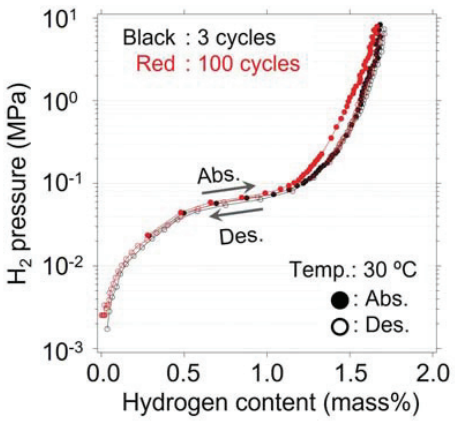

# Hydrogen storage methods

Hydrogen storage as Molecular state

Hydrogen storage as Atomic state

| | Gaseous $H_2$ | Liquid $H_2$ | Hydride |
|---|---|---|---|
| |  |  |  |
| Adv. | Gravimetric density | Volumetric density | Volumetric density |
| DA. | Volumetric density | Temperature | Gravimetric density |
| Ex. |  |  |  |

https://toyota.jp/mirai/gallery/?padid=from_mirai_forexecutive_navi-menu_gallery
https://www.khi.co.jp/news/detail/20220725_1.html
https://www.global.toshiba/jp/news/corporate/2017/06/pr2001.html

E-IMR International Workshop 2024, Nov. 26, 2024

# Hydrogen storage capacity

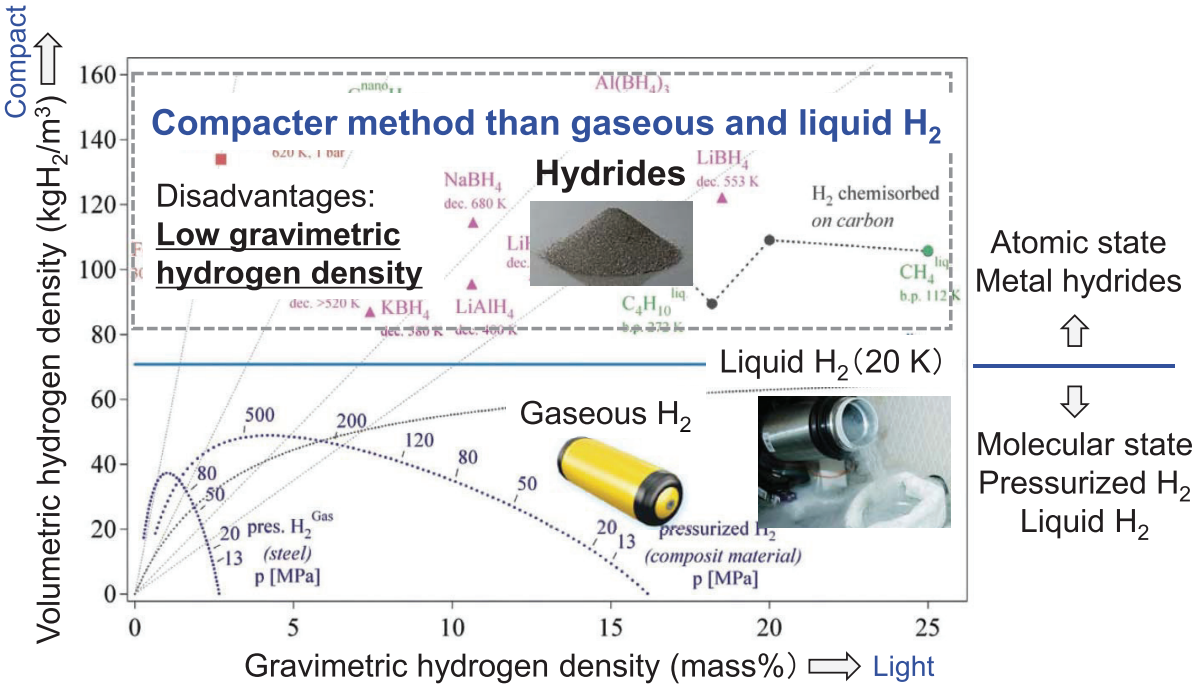


A. Züttel *Mater. Today* **6**, 24–33, (2003).

# Candidates for hydrogen storage materials

## Hydrogen absorption/desorption reactions

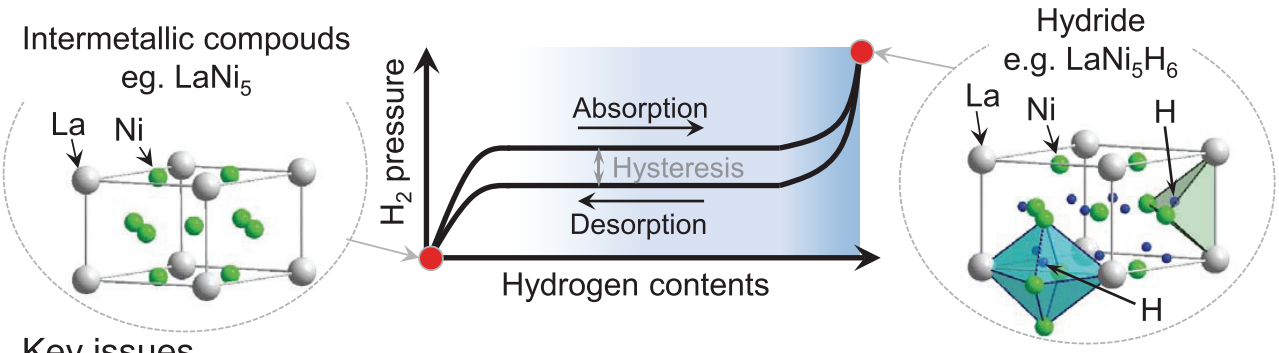


## Key issues

- Low gravimetric hydrogen density ($LaNi_5$ : 1.4 mass%)
- Temperature
- Hysteresis
- Degradation after hydrogen absorption/desorption reactions

## Candidate materials

Intermetallic compounds (e.g. $LaNi_5H_6$), Complex hydrides (e.g. $NaAlH_4$), Ionic hydrides (e.g. $MgH_2$), Porous materials (e.g. MOF-5), etc.



# Intermetallic compounds for hydrogen storage material

Typical intermetallic compounds for hydrogen storage materials: $AB_2$, $AB_3$, $AB_5$

Higher affinity to hydrogen

Lower affinity to hydrogen

| 1 | 2 | 3 | 4 | 5 | 6 | 7 | 8 | 9 | 10 | 11 | 12 | 13 | 14 | 15 | 16 | 17 | 18 |
|---|---|---|---|---|---|---|---|---|---|---|---|---|---|---|---|---|---|
| H | | | | | | | | | | | | | | | | | He |
| Li | | | | | | | | | | | | B | C | N | O | F | Ne |
| Na | Mg | | | | | | | | | | | Al | Si | P | S | Cl | Ar |
| K | Ca | Sc | Ti | V | Cr | Mn | Fe | Co | Ni | Cu | Zn | Ga | Ge | As | Se | Br | Kr |
| Rb | Sr | Y | Zr | Nb | Mo | Tc | Ru | Rh | Pd | Ag | Cd | In | Sn | Sb | Te | I | Xe |
| Cs | Ba | La | Hf | Ta | W | Re | Os | Ir | Pt | Au | Hg | Tl | Pb | Bi | Po | At | Rn |

Component A

Component B

AB$x$ ($x$ = 1–5)

# Our studies on $(Y, Mg)Co_3$ as a hydrogen storage material

- Studies on $YMgNi_4$-based alloys ($\approx AB_2$) for hydrogen storage materials

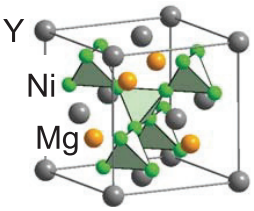


Partial Co-substitution

$(1\text{-}x)YNi_2 + xMgCo_2 \rightarrow (Y, Mg)(Ni, Co)_2$

$YMgNi_4 = (Y, Mg)Ni_2$

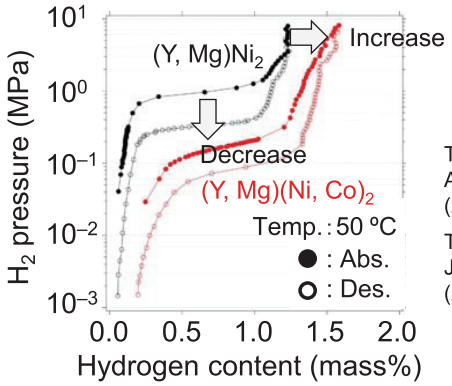


T. Sato et al., ACS Omega, (2020).

T. Sato et al., J. Phys. Chem. C, (2022).

E-IMR International Workshop 2024, Nov. 26, 2024

# Our studies on $(Y, Mg)Co_3$ as a hydrogen storage material

- Studies on $YMgNi_4$-based alloys ($\approx AB_2$) for hydrogen storage materials

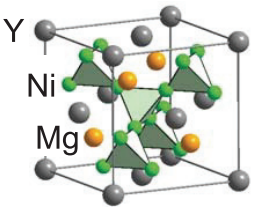


Partial Co-substitution

$(1\text{-}x)YNi_2 + xMgCo_2 \rightarrow (Y, Mg)(Ni, Co)_2$

$YMgNi_4 = (Y, Mg)Ni_2$

Ni replaced by Co

Reaction between $(1\text{-}x)YCo_2 + xMgCo_2$ at 900 °C

- **$(Y, Mg)Co_3$ ($AB_3$-based alloy)**

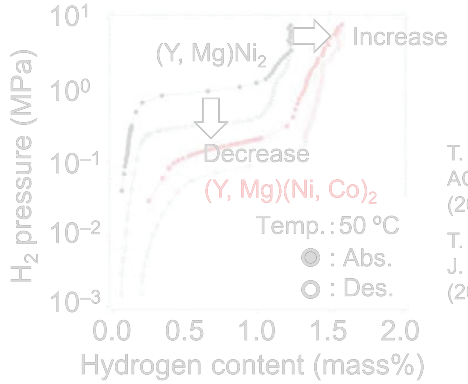


T. Sato et al., ACS Omega, (2020).

T. Sato et al., J. Phys. Chem. C, (2022).

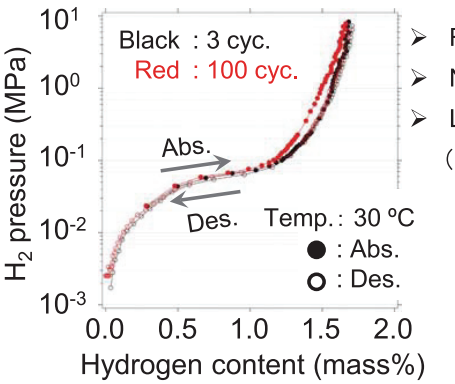


- Reversible
- Narrow hysteresis
- Less degradation (< 100 cycles)

Sato et al., in preparation

# Cycling at 30 ºC (1.2$YCo_2$ + 0.8$MgCo_2$)

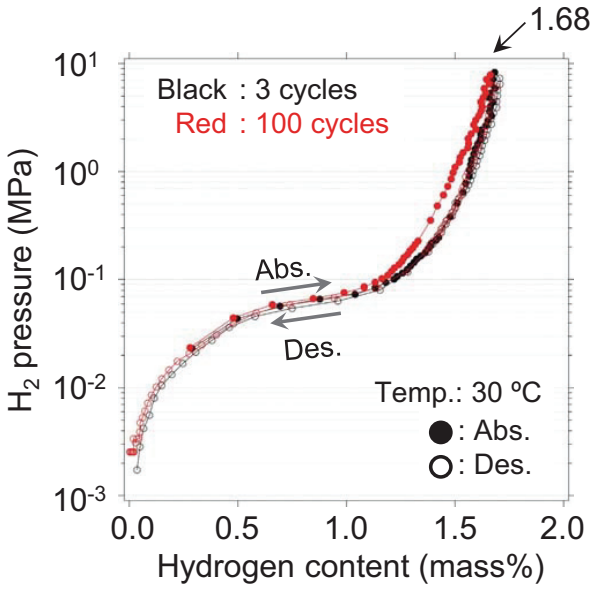


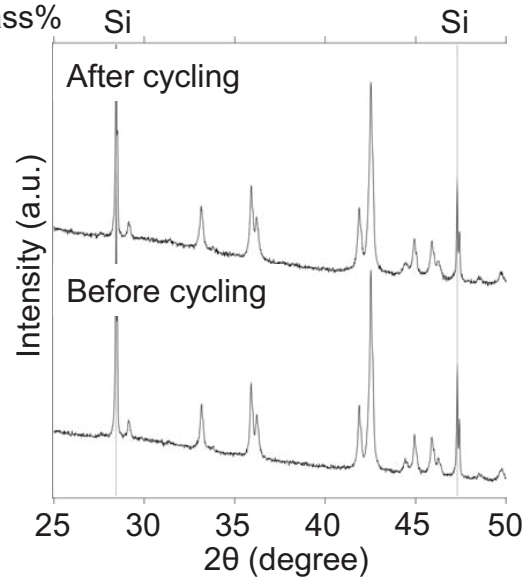


Less degradation after the cycling up to 100 cycles



# Crystal structures (Neutron diffraction in $D_2$ pressure)

$Y_{0.68}Mg_{0.32}Co_{3.00}$ (Trigonal)
a = 4.99719(67) Å, c = 24.16062(533) Å
V = 522.51(18) Å$^3$

118%

$Y_{0.68}Mg_{0.32}Co_{3.00}D_{3.76}$ (Trigonal)
a = 5.27370(64) Å, c = 25.68827(553) Å
V = 618.72(22) Å$^3$

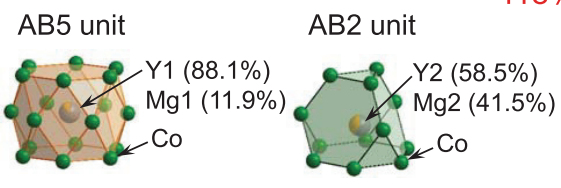


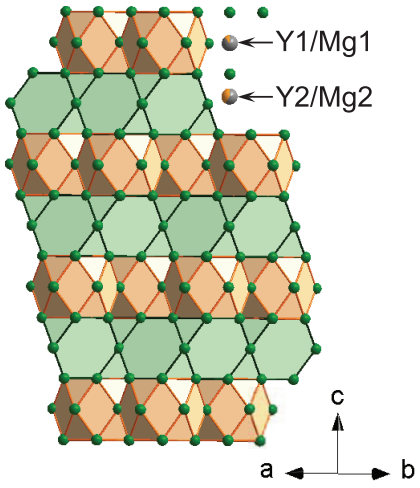


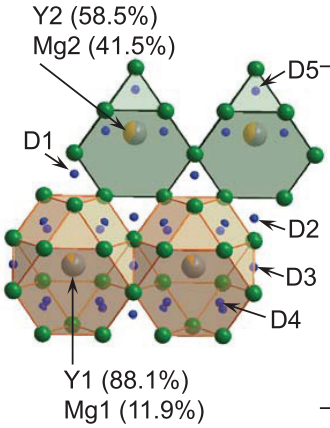


| D atoms (Site, Occu.) | location |
|---|---|
| D1 (6c, 33%) | Inter-unit |
| D2 (6c, 33%) | Inter-unit |
| D3 (9e, 54%) | Intra-unit AB5 unit |
| D4 (18h, 78%) | Intra-unit AB5 unit |
| D5 (18h, 61%) | Intra-unit AB2 unit |

# Conclusions

- **Syntheses**

  $AB_3$ based alloys, $(Y, Mg)Co_3$ : Synthesized from $YCo_2$ and $MgCo_2$
  (Y and Mg ratios: controlled by initial material ratios)

- **Hydrogen storage properties**

  Cycling : Less degradation up to 100 cycles

  Hydrogen storage capacity : 1.68 mass% at 30 ºC

- **Crystal structure**

  Mg atomic positions : The same positions with Y atoms

  D atomic positions : spaces in the inter- and intra- $AB_2$ and $AB_5$ units
  (D atoms: $AB_5$ units > $AB_2$ units)

E-IMR International Workshop 2024, Nov. 26, 2024

# Acknowledgements

This research was supported by

the JST SICORP (grant number JPMJSC1802)

the JSPS KAKENHI (grant numbers 16K06766, 18H05513, 18H05518, 19K05051),

the GIMRT Program of the Institute for Materials Research, Tohoku University

the JST GteX (grant number JPMJGX23H1)

2024.11.26
E-IMR International Workshop

Structure-Controlled Functional Materials Laboratory,
Institute for Mateirals Research, Tohoku University
市坪研究室

# Interface Design for Room-Temperature Rechargeable Magnesium Batteries with Transition Metal Oxide Cathodes

Hongyi Li, Xiatong Ye, Yue Qi,
Norihiko L. Okamoto, Tetsu Ichitsubo

*Institute for Materials Research, Tohoku University*



## Rechargeable batteries with minimal resource constraints

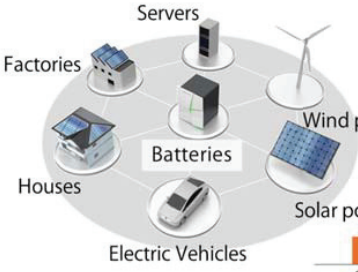


**Demand** for rechargeable batteries

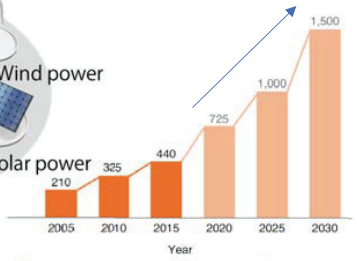


F. Duffner et al, *Nat. Energy* 6, 123 (2021).

**Resource abundance**

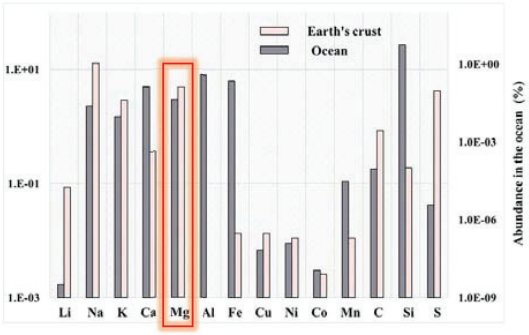


**Commercial Li-ion batteries（LIBs）**

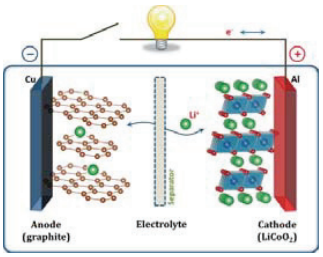


J. B. Goodenough and K. S. Park, *J. Am. Chem. Soc.* 135, 1167 (2013).

Na-ion
Metal-air
Multivalent cation

**What is next?**

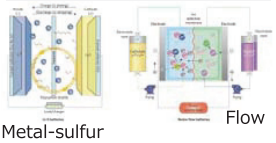

Metal-sulfur
Flow

C. P. Grey and J. M. Tarascon, *Nat. Mater.* 16, 45 (2016).

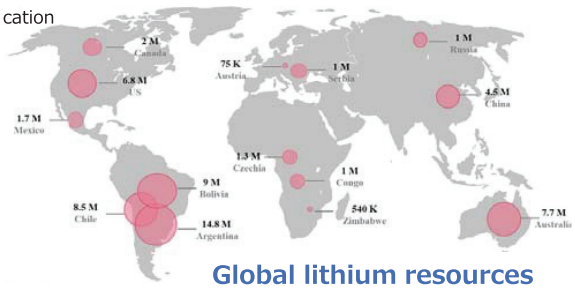


**Global lithium resources**

E. Fan et al, *Chem. Rev.* 120, 7020 (2020)

**Rechargeable Magnesium batteries** are a promising candidate for constructing low-cost large-scale energy storage systems.

## **Prototype** of rechargeable magnesium batteries

D. Aurbach *et al. Nature* **407**, 724 (2000).

| Anode | Electrolyte | Cathode | |
|---|---|---|---|
| Mg metal | $Mg(AlCl_3R)_2$ or $Mg(AlCl_2RR')_2$/THF<br>R = $C_4H_9$, $C_2H_5$ etc. | $Mo_6S_8$ | Aurbach's prototype |

### Deposition morphology
in $Mg(AlCl_2BuEt)_2$/THF

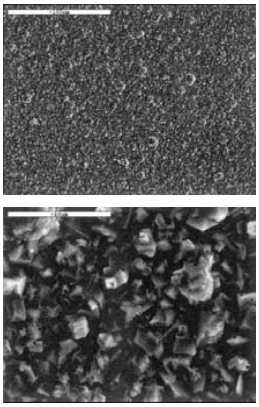

D. Aurbach *et al. J. Power Sources* **97-98**, 269 (2001).

- Non-dendritic
- Reversible Mg deposition and dissolution

### Potential window

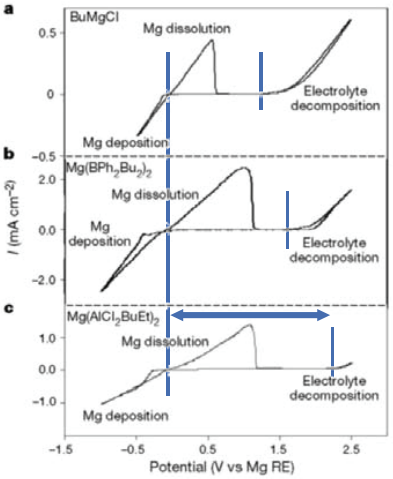


- Up to ~2.4 V

### Intercalation behavior

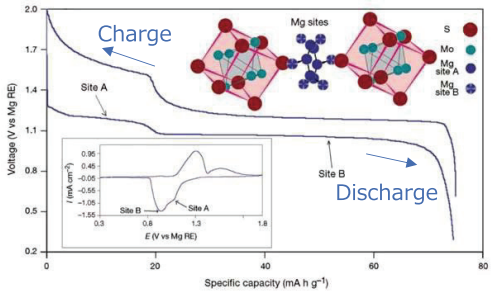


- High reversibility
- Low capacity
- Low operating potential

Energy density (based on active materials)

**$Mg||Mo_6S_8$ ~ 130 Wh kg$^{-1}$**

Lower than LIBs

e.g. $C_6||LiCoO_2$ ~ 386 Wh kg$^{-1}$



## Developing **electrolytes** with reversible Mg anode and high stability

Solvent: THF, DME, Triglyme(G3) etc.

### Cl-contained

- $PhMgCl + AlCl_3$ (APC) — O. Mizrahi et al, *J. Electrochem. Soc.* 155, A103 (2008).
- $Mg[HMDS]_2 - AlCl_3$ — Z. Zhao-Karger et al, *RSC Adv.* 3, 16330 (2013).
- $MgCl_2 - AlCl_3$ (MACC) — R. E. Doe et al, *Chem. Commun.* 50, 243 (2014).
- $MgTFSA_2 - MgCl_2$ — I. Shterenberg et al, *J. Electrochem. Soc.* 162, A7118 (2015).

### Cl-free

- $Mg(BH_4)_2$ — R. Mohtadi et al, *Angew. Chemie Int. Ed.* 51, 9780 (2012).
- $Mg[TFSA]_2$ — B. Gao et al, In Molten Salts Chemistry and Technology, 365–372. John Wiley & Sons, Ltd, 2014.
- $Mg[Al(hfip)_4]_2$ — J. T. Herb et al, *ACS Energy Lett.* 1, 1227 (2016).
- $Mg[B(hfip)_4]_2$ — Z. Zhao-Karger et al, *J. Mater. Chem. A* 5, 10815 (2017).

e.g. $Mg[HMDS]_2$ - $AlCl_3$/THF
Z. Zhao-Karger et al, *RSC Adv.* 3, 16330 (2013).

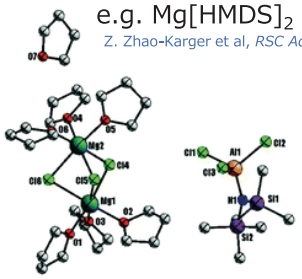

**$[Mg_2Cl_3 \cdot 6THF]^+$** + $[[HMDS]AlCl_3]^-$ $[HMDS]_2AlCl_2$

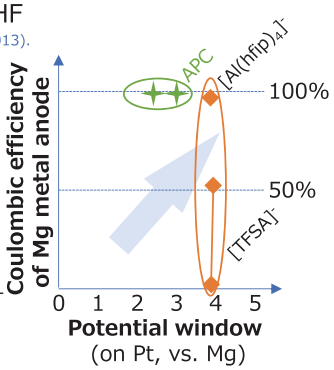


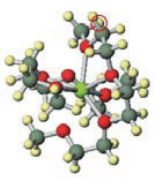

**$[Mg(G3)_2]^{2+}$**

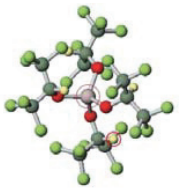

$[Al(hfip)_4]^-$

Solvent-separated ion pair (SSIPs)

- Reversible Mg deposition
- Corrosive • Poor stability

- Good stability
- Easily passivation

## Exploring **cathode materials** with high capacity and potential

### Spinel-type oxides

| | |
|---|---|
| $MgCo_2O_4$ | S. Okamoto, T. Ichitsubo et al, *Adv. Sci.* 2, 1500072 (2015) |
| $ZnFe_2O_4$ | K. Shimokawa, T. Ichitsubo et al, *J. Mater. Chem. A* 7, 12225 (2019) |
| $ZnMnO_3$ | K. Shimokawa, T. Ichitsubo et al, *Adv. Mater.*33, 2007539 (2021) |

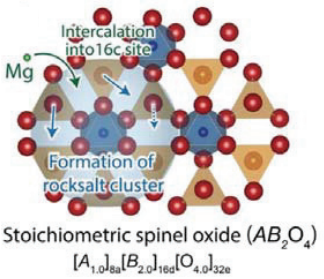


Stoichiometric spinel oxide ($AB_2O_4$)
$[A_{1.0}]_{8a}[B_{2.0}]_{16d}[O_{4.0}]_{32e}$

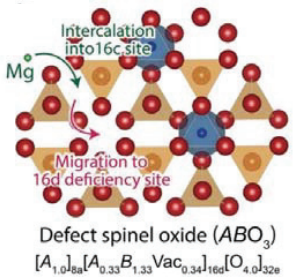


Defect spinel oxide ($ABO_3$)
$[A_{1.0}]_{8a}[A_{0.33}B_{1.33}Vac_{0.34}]_{16d}[O_{4.0}]_{32e}$

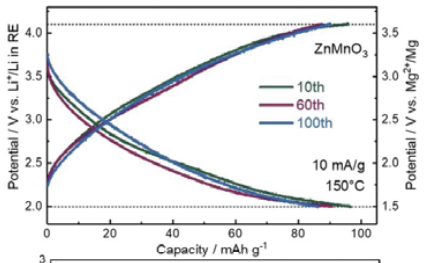


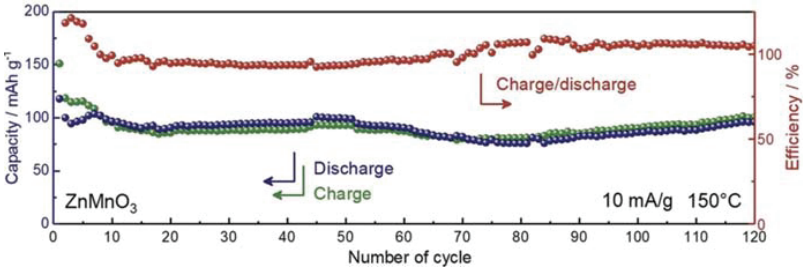


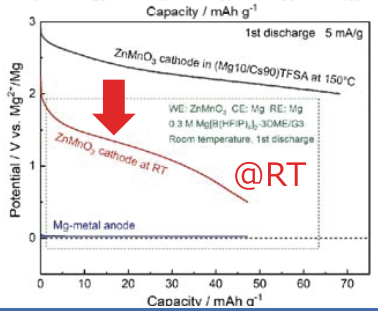


- Reversible $Mg^{2+}$ intercalation has demonstrated at elevated temperature (~ 150℃).
- Operating potential and capacity are markedly decreased at room temperature due to the sluggish $Mg^{2+}$ migration in host structure.



## Suitable host structure for room-temperature operation

### $MnO_2$ polymorphs

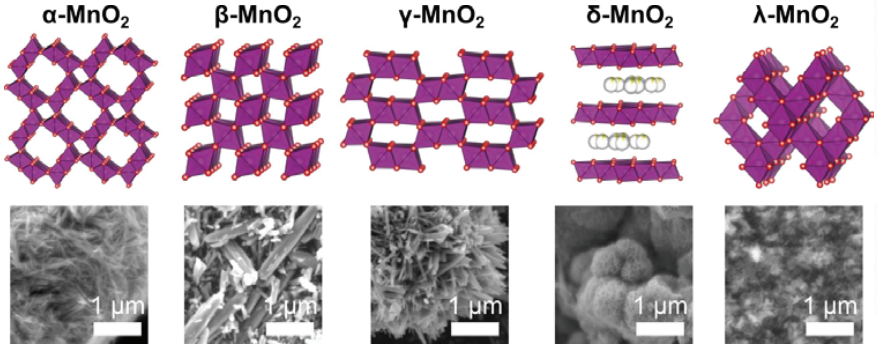


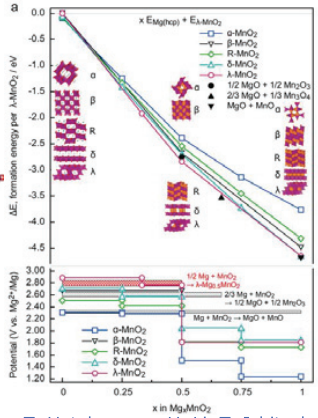


T. Hatakeyama, H. Li, T. Ichitsubo et al, *Chem. Mater.* 33, 6983 (2021).

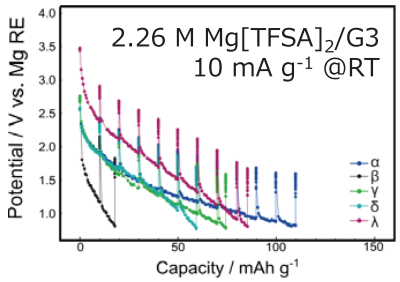


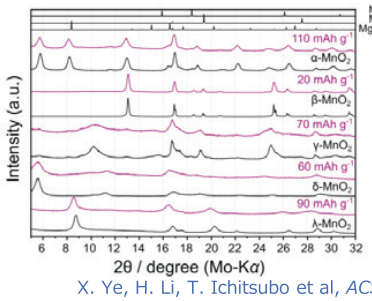


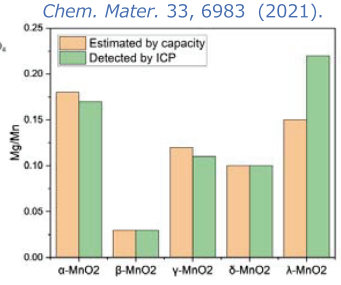


X. Ye, H. Li, T. Ichitsubo et al, *ACS Appl. Mater. Interfaces* 14, 56685 (2022).

α-$MnO_2$ showed a metastable phase transformation pathway for genuine $Mg^{2+}$ intercalation and a reversible capacity over 100 mAh $g^{-1}$ at RT.

## Combination of **α-$MnO_2$** cathode and **SSIP-dominated** electrolytes

### In **CIP-dominated** 2.26 M $Mg[TFSA]_2$/G3 electrolyte

Association

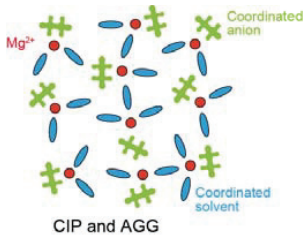


Contact-ion pair (CIP)

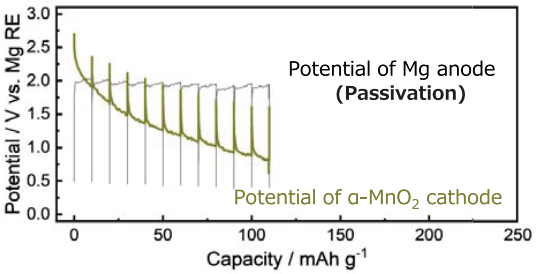



Capacity from Side reactions

Capacity from $Mg^{2+}$ intercalation

**Solvation structure** — **Discharge profile** — **Composition**

### In **SSIP-dominated** 0.3 M $Mg[Al(hfip)_4]_2$/G3 electrolyte

Dissociation

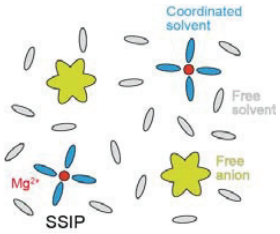


Solvent-separated ion pairs (SSIPs)

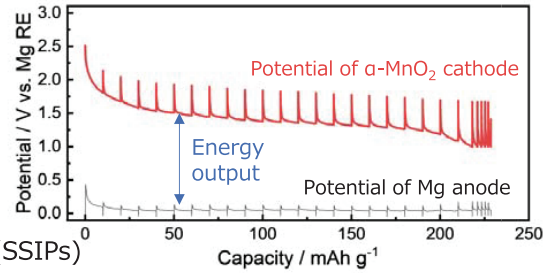



Capacity from Side reactions

Capacity from $Mg^{2+}$ intercalation

Large discharge capacity was obtained without corresponding $Mg^{2+}$ intercalation, suggesting the occurrence of side reactions.



## Clarifying **side reactions** in SSIP-dominated electrolytes

**XRD patterns**

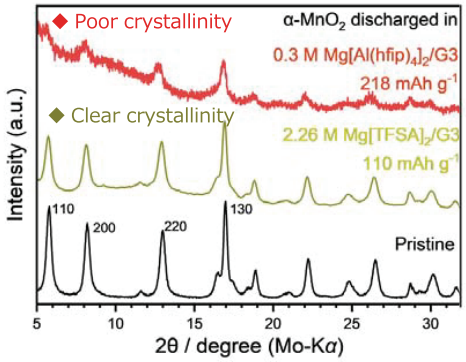


**Soft X-ray emission spectrometry (SXES)**

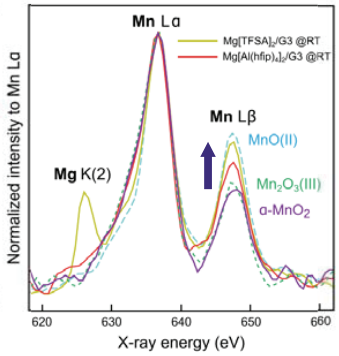


**EDX**

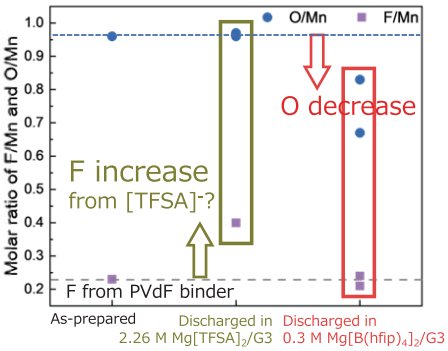


- Significant structural degradation in the SSIP-dominated electrolyte
- $Mn^{4+/2+}$ reduction with $O^{2-}$ release rather than $Mg^{2+}$ insertion ($MnO_2 + 2e^- \rightarrow MnO + O^{2-}$)

**STEM-EDX images**

Discharged in **CIP-dominated electrolyte**

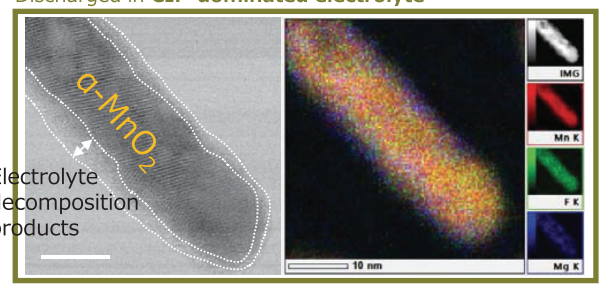


Discharged in **SSIP-dominated electrolyte**

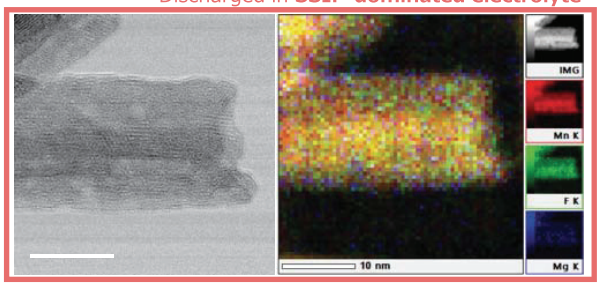


Amorphous surface layer formed on α-$MnO_2$ crystal

Degraded crystallinity with no obvious surface layer

## **Origin of the side reactions** in SSIP-dominated electrolytes

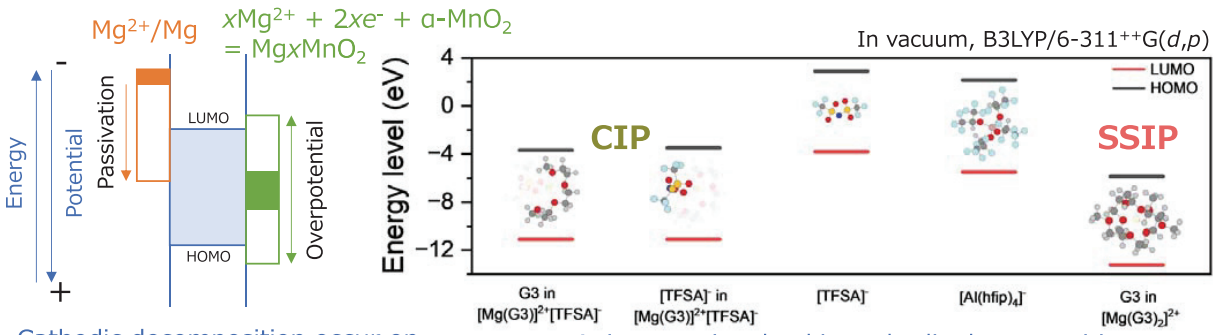


Cathodic decomposition occur on both sides during discharging

Anions are involved in cathodic decomposition in CIP-dominated electrolyte

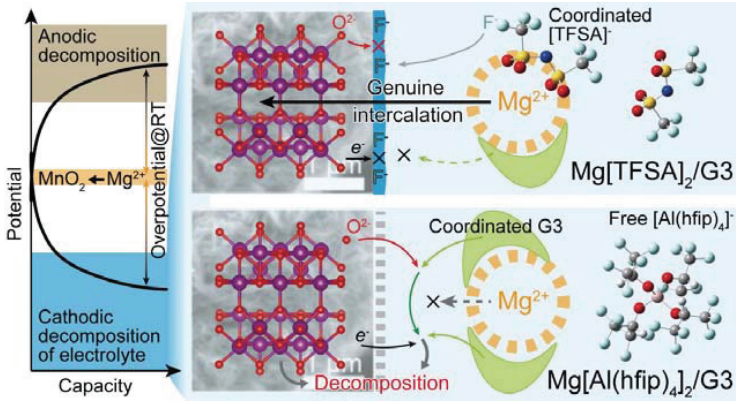


**CIP-dominated** electrolyte

Anion-derived decomposition products protect a-$MnO_2$ but passivate Mg metal

**SSIP-dominated** electrolyte

Solvent-derived decomposition products cause side reactions on a-$MnO_2$ but prevent the passivation on Mg metal.

Interface design is required to use the a-$MnO_2$ cathode in SSIP-dominated electrolytes



## Summary

- The combination of transition metal oxide cathodes (a-$MnO_2$) and SSIP-dominated electrolytes is a promising approach for the construction of room-temperature rechargeable magnesium batteries.
- In SSIP-dominated electrolytes, ether solvent is involved in the cathodic decomposition during discharging, where a stable passivation film is difficult to form to block the electron and oxygen (ion) conduction from the oxide cathodes to the electrolyte.
- These side reactions cause significant structural degradation of the oxide cathode and impede the genuine $Mg^{2+}$ intercalation.
- Preparing an artificial interface on a-$MnO_2$ cathodes is a promising strategy to suppress the side reactions and enhance the performance.

### Acknowledgements

This work is supported by Green Technologies of Excellence (GteX) Program.

GteX Green Technologies of Excellence

Thank you for the kind attention!

MEMO

# Recent advances of silicon crystal for solar cells

Deren YANG

State Key Laboratory of Silicon and Advanced Semiconductor Materials, Zhejiang University

## CONTENTS

01 Si for solar cells

02 Polycrystalline Si

03 Crystalline Si

- 01 Czochralski (Cz) Si
- 02 Oxygen in Cz Si
- 03 Si growth technology

# CONTENTS


01 Si for solar cells

02 Polycrystalline Si

03 Crystalline Si

- 01 Czochralski (Cz) Si
- 02 Impurity (oxygen) in Cz Si
- 03 Si growth technology




# Si solar cells

- In 1954, Si solar cells with the efficiency of ~ 6% were invented in Bell Lab by D. M. Chapin et al.

Gerald Pearson, Daryl Chapin, and Calvin Fuller (left-to-right), inventors of the Bell Solar Battery. Photo credit: NREL, *The Silicon Cell; Turns 50*, with permission from AT&T Bell Labs

SIMPLE AND EFFICIENT—The *Bell Solar Battery* is made of thin, specially treated strips of silicon, an ingredient of common sand. It needs no fuel other than the light from the sun itself. Since it has no moving parts and nothing is consumed to destroyed, the *Bell Solar Battery* should theoretically last indefinitely.

**New Bell Solar Battery Converts Sun's Rays Into Electricity**

**Bell Telephone Laboratories demonstrate new device for using power from the sun**

Scientists have long reached for the secret of the sun. For they have known that it sends us nearly as much energy daily as is contained in all known reserves of coal, oil and uranium.

If this energy could be put to use there would be enough to turn every wheel and light every lamp that mankind would ever need.

Now the dream of the ages is closer to realization. For out of the Bell Telephone Laboratories has come the *Bell Solar Battery*—a device to convert energy from the sun directly and efficiently into usable amounts of electricity.

Though much development remains to be done, this new battery gives a glimpse of future progress in many fields. Its use with transistors (also invented at Bell Laboratories) offers many opportunities for improvements and economies in telephone service.

A small *Bell Solar Battery* has shown that it can send voices over telephone wires and operate low power radio transmitters. Made to cover a square yard, it can deliver enough power from the sun to light an ordinary reading lamp.

Great benefits for telephone users and for all mankind will come from this forward step in harnessing the limitless power of the sun.

BELL TELEPHONE SYSTEM

# PV Installation

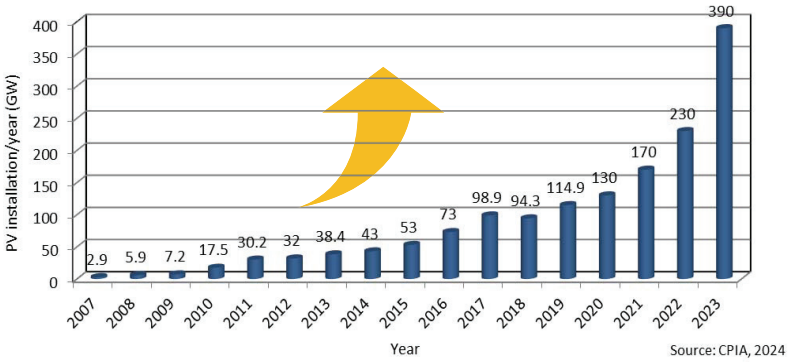


- **Annual Installation: ~ 130**
  - In 2007, 2.9 GW
  - In 2023, 390.0 GW
- **Accumulated installation: ~140**
  - 2007年
  - 2023年, 1546 GW

# Levelized cost

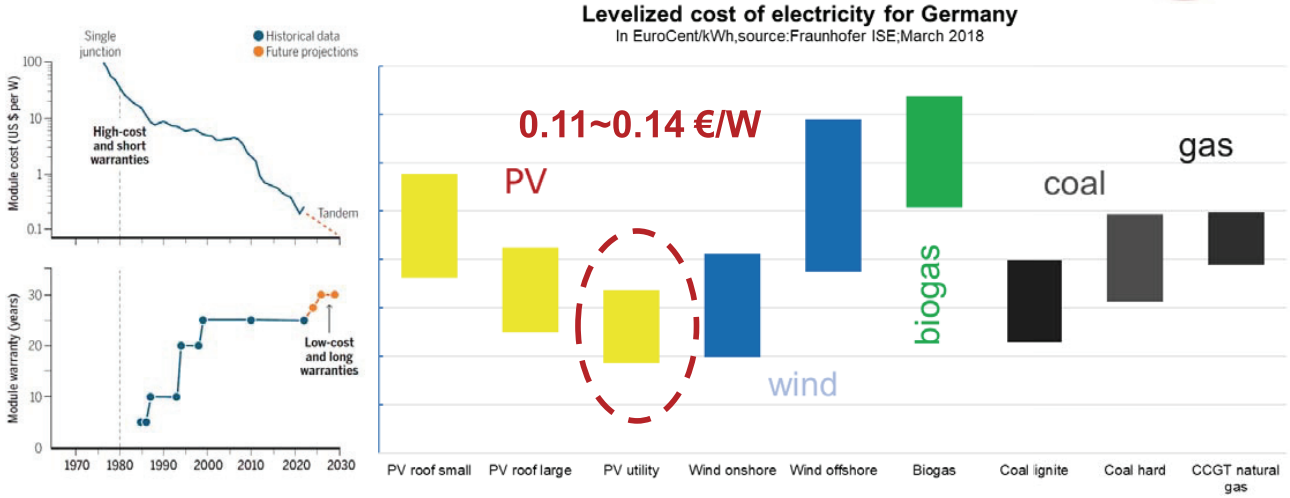


*Aydin et al., Science 383, 162 (2024)*

# Crystal Si for solar cells

- Crystalline Si
- Thin film
  - GaAs
  - CdTe
  - CuInGaSe (CIGS)
- New concept
  - Perovskite
  - Organic




# Si PV industry chain

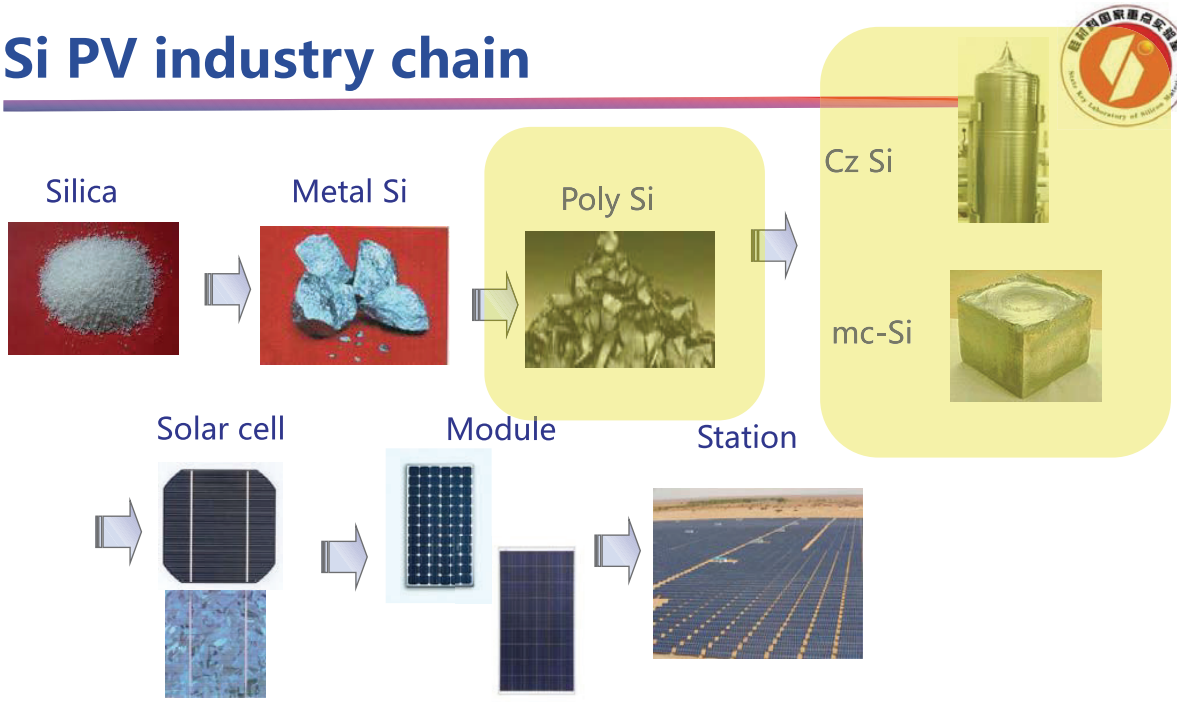

## CONTENTS


01 Si for solar cells

02 **Polycrystalline Si**

03 Crystalline Si

- 01 Czochralski (Cz) Si
- 02 Oxygen in Cz Si
- 03 Si growth technology




## Polycrystalline Si

- Trichlorosilane (TCS) process:
  rod -- (Siemens process)

- Fluidized bed silane (FBS) process:
  granular

# Trichlorosilane (TCS) process

$$Si + 3HCl \xrightarrow{280\sim300^{o}C} SiHCl_3 + H_2$$

$$SiHCl_3 + H_2 \xrightarrow{1100^{o}C} Si + 3HCl$$

- Large production （200 kiloton /line）
- Lowe energy consumption (~50 kilowatt/kg)
- Lower cost (~4 US$/kg)



# Trichlorosilane (TCS) process

- 48 or 72 pair rods
- 600~1000 kg/furnace
- more than 50% for N-type Cz Si
  - Reduction power consumption：37~44 kWh/kg-S
  - Total power consumption：50~56 kWh/kg-Si
  - Si consumption： ~1.08 kg/kg-Si

Source：2024 Development Report on Chinese PV Technology

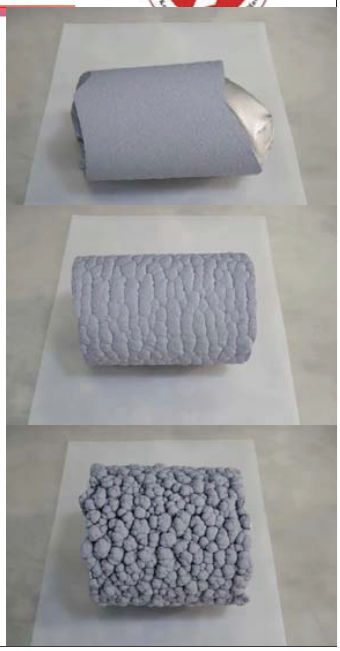

# Fluidized bed silane (FBS) process:

$$2SiHCl_3 \longrightarrow SiH_2Cl_2 + SiCl_4$$

$$3SiH_2Cl_2 \longrightarrow SiH_4 + 2SiHCl_3$$

$$SiH_4 \xrightarrow{800^oC} Si + 2H_2$$

- Simple process
- More lower energy consumption (~40~50% TCS)
- Easy treatment of waste gases
- Continous working process (> 200 days)

**Drawback: fire and explosion**



# Fluidized bed silane (FBS) process:

- Technical challenge:
  - Reduce Si powder
  - Decrease hydrogen conc.
  - Decrease surface metal conc. and carbon conc.

Diameter: ~ 2 mm

# Granular (FBS) Si (2023)

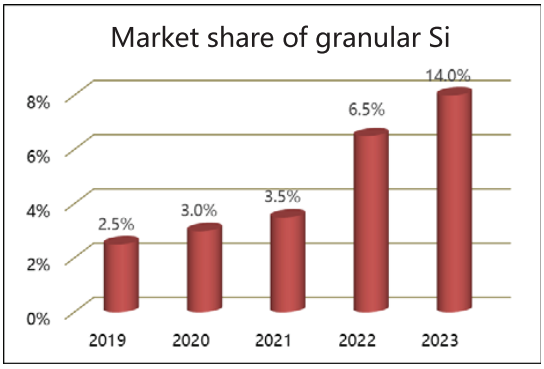


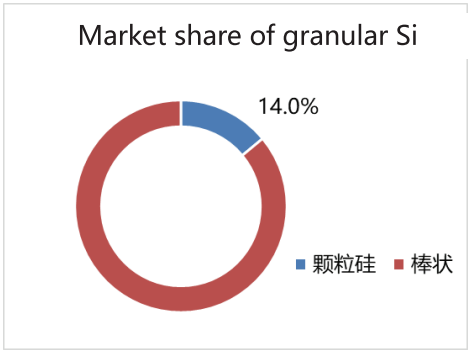




## CONTENTS

01 Si for solar cells

02 Polycrystalline Si

03 **Crystalline Si**

- 01 Czochralski (Cz) Si
- 02 Oxygen in Cz Si
- 03 Si growth technology

# Cz Si and mc-Si

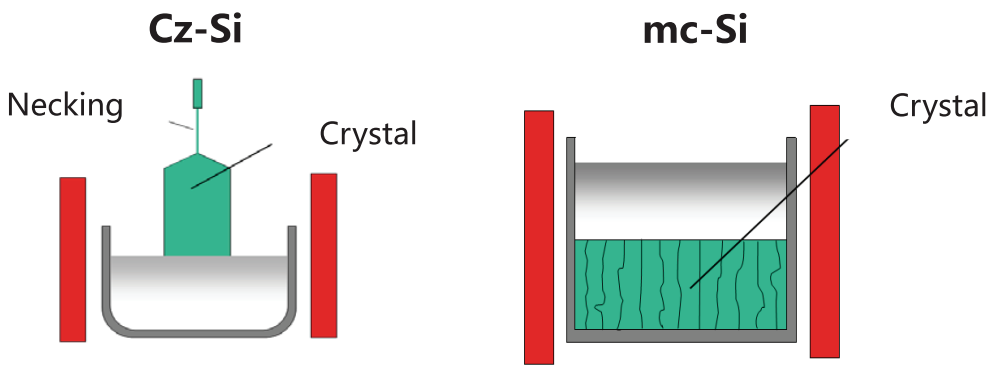


- Cz-Si: better crystal quality, high efficiency, but high cost
- mc-Si: low cost, but inferior quality, low efficiency



# 3.1 Czochralski silicon (Cz-Si)

- In 1917, Polish scientist Czochralski invented.
- In 1952, Teal and Buehler successfully grew Czochralski (Cz) single-crystal silicon.
- In 1958, Dash proposed the dislocation free single-crystal silicon growth process, known as the "necking" technique.

# Progress of Cz Si

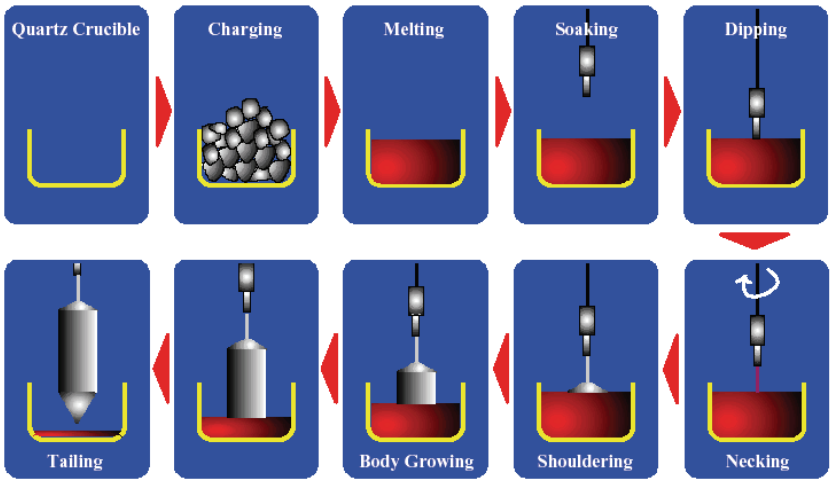




# Cz-Si Growth Technology: RCz-Si

- Recharge Czochralski (RCz-Si)

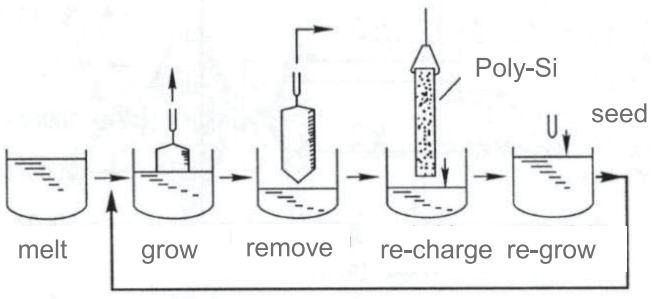


6100 mm（Liton）

# RCz-Si Growth

- Inner diameter of furnace: 1600 ~1800 mm
- Crucible size: 32/36 Inch
- Pulling time: > 500 hours
- Production yield: 6 ~ 7 kg/h
- Power consumption: 23.9 kWh/kg-Si



# Dopant of Cz-Si

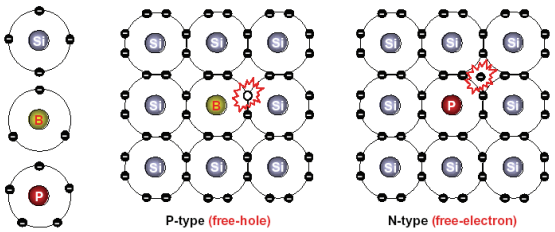



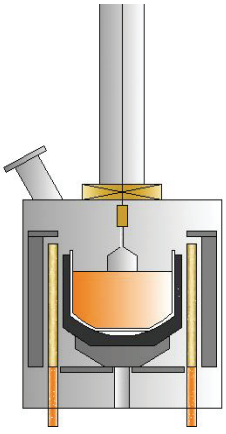

- P type: Ga instead of B
- N type: Sb instead of P

# p-type and n-type Cz Si

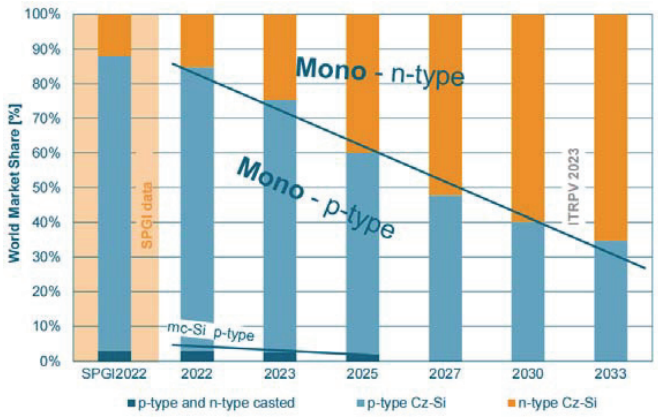


ITRPV 2023 International Technology Roadmap for Photovoltaic

- *p*-type Si will stay mainstream as base for p-PERC technology at least until 2025.
- *n*-type Si expected to dominate after 2026.



# Property of CCz-Si

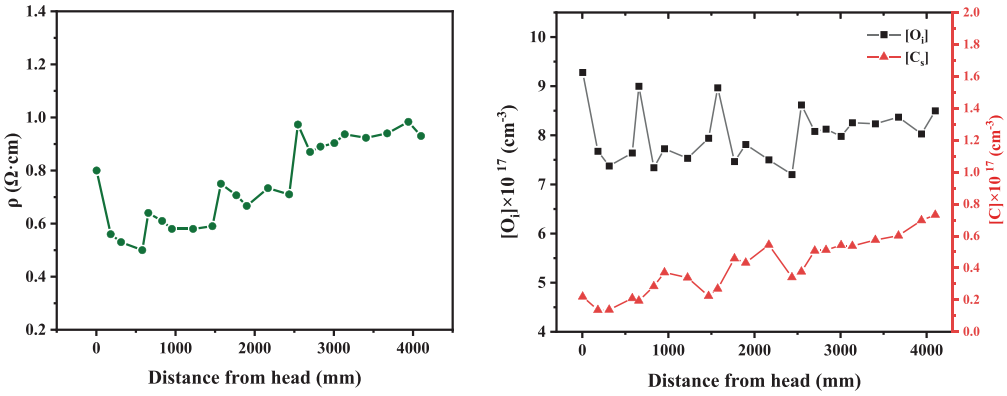


- 8-inch *p*-type CCz-Si，Ga-doped, pulling rate 1.45 mm/min

# Property of CCz-Si

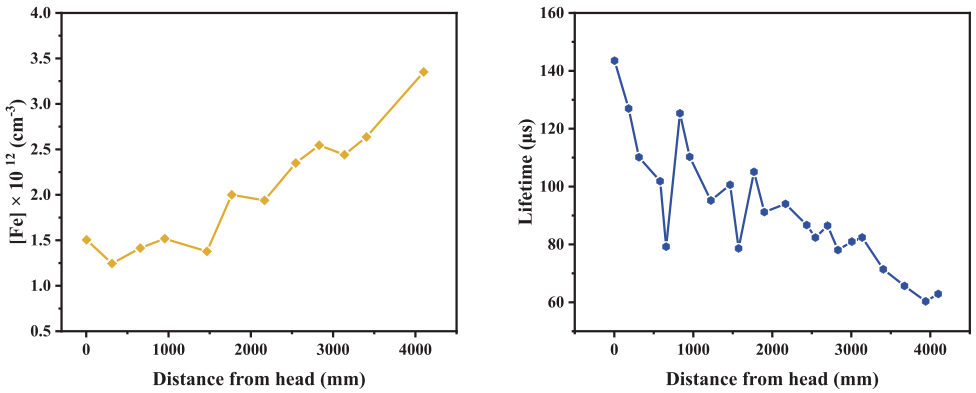


- 8-inch *p*-type CCz-Si，Ga-doped, pulling rate 1.45 mm/min



# Wafer size of Cz-Si (2023)

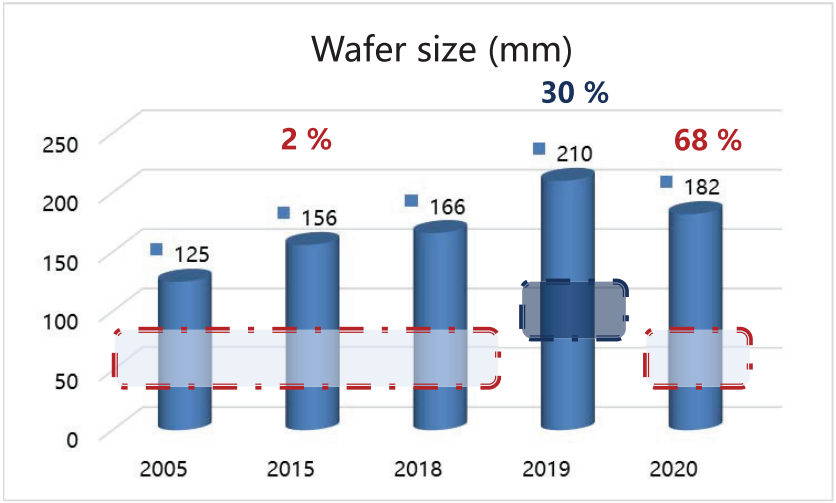


- Compare to M2 wafer, area increase: 12.2%， 80%， 35.1%, respectively

# Wafer thickness of Cz-Si (2023)

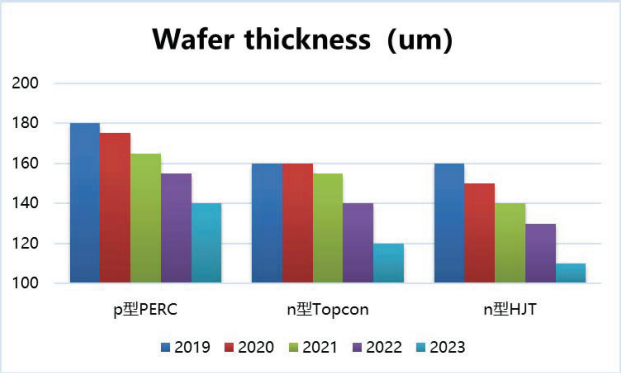


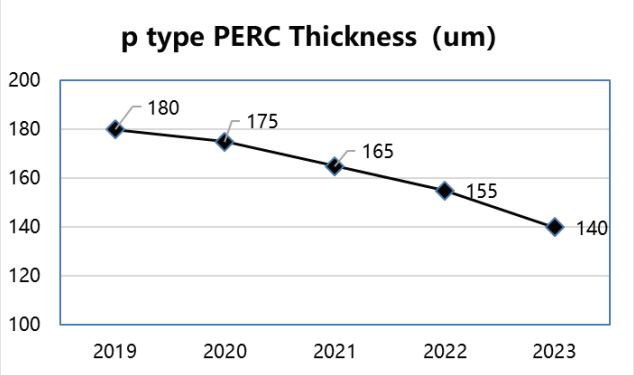




## CONTENTS

01 Si for solar cells

02 Polycrystalline Si

03 **Crystalline Si**

- 01 Czochralski (Cz) Si
- 02 Oxygen in Cz Si
- 03 Si growth technology

# 3.2 Oxygen in Cz-Si

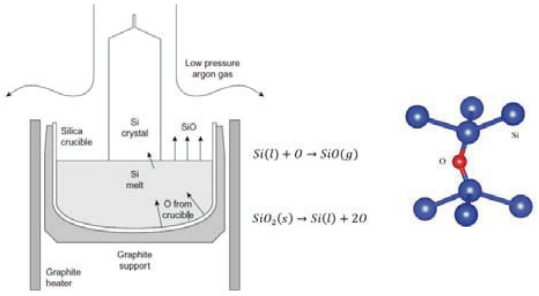





**< 5.5*10$^{17}$ cm$^{-3}$**

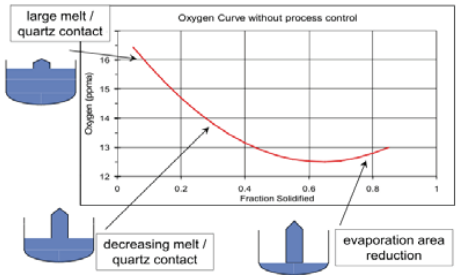


- Oxygen mainly comes from the quartz crucible.
- Interstitial oxygen concentration [$O_i$]=$10^{17}$-$10^{18}$ cm$^{-3}$.
- [$O_i$] distribution: High [$O_i$] in head, low [$O_i$] in tail.

*A. Borghesi et al. Journal of Applied Physics, 1995, 77(9): 4169-4244.*
*M. Tilli et al. Handbook of silicon based MEMS materials and technologies. Elsevier, 2020.*



# Oxygen precipitate (OP)

- Formation temperature: 600~1100℃

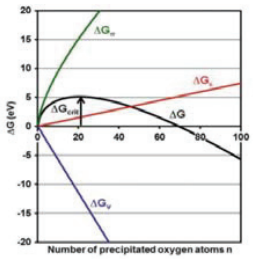


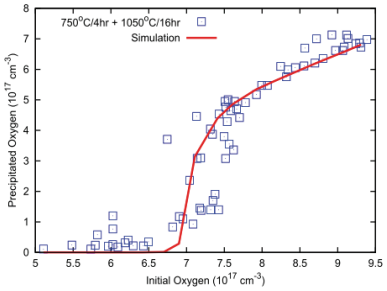


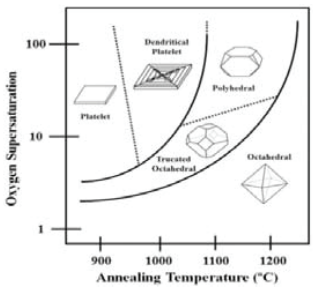


$$(1+\gamma)\ \mathrm{Si}+\chi\mathrm{O}_i+\beta\mathrm{V}\leftrightarrow\mathrm{SiO}\chi+\gamma\mathrm{I}+\varphi_{\mathrm{stress}}$$

*Y. Yoshida et al. Defects and impurities in silicon materials [M]. Springer, 2015.*
*B. Trzynadlowski et al. Journal of Applied Physics, 2013, 114(24): 243508.*
*H. Fujimori. Journal of the Electrochemical Society, 1997, 144(9): 3180-3184.*

# Thermal donor (TD)

- Formation temperature: 300~500℃

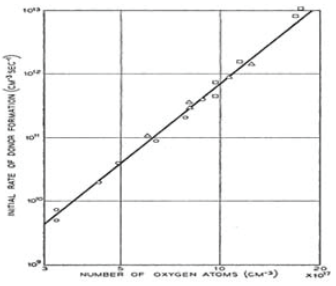


Kaiser et al. Physical Review, 1958, 112(5).

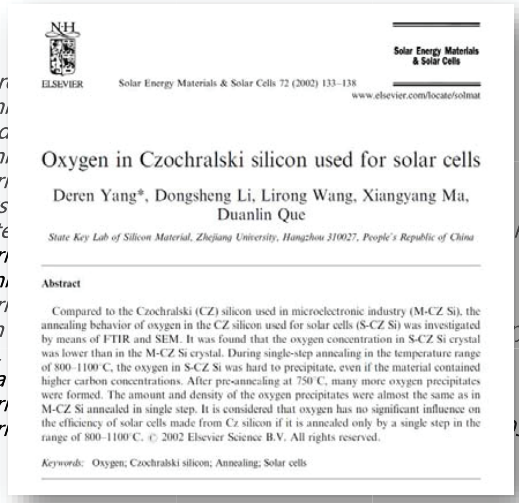

NH ELSEVIER

Solar Energy Materials & Solar Cells

Solar Energy Materials & Solar Cells 72 (2002) 133–138

www.elsevier.com/locate/solmat

Oxygen in Czochralski silicon used for solar cells

Deren Yang*, Dongsheng Li, Lirong Wang, Xiangyang Ma, Duanlin Que

*State Key Lab of Silicon Material, Zhejiang University, Hangzhou 310027, People's Republic of China*

Abstract

Compared to the Czochralski (CZ) silicon used in microelectronic industry (M-CZ Si), the annealing behavior of oxygen in the CZ silicon used for solar cells (S-CZ Si) was investigated by means of FTIR and SEM. It was found that the oxygen concentration in S-CZ Si crystal was lower than in the M-CZ Si crystal. During single-step annealing in the temperature range of 800–1100°C, the oxygen in S-CZ Si was hard to precipitate, even if the material contained higher carbon concentrations. After pre-annealing at 750°C, many more oxygen precipitates were formed. The amount and density of the oxygen precipitates were almost the same as in M-CZ Si annealed in single step. It is considered that oxygen has no significant influence on the efficiency of solar cells made from Cz silicon if it is annealed only by a single step in the range of 800–1100°C. © 2002 Elsevier Science B.V. All rights reserved.

*Keywords:* Oxygen; Czochralski silicon; Annealing; Solar cells

- *Micr*
- *Sem*
- *Solic*
- *Sem*
- *Jour*
- *Phys*
- *Mate*
- *Jour*
- *Sem*
- *Jour*
- *Thin 324,*
- *Acta*
- *Jour*
- *Jour*

*P.600-605*

*ystal Growth*

*39-5044*



# RCz-Si

➢ Difference of Cz-Si and RCz-Si

- Ga-doping
- Fast growth rate（1.5-1.8 mm/min）
- 7~10 ingots using one crucible
- Length: ~ 4.5 m

6100 mm（Liton）

# Thermal donor (TD)

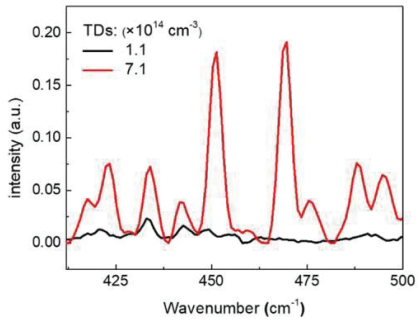


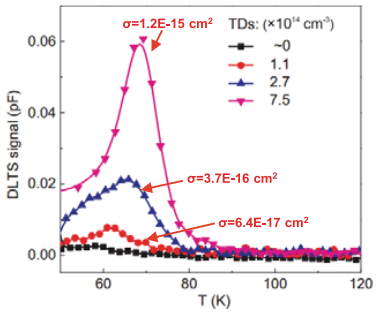


- TDs showing ionization levels at about 0.04–0.07 eV.
- σ of TD-related energy level increase with the increase of TD concentrations.

*Solar Energy Materials and Solar Cells 179 (2018) 17–21*
*Journal of Crystal Growth 630 (2024) 127602*



# Thermal donor

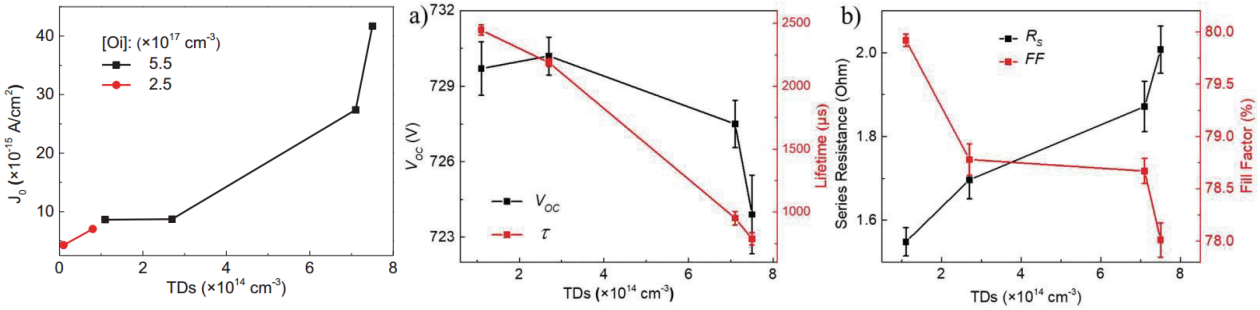


- TDs cause recombination centers. With the increase of [TD] , $J_o$, and $R_s$ increase , $V_{oc}$ and *FF* decrease

*Solar Energy Materials and Solar Cells 179 (2018) 17–21*
*Journal of Crystal Growth 630 (2024) 127602*

# Oxygen precipitates: Electrical

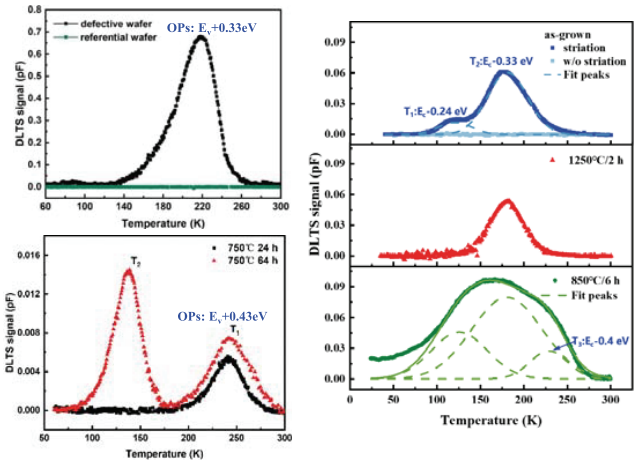


- ***p*-type Cz-Si**
  - $E_T = E_V + 0.33$ eV, $\sigma_p = 2.3\times10^{-15}$ cm$^2$
  - $E_T = E_V + 0.43$ eV, $\sigma_p = 4.3\times10^{-15}$ cm$^2$
- ***n*-type Cz-Si**
  - $E_T = E_C - 0.24$ eV, $\sigma_n = 5.1\times10^{-16}$ cm$^2$
  - $E_T = E_C - 0.4$ eV, $\sigma_n = 8.8\times10^{-15}$ cm$^2$

*Solar Energy Materials and Solar Cells 236 (2022) 111533*



# Oxygen precipitates: PL

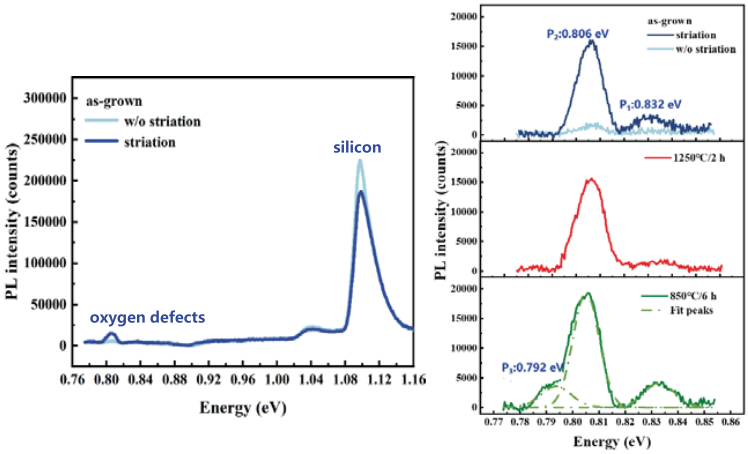


- PL peaks at 20K:
  - OPs: 0.832 eV、0.792 eV
  - OPs induced dislocation: 0.806 eV

# Oxygen precipitates: dislocation

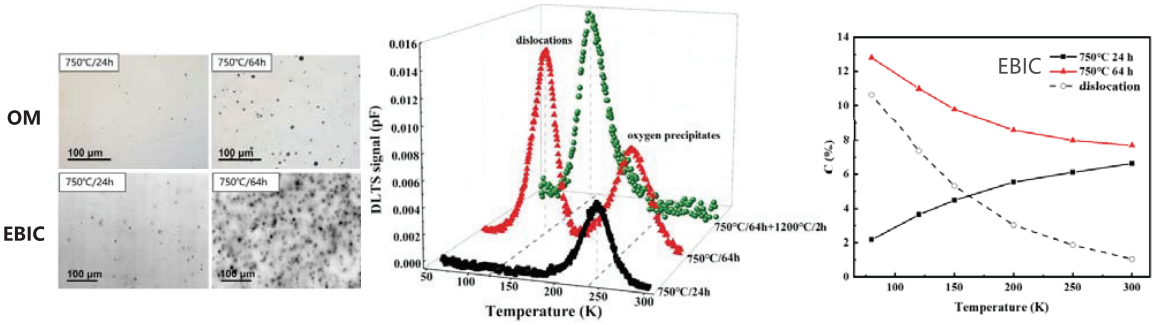


- Dislocations: $E_T = E_V + 0.26$ eV, $\sigma_p = 6.8\times10^{-16}$ cm$^2$.
- Dislocations enhance the defect recombination activity at low temperature.

*Appl. Phys. Express 15, 071004 (2022)*



# Oxygen precipitates: stacking faults

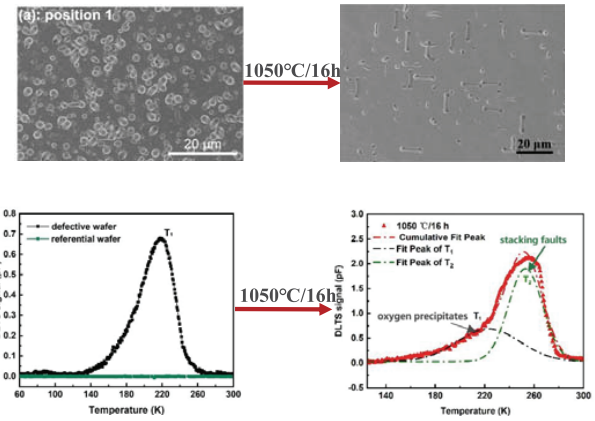


- Stacking faults will be induced during high temperature growth （>1000℃）of oxygen precipitates.
- Stacking faults: $E_T = E_V + 0.42$ eV, $\sigma_p = 1.0\times10^{-14}$ cm$^2$.

*Solar Energy Materials and Solar Cells 236 (2022) 111533*

# Oxygen precipitates: lifetime

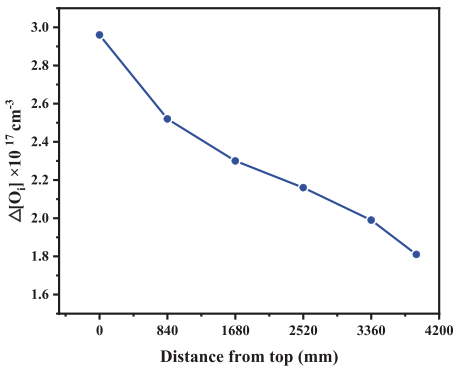


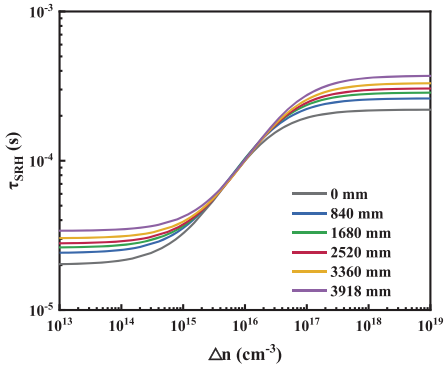




# Oxygen precipitates: cell performance

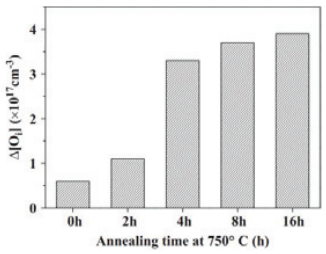


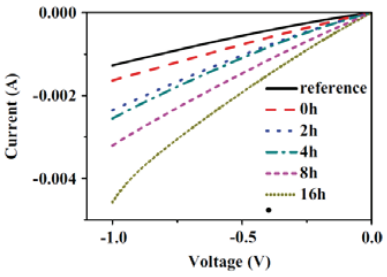


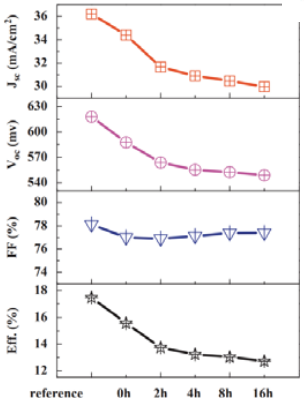


- The higher the OP density, the more pronounced the leakage current.
- OPs reduce the $J_{sc}$, $V_{oc}$, *FF*, and efficiency of solar cells.

*Solar Energy Materials & Solar Cells 95 (2011) 3148–3151*

# Formation of Swirl striations

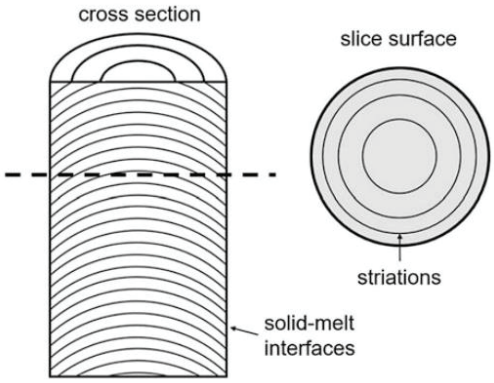


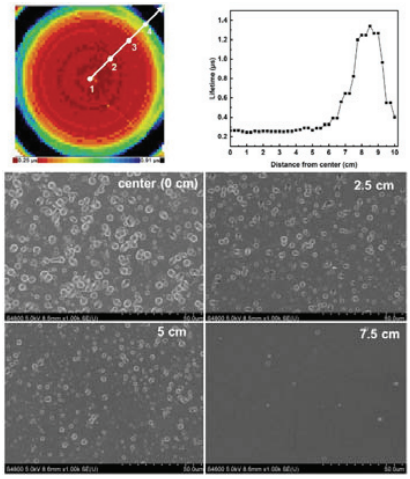


- Oxygen precipitates are the vital component of the striations.

*Solar Energy Materials and Solar Cells 236 (2022) 111533*



# Swirl Striations

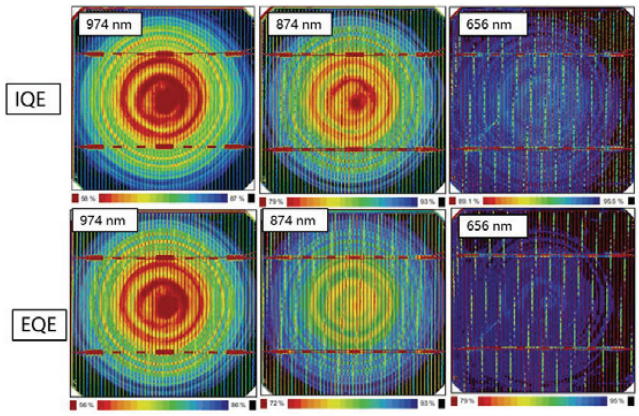


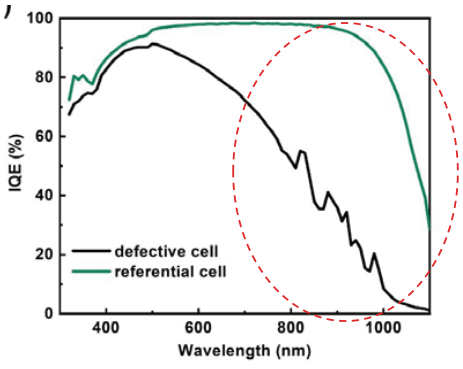


- Swirl defects lead to a decrease in QE, especially in the long wavelength range.

*Solar Energy Materials and Solar Cells 236 (2022) 111533*

# Oxygen precipitates: H passivation

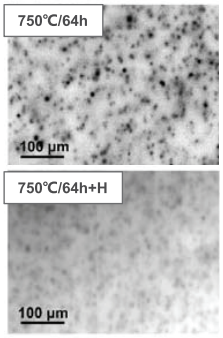


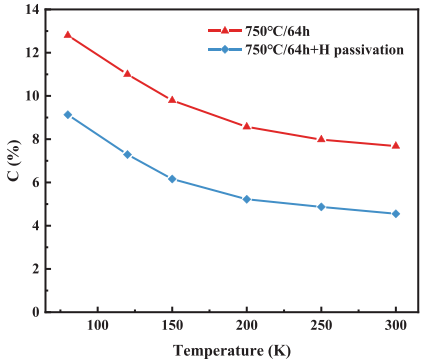


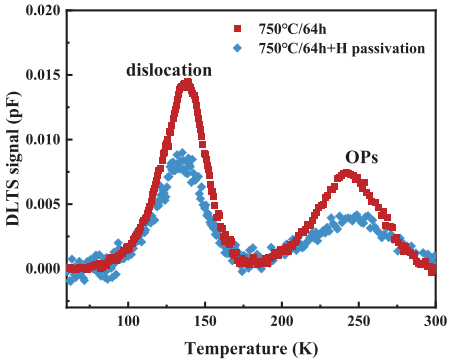


- Hydrogen can successfully passivate about one-third of the oxygen precipitates defect states and about half of the dislocation defect states.

*Appl. Phys. Express 15, 071004 (2022)*



## CONTENTS

01 Si for solar cells

02 Polycrystalline Si

03 **Crystalline Si**

- 01 Czochralski (Cz) Si
- 02 Oxygen in Cz Si
- 03 Si growth technology

# Cz-Si Growth Technology: CCz-Si

➢ Continuous Czochralski (CCz-Si)

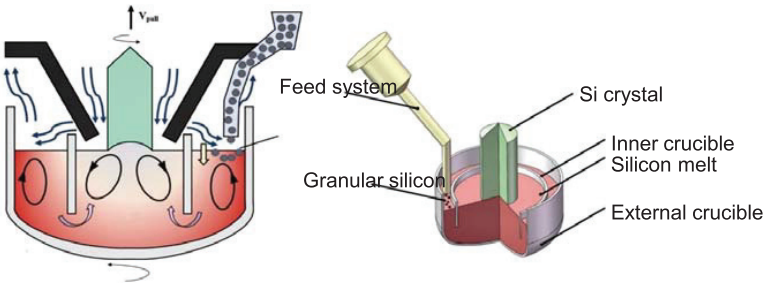


- Better uniformity of resistivity
- Better uniformity of oxygen along with growth direction
- Ingot: 8~10



# Cz-Si Growth Technology: MCz-Si

➢ Magnetic field applied Czochralski (MCz)

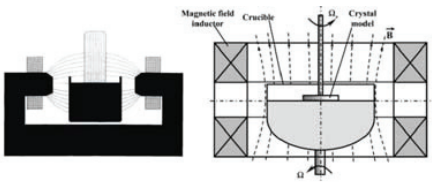


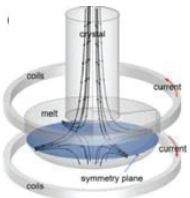


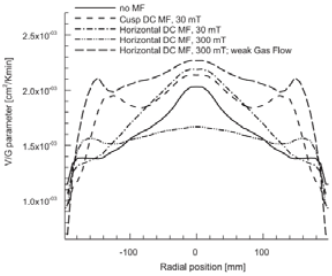


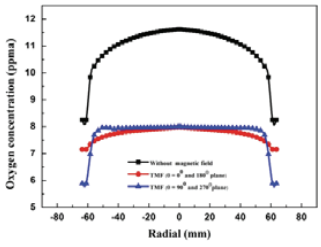


- Restrain the conversion
- Reduce oxygen content

*R. Series et al. Journal of Crystal Growth, 1991, 113(1-2): 305-328.*
*J. Ding et al. Physics of Fluids, 2022, 34(2): 025117.*
*V. Kalaev. Journal of Crystal Growth, 2007, 303(1): 203-210.*
*J. Chen. Journal of Crystal Growth, 2014, 401:813-819.*

# Cast mono Si technology

- **Cast mono:**
  - quasi-single crystalline Si
  - mono-like Si

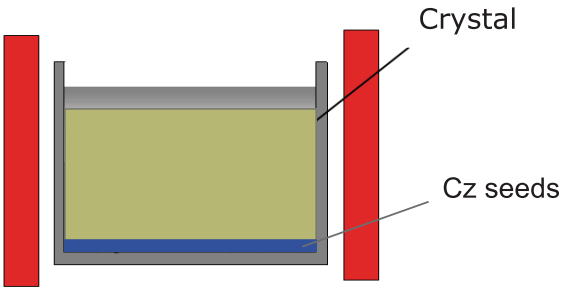


- Inheriting the advantages of both Cz-Si and mc-Si.



# Direct Si wafer

1366 technologies

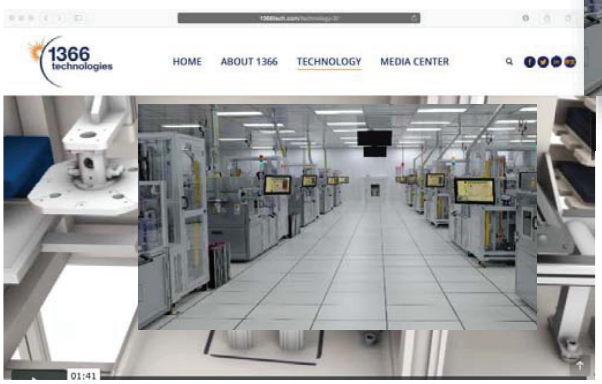


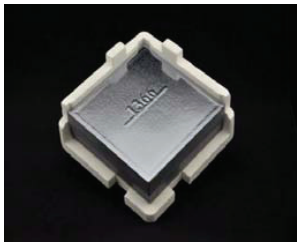

- Poly Si wafer
- Acid texture
- Effi：20.1%

- In 2021，Rebuilt to be Cubic PV，Si based perovskite

*Source：http://1366tech.com*

# Epi-Si wafer

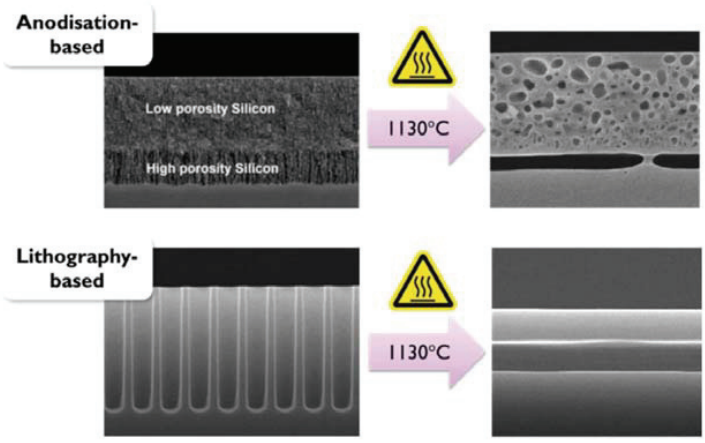


Crystal Solar, SPB, NexWafe

- 50 um
- 效率：20.5%

*J. Govaerts et al，Energy Procedia 77 (2015) 871 – 880*



# Summary

- Cz-Si is currently the mainstream material for PV.
- Oxygen related defects, including thermal donors, oxygen precipitates and swirl defects have a negative impact on the performance of solar cells.
- Except for Cz technique, several new growth techniques of crystal Si have been developed, but have not applied in mass production.

# Thanks

# Electrical and optical detection of the Berry Curvature Multipole in Magnetization Space

Wenzhi Peng[#], Zheng Liu[#], Haolin Pan, Peng Wang, Yulong Chen, Jiachen Zhang, Xuhao Yu, Jinhui Shen, Mingmin Yang, Qian Niu[*], Yang Gao[*], Dazhi Hou[*]

ICQD, School of Emerging Technology, University of Science and Technology of China, Hefei, Anhui 230026, China



## Academic and other activities

Group members @USTC


@USTC, China 2024

Serious Skier

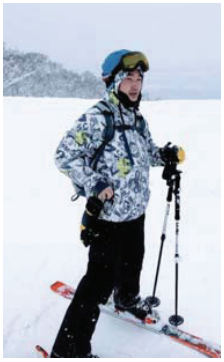

@Niseko 2018

Previous member of IMR


@IMR, Sendai 2017

# Anomalous Hall effect

Dr. E.H. Hall
1855 –1938

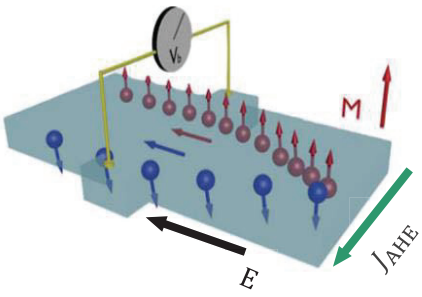


$$\rho_{xy} = R_0 H_z + R_s M_z$$

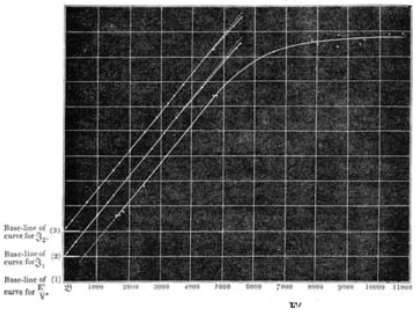

Ph.D. (1881) XVIII. On the "Rotational Coefficient" in nickel and cobalt , Philosophical Magazine Series 5, 12:74, 157-172





Fe(001)

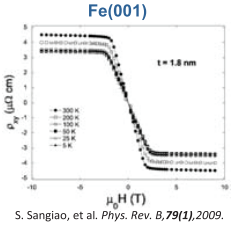

S. Sangiao, et al. *Phys. Rev. B,* ***79(1)****,2009.*

Mn3Sn

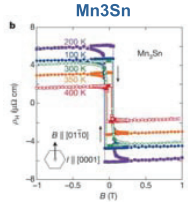

Nakatsuji, S. et.al, Nature 527, 212–215 (2015).

Pt/Co/AlOx

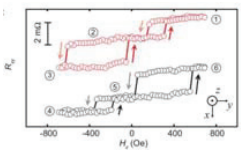

Zhaochu Luo et al.,Science, 363,1435-1439(2019)

FeCo/Gd

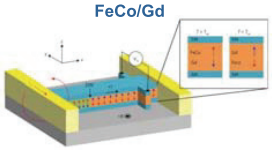

Kim, KJ. et al. Nature Mater 16, 1187(2017)

$Co_3Sn_2S_2$

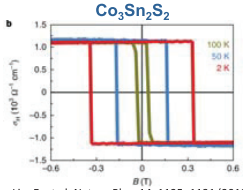

Liu, E. et al. Nature Phys 14, 1125–1131 (2018)

Cr-doped $(Bi,Sb)_2Te_3$

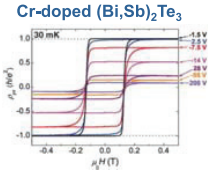

C.Z. Chang, et al. Science,340(6129),2013.

① Orthogonality

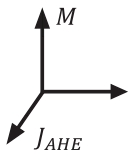


② Linear to M

$$J_{AHE} \propto E \times M$$

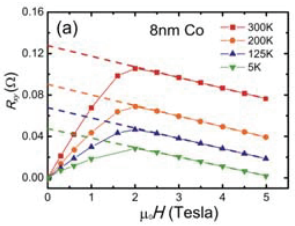


Dazhi Hou *et al.,* JPCM, 24 482001 (2012)

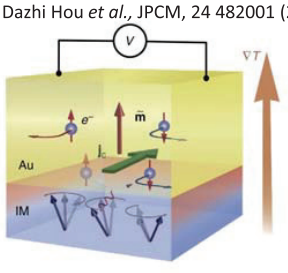


Dazhi Hou *et al.,* Nat. Commun. 7:12265 (2016)

The AHE sensitize to out-of-plane ***M***

AHE signal indued by in-plane M, Why?

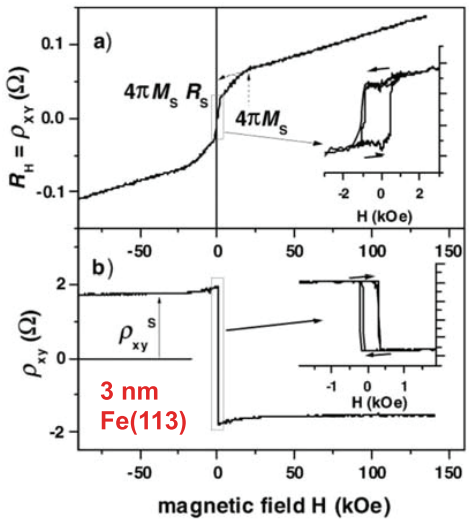


K-J Friedland *et al.*, Physica E 10 442 (2001)

10nm Fe(113)/GaAs(113)

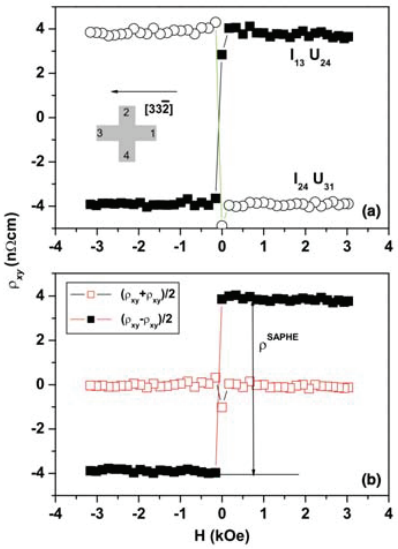


K-J Friedland *et al.*,JPCM,18, 2641 (2006)





Consider the conductivity tensor:

$$\vec{\vec{\sigma}} = \begin{pmatrix} \sigma_{xx} & \sigma_{xy} & -\sigma_{zx} \\ -\sigma_{xy} & \sigma_{yy} & \sigma_{yz} \\ \sigma_{zx} & -\sigma_{yz} & \sigma_{zz} \end{pmatrix}$$

$$\vec{\sigma}_{AHE} = ( \sigma_{yz} , \sigma_{zx} , \sigma_{xy} )$$

① Orthogonality

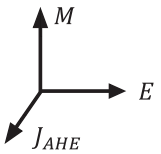


② Linear to M

$J_{AHE} \propto E \times M$

Phenomenological formulation of the AHE

$$\boldsymbol{J}_{\mathrm{AHE}} = \boldsymbol{\sigma}_{\mathrm{AHE}} \times \boldsymbol{E}$$

Assuming a **linear response** of ***M*** in $\sigma_{AHE}$:

$$\boldsymbol{\sigma}_{\mathrm{AHE}} = p\boldsymbol{M} = \sigma_{\mathrm{AHE}}\hat{M}$$

Effectively we have:

$$\boldsymbol{J}_{\mathrm{AHE}} = \sigma_{\mathrm{AHE}}\hat{M} \times \boldsymbol{E}$$

That is why AHE sensitize to out-of-plane ***M***

## Anisotropy of the Anomalous Hall effect

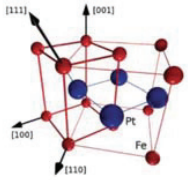


$$\boldsymbol{\sigma} = \sigma_{\parallel}\hat{\mathbf{M}} + \sigma_{\perp}\mathbf{n}$$

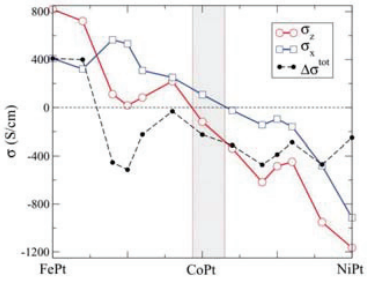


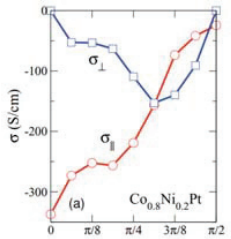


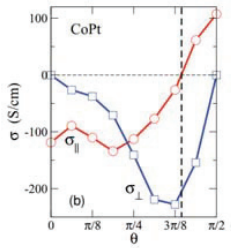


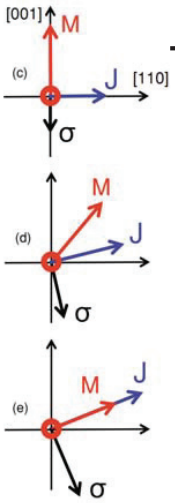


$$\sigma_{\mathrm{AHE}} = pM = \sigma_{\mathrm{AHE}}\hat{M}$$

$$\vec{\sigma}_{AHE} = \begin{pmatrix} p_{11} & p_{12} & p_{13} \\ p_{21} & p_{22} & p_{23} \\ p_{31} & p_{32} & p_{33} \end{pmatrix} \cdot \vec{M}$$

$$\boldsymbol{\sigma} \nparallel \boldsymbol{M} \; or \; \boldsymbol{\sigma} \perp \boldsymbol{M}$$

Eric Roman, Yuriy Mokrousov, and Ivo Souza, PRL 103, 097203 (2009)

Hongbin Zhang, Stefan Blügel, and Yuriy Mokrousov, *Phys. Rev. B* 84, 024401 (2011)



## Recent proposal of the In-plane Anomalous Hall effect



**When symmetry of the ferromagnet is low enough, in-plane AHE can appear**

$$\boldsymbol{\sigma} \parallel \boldsymbol{M}$$

$$\boldsymbol{\sigma} \nparallel \boldsymbol{M} \; or \; \boldsymbol{\sigma} \perp \boldsymbol{M}$$

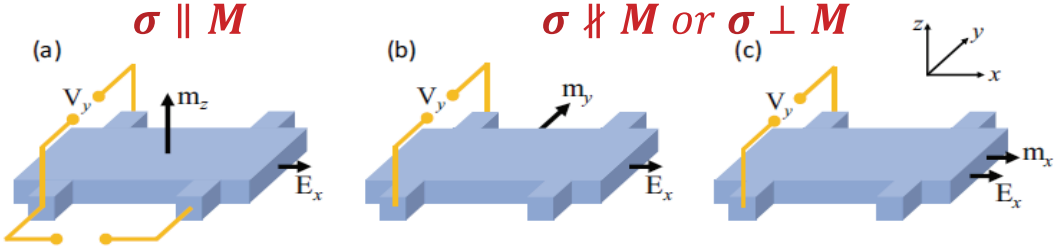


H.X. Tan, Y.Z. Liu, and B.H. Yan. *Phys. Rev. B,**103(21)**,2021*

$$\sigma_{\mathrm{AHE}} = pM = \sigma_{\mathrm{AHE}}\hat{M}$$

$$\vec{\sigma}_{AHE} = \begin{pmatrix} p_{11} & p_{12} & p_{13} \\ p_{21} & p_{22} & p_{23} \\ p_{31} & p_{32} & p_{33} \end{pmatrix} \cdot \vec{M}$$

**But most ferromagnets, e.g. Fe and Ni, are highly symmetric……**

**in-plane AHE seems impossible**

## In-plane AHE as a result of BC multipole in magnetization space

Let us have a close look at the linear dependence:

$$\boldsymbol{\sigma}_{\mathrm{AHE}} = p\boldsymbol{M} = \sigma_{\mathrm{AHE}}\hat{M}$$

The Onsager relation dictates that:

$$\boldsymbol{\sigma}_{\mathrm{AHE}}(-\boldsymbol{M}) = -\boldsymbol{\sigma}_{\mathrm{AHE}}(\boldsymbol{M})$$

So there can also be higher-order terms of $\boldsymbol{M}$ in $\boldsymbol{\sigma_{AHE}}$

$$\sigma_H = \frac{e^2}{h}\sum_n \int \frac{dk_x dk_y}{2\pi}\Omega_n f(E_{n\mathbf{k}})$$

**Multipolar Anisotropy in Anomalous Hall Effect from Spin-Group Symmetry Breaking** Arxiv: 2408.08810

Zheng Liu,[1] Mengjie Wei,[1] Dazhi Hou,[2] Yang Gao,[1,2,*] and Qian Niu[1]
[1]CAS Key Laboratory of Strongly-Coupled Quantum Matter Physics, and Department of Physics, University of Science and Technology of China, Hefei, Anhui 230026, China
[2]ICQD, Hefei National Laboratory for Physical Sciences at Microscale, University of Science and Technology of China, Hefei, Anhui 230026, China
(Dated: August 19, 2024)

**Berry curvature multipole in magnetization space**

$$\sigma^i_{\mathrm{AHE}} = p^{(1)}_{ii_1}P^{(1)}_{i_1} + \sum_{N\geq 3}^{odd} p^{(N)}_{ii_1i_2\cdots i_N}P^{(N)}_{i_1i_2\cdots i_N}$$

TABLE I. The Hall-type current due to the multipole of the Berry curvature in the momentum and magnetic-order space.

| | in momentum space | in magnetic-order space |
|---|---|---|
| Monopole $c_i$ | $\boldsymbol{J} = \boldsymbol{E}\times\boldsymbol{c}$ [6] | Zero |
| Dipole $p_{ij}$ | $\boldsymbol{J} = \tau\boldsymbol{E}\times\boldsymbol{p}\cdot\boldsymbol{E}$ [62] | $\boldsymbol{J} = \boldsymbol{E}\times\boldsymbol{p}\cdot\hat{\boldsymbol{M}}$ |
| Quadrupole $q_{ijk}$ | $\boldsymbol{J} = \tau^2\boldsymbol{E}\times\boldsymbol{q}\cdot\boldsymbol{EE}$ [63, 64] | Zero |
| Octupole $o_{ijk\ell}$ | $\boldsymbol{J} = \tau^3\boldsymbol{E}\times\boldsymbol{o}\cdot\boldsymbol{EEE}$ [64] | $\boldsymbol{J} = \boldsymbol{E}\times\boldsymbol{o}\cdot\hat{\boldsymbol{M}}\hat{\boldsymbol{M}}\hat{\boldsymbol{M}}$ |



## How to imagine the multipolar structure of Berry curvature in M-space?

Dipole

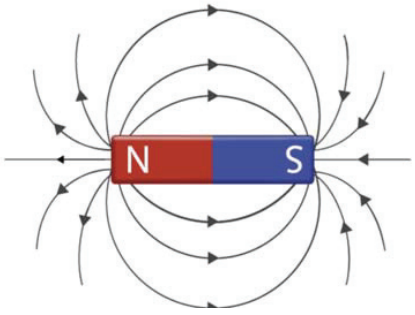


Octupole

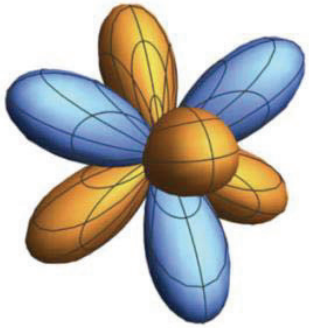

$$\sigma^i_{\mathrm{AHE}} = \underbrace{p^{(1)}_{ii_1}P^{(1)}_{i_1}}_{\text{Dipole}} + \underbrace{\sum_{N\geq 3}^{odd} p^{(N)}_{ii_1i_2\cdots i_N}P^{(N)}_{i_1i_2\cdots i_N}}_{\text{Higher-order poles}}$$

cubic FM, e.g. Fe, as example:

$$\sigma^i_{\mathrm{AHE}} = \alpha\hat{M}_i + \beta\hat{M}_i^3 \text{ + high-order poles}$$

## Let us reconsider the AHE in Fe:

$$\sigma^{i}_{\mathrm{AHE}} = \alpha\hat{M}_i + \beta\hat{M}_i^3 + \text{high-order poles}$$

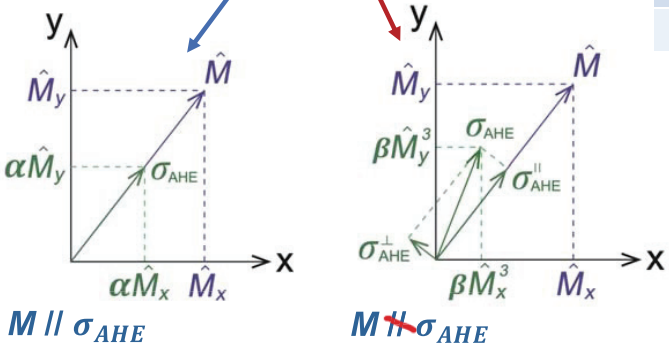


$M \parallel \sigma_{AHE}$ $M \nparallel \sigma_{AHE}$

| $M$ | $(M_x^3, M_y^3, M_z^3)$ | alignment between $M$ and $(M_x^3, M_y^3, M_z^3)$ |
|---|---|---|
| (001) | (001) | Collinear |
| (111) | (111) | Collinear |
| (103) | (1,0,27) | Non-collinear |
| (112) | (118) | Non-collinear |

**Practical design for the in-plane AHE measurement in Fe**

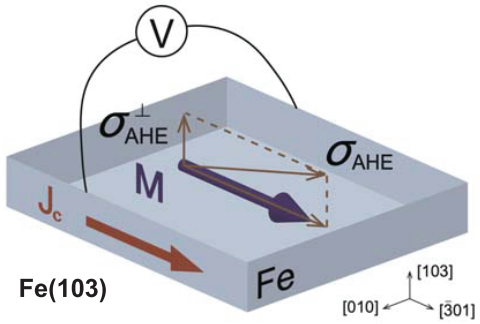






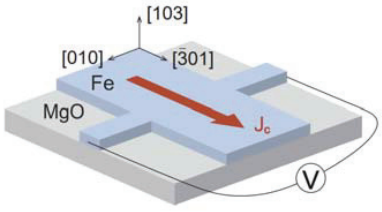


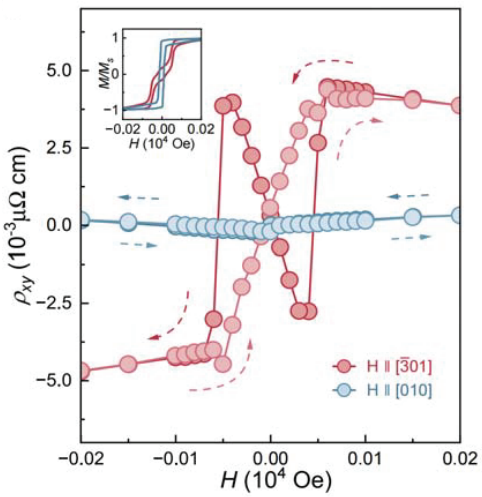


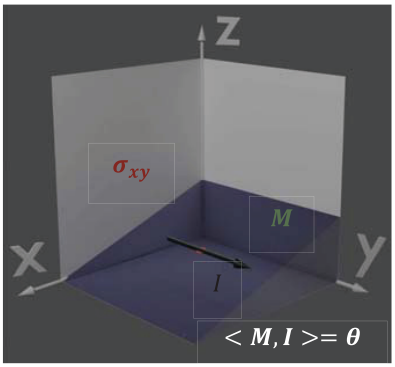


Wenzhi Peng et al., arXiv:2402.15741 (2024)

## In-plane AHE in 100-nm Fe(103) film: high magnetic field dependence

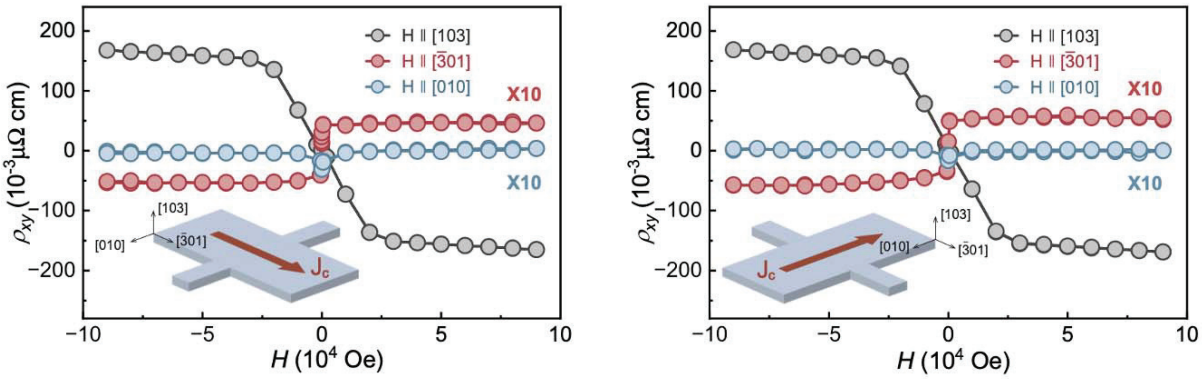


**Excluding the trial origin of the AHE by tilting out-of-plane *M***

Wenzhi Peng et al., arXiv:2402.15741 (2024)



## In-plane AHE in 80nm Ni(111)/MgO(111)

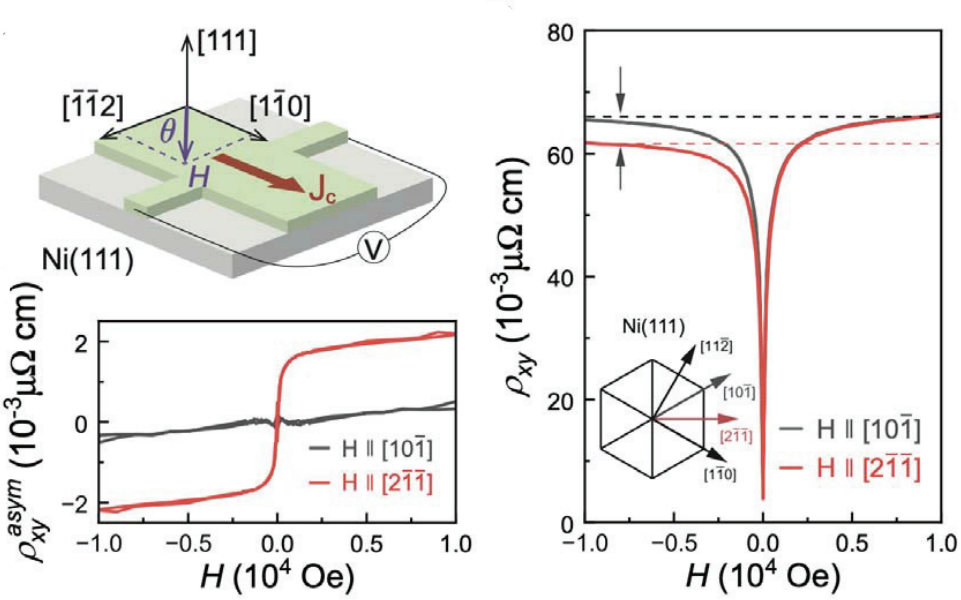


Wenzhi Peng et al., arXiv:2402.15741 (2024)

## Fe(001) @|H| = 90000 Oe

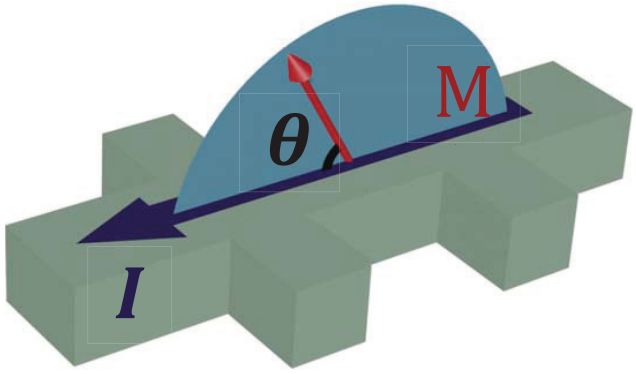


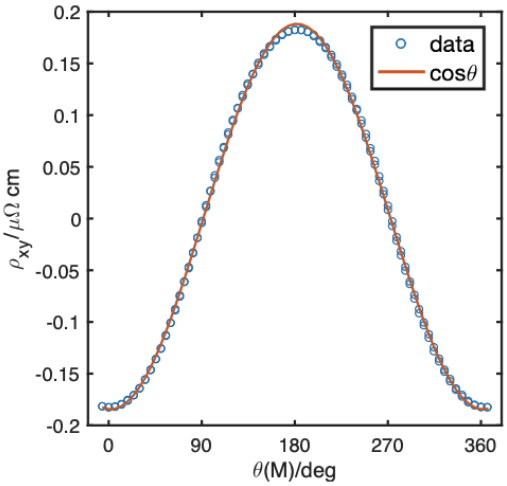






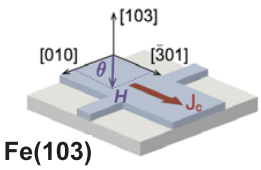


Fe(103)

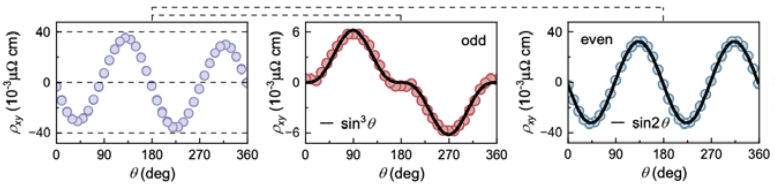


$$|\sigma^{\perp}_{\mathrm{AHE}}|_{\mathrm{Fe(103)}} = \frac{6}{25}\beta_{\mathrm{Fe}}\sin^3\theta$$

$$\sigma^{i}_{\mathrm{AHE}} = \alpha\hat{M}_i + \beta\hat{M}_i^3$$

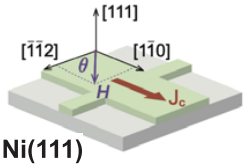


Ni(111)

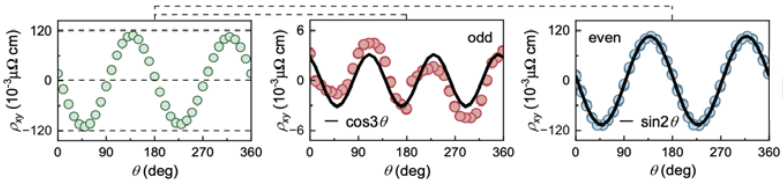


$$|\sigma^{\perp}_{\mathrm{AHE}}|_{\mathrm{Ni(111)}} = \frac{\sqrt{2}}{6}\beta_{\mathrm{Ni}}\cos(3\theta)$$

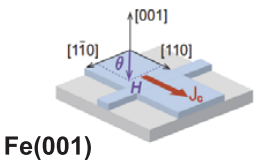


Fe(001)

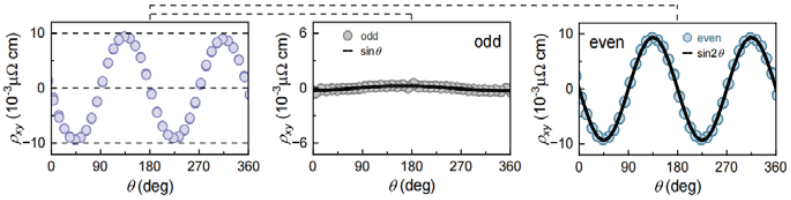


No in-plane AHE

Wenzhi Peng et al., arXiv:2402.15741 (2024)

$Co_3Sn_2S_2$

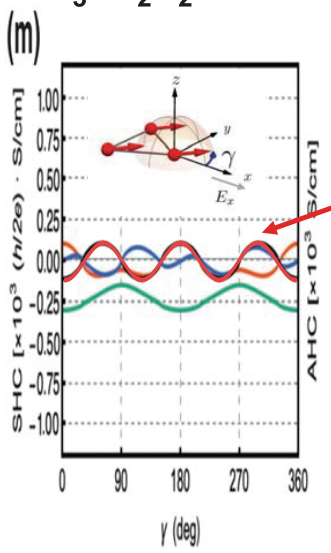


A. Ozawa,K. Kobayashi, K. Nomura, PRA,21, 014041 (2024)

$Fe_3Sn_2$

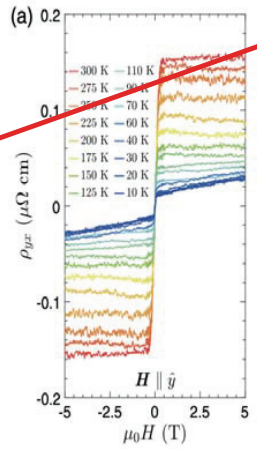


$\rho_{AHE} = A\cos(3\phi)$

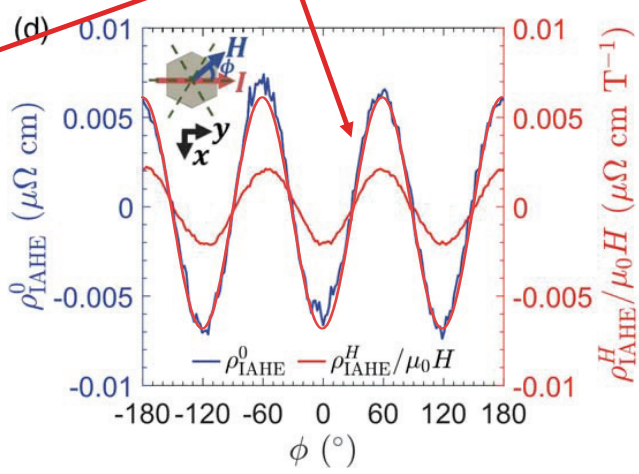


Lujunyu Wang et. al, Phys. Rev. Lett. 132, 106601 (2024)





$$\sigma^i_{\mathrm{AHE}} = \alpha \hat{M}_i + \beta \hat{M}_i^3$$

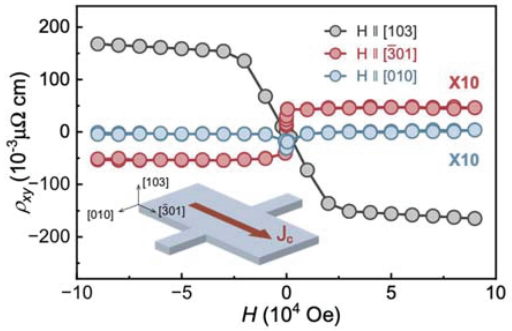


$\alpha = 840.682\ \Omega^{-1}cm^{-1}$

$\beta = -136.811\ \Omega^{-1}cm^{-1}$

in Fe

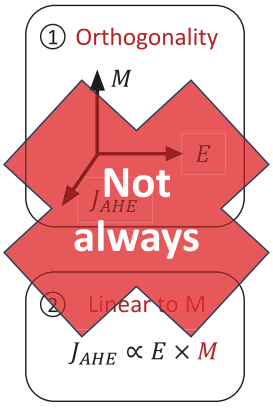


Features of the Octupole AHE:

- Hall measurement of in-plane ***M***
- Allowed in all space groups
- Showing various angle dependence

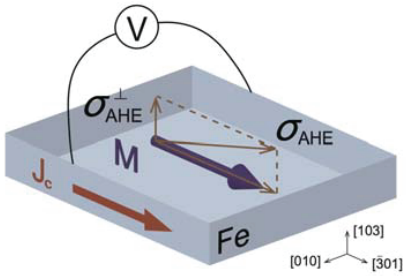


**Octupole AHE contribution is significant!**

Anomalous Hall effect

Magneto-optical Kerr effect(MOKE)

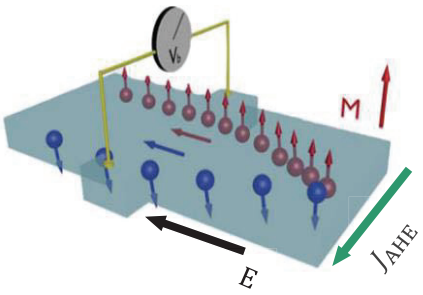


$\sigma_{xy}(f)$

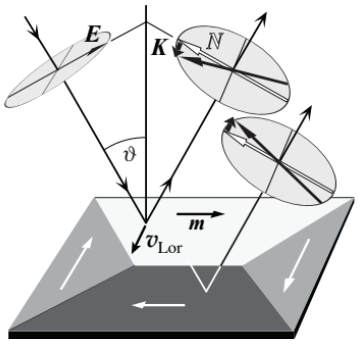


$E_{xx} \rightarrow E_{xy}$@few Hz

$E_{xx} \rightarrow E_{xy}$@~$10^{14}$ Hz





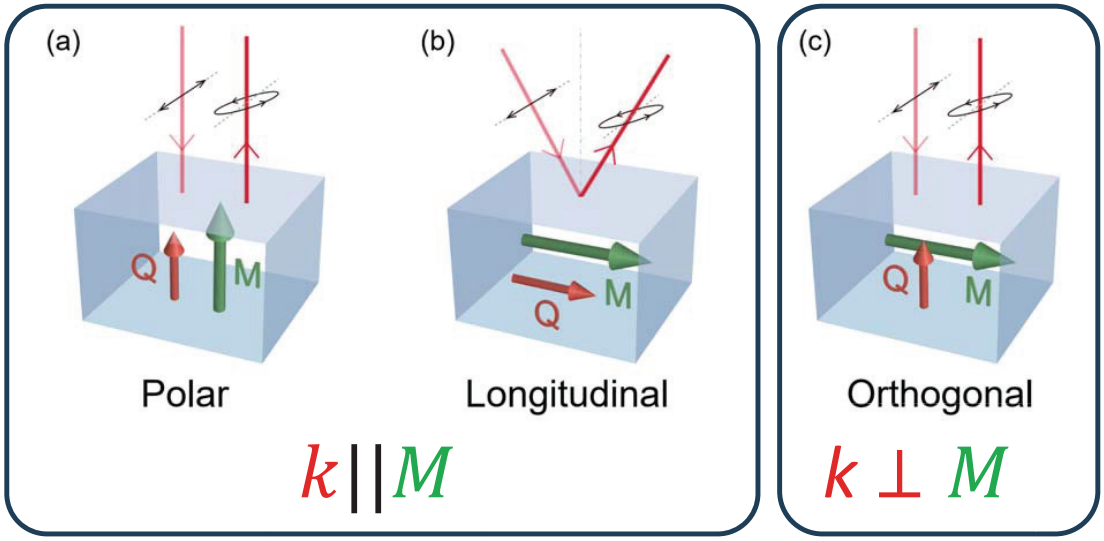

## Orthogonal MOKE in Tb:BIG

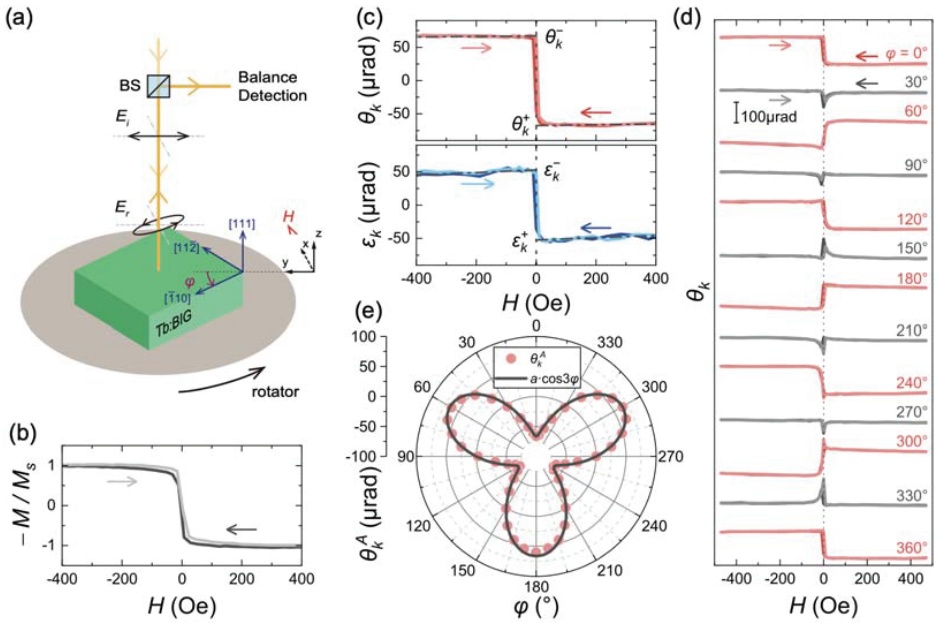




## Orthogonal MOKE in Ni(111)

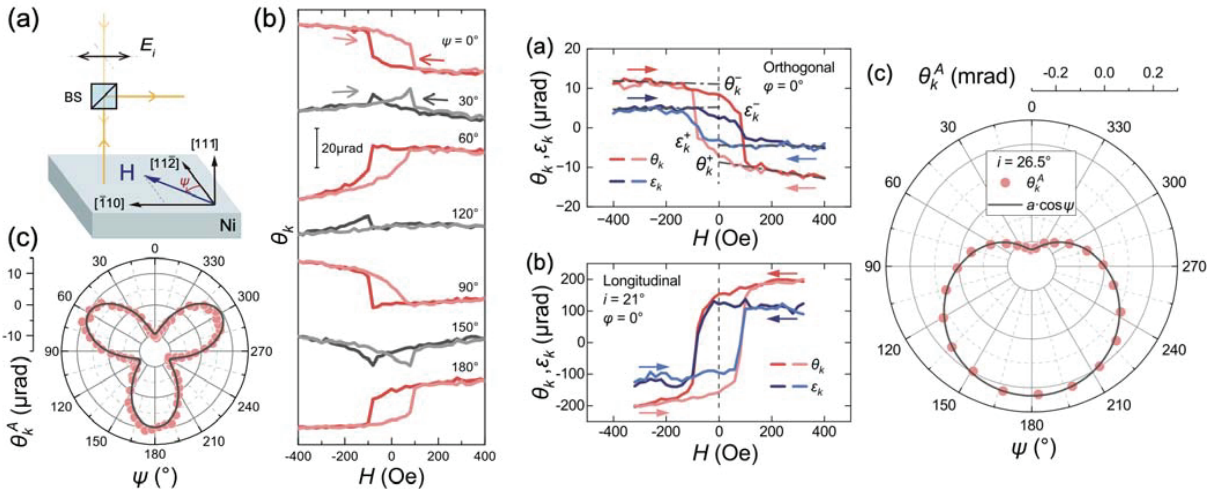

## Orthogonal MOKE in FGT

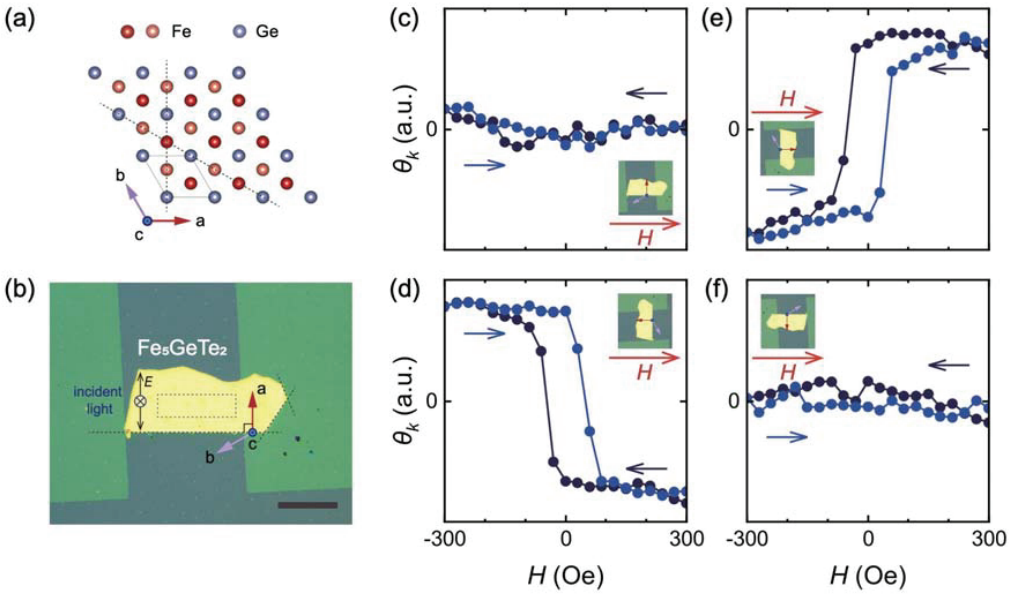




## Summary

$$\sigma^i_{\mathrm{AHE}} = p_{ij}\hat{M}_i + \frac{1}{15}o_{ijkl}\hat{M}_j\hat{M}_k\hat{M}_l \cdots$$

**Dipole** **Multipolar structure**

### In-plane AHE

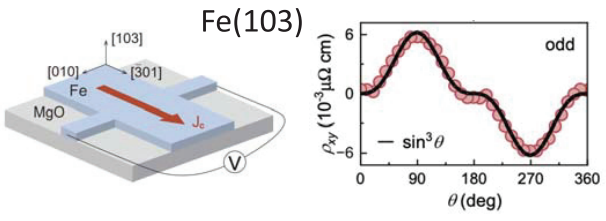


### Orthogonal MOKE

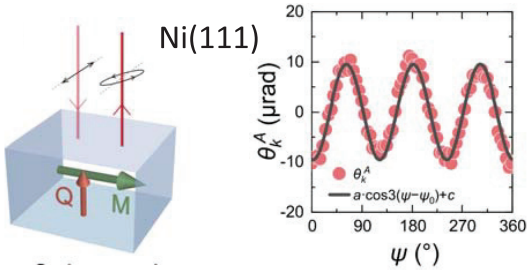

## Acknowledgement

### Hou group

Wenzhi Peng

Haolin Pan

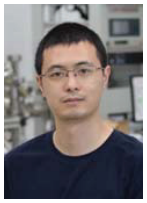

### Theorists

Dr. Zheng Liu

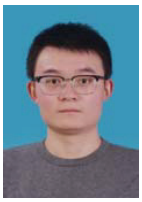

Prof. Yang Gao

Prof. Qian Niu

### Fundings

NSFC
National Natural Science Foundation of China

LUXET 凌光红外 Lingguang Infrared Tech Co., Ltd

中华人民共和国 科学技术部

MEMO

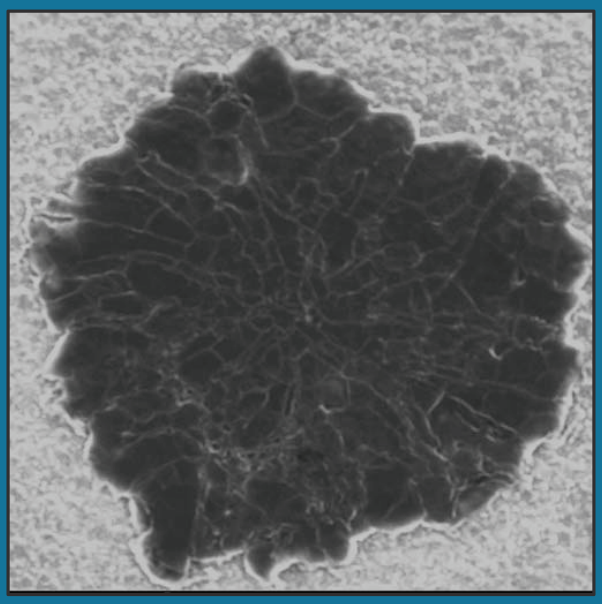

*Lithium plated on Cu*

# Formation Rate as a Key Factor in Enhancing the Stability of Anode-Less Lithium Metal Batteries

**E-IMR Conference, November 26th, 2024**

**Soochan Kim, Michael De Volder**

**University of Cambridge**

THE FARADAY INSTITUTION
EXTENDING BATTERY LIFE

UNIVERSITY OF CAMBRIDGE

## What are anode-less batteries?

Historic perspective (three contributions to Nobel Prize):

**Stanley Whittingham (1973)** | **John B. Goodenough (1980)** | **Akira Yoshino (1991)**

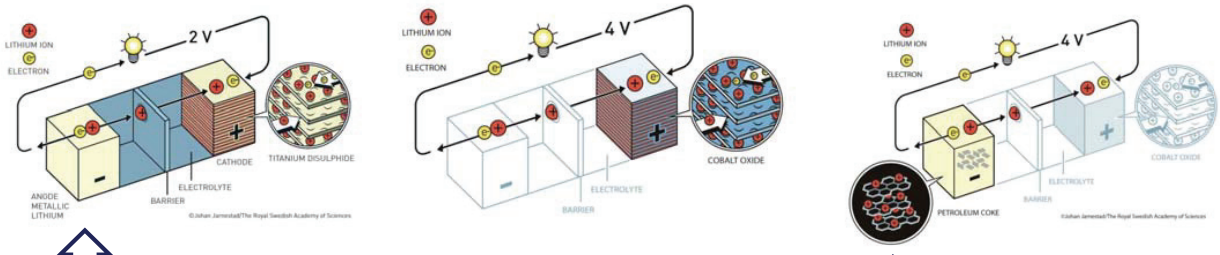


Dramatic improvements possible by revisiting 50 year old anode technology

Past 30 years only industrial anode development has been on adding Si to Gr and controlling SEI better

UNIVERSITY OF CAMBRIDGE

## What are anode-less batteries?

### Historic perspective

**Whittingham (1973) / Half-cell**

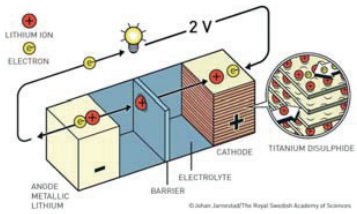


>250 µm Lithium

**Li metal anode**

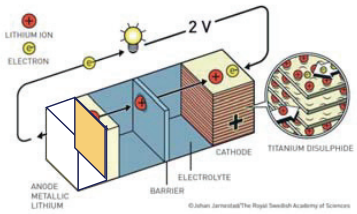


<50 µm Li on Cu foil

**Anode-Less**

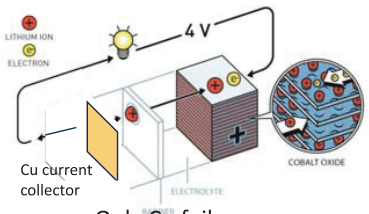


Only Cu foil

Why Anode-less (anode free) rather than Li metal?

- Manufacturing thin lithium foils (<50 µm thickness) over large areas is challenging
- Processing batteries with Li metal foils requires controlled environment
- N/P ratio = 1, lean design, but no additional Li inventory to artificially increase lifetime

UNIVERSITY OF CAMBRIDGE

## "Half cells" versus "Li metal anode" versus "Anode free"

**Half Cell**

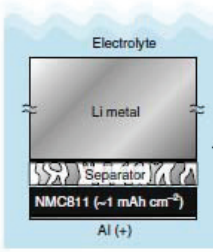


Thick Li disk
Lots of electrolyte
Low areal loading

**Li metal anode**

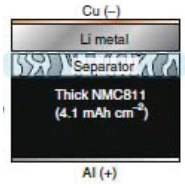


Thin Li sheet
Little electrolyte
High areal loading

**Anode free**

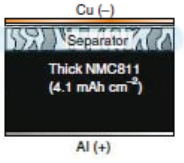


No Li sheet
Little electrolyte
High areal loading

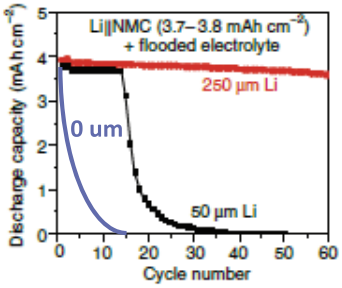


Half cells are very different from Anode Free!

4

UNIVERSITY OF CAMBRIDGE

*[Adapted from J. Liu, Nature Energy | VOL 4 | MARCH 2019 | 180–186]*

## What are the benefits if we get anode free batteries right?

The benefits:

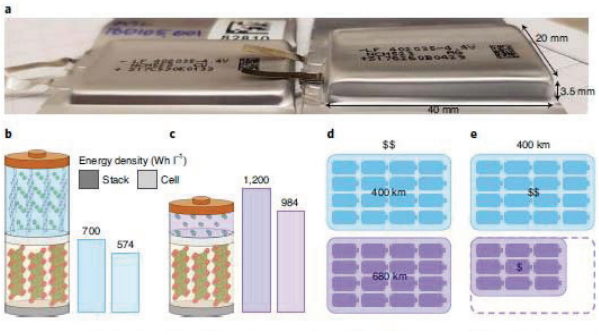


*[R. Weber, Nature Energy, 4, 683–689, **2019**]*

The challenge:

*Recording in collaboration with Prof H. Arai*

UNIVERSITY OF CAMBRIDGE

## Existing strategies to extend lifetime of anode-less batteries

**Degradation Mitigation**

- **Electrolytes**
- **Pressure & Dilatom.**
- **SEI, Current collector**
- **Formation & Cycling protocols**

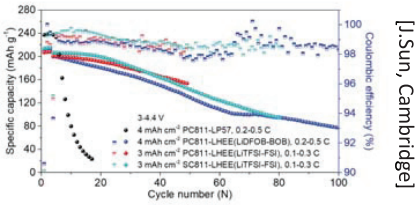


[J.Sun, Cambridge]

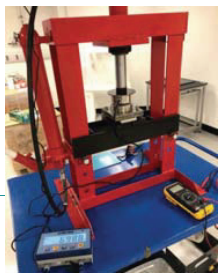

[G. Bree – Warwick]

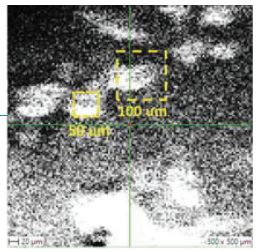


[A. Huang - Imperial]

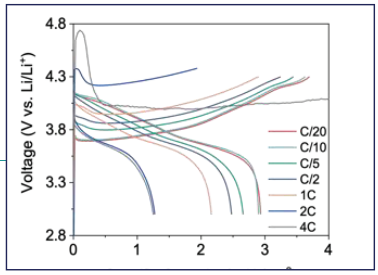


This presentations

UNIVERSITY OF CAMBRIDGE

## Formation protocol background

Cell formation has a strong impact on battery life time

- In academia:
  - Rest cells ~ 1 day after electrolyte filling
  - Cycle 3 times at C/10
- In industry:
  - Protocols are much more complex
  - C/20, C/10, C/4 with long rests and de-gassing
  - Protocol kept secret
- Common understanding:
  - Slow charge/discharge improves Graphite SEI

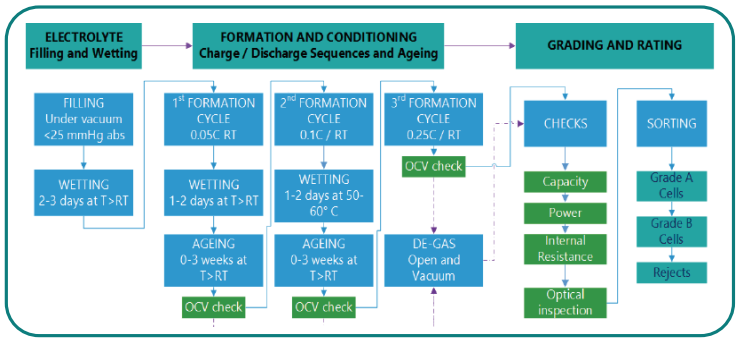


Anode-less literature: Suggests temperature control is important

Our approach: Check if slow formation protocols developed for Gr are good for anode-less



## Cycling results: Cycling protocol

One formation C-D at different C-rates (C/20 to 4C) + Asymmetric cycling at C/5 and D/2

Only the first cycle is changed

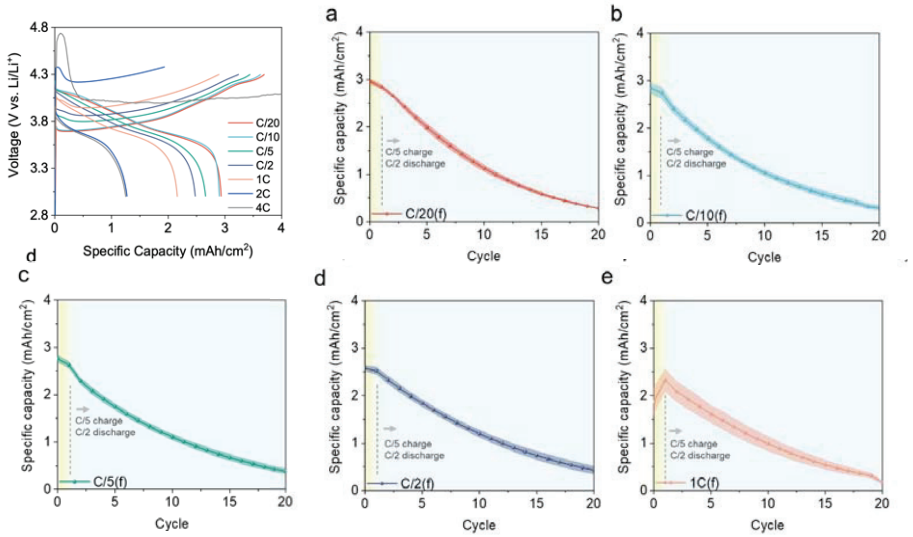


**Cell design:**
NMC 811 vs Cu
Areal capacity: 3 mAh/cm$^2$,
1M $LiPF_6$ in EC:DEC, 1:1, *v:v*

(2C and 4C formation failed)

## Cycling results: Coulombic efficiency

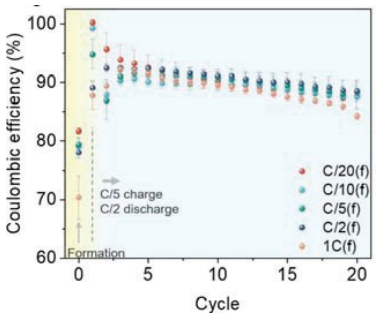


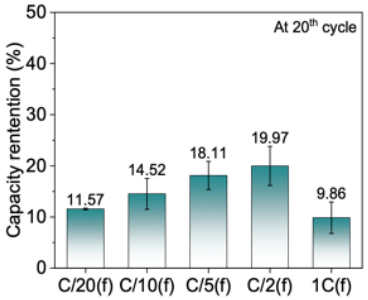


**Observations:**

- Small difference in formation rate has huge impact on CE!
- Very slow and very fast formation leads to poor performance
- Highest capacity retention (20%) @ C/2 formation
- Capacity retention can be doubled by changing the formation cycle

**Hypothesis**:

- Initial Li deposition leave traces templating subsequent plating



## EIS – DRT Analysis

Impedance analysis to study SEI formation

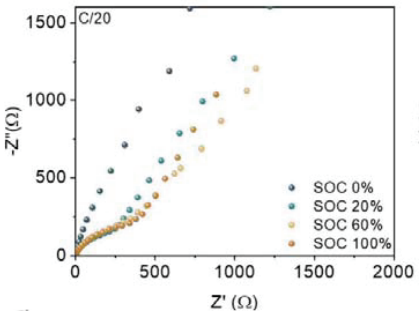


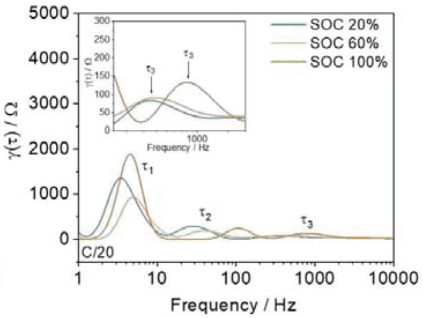


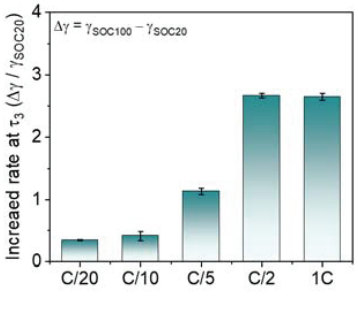


- EIS: Data overlaps, therefore moved to DRT analysis.
- DRT: Distribution of relaxation times. $\tau_3$ supposedly captures interfacial phenomenon
- $\tau_3$ peak increases more with SOC at fast formation than C/2, which suggesting a different behaviour of the SEI

## Post-mortem SEM analysis: First Plating

Plated Li structure decrease in size with C-rate

At 1C dendrites are observed (in agreement with low CE)

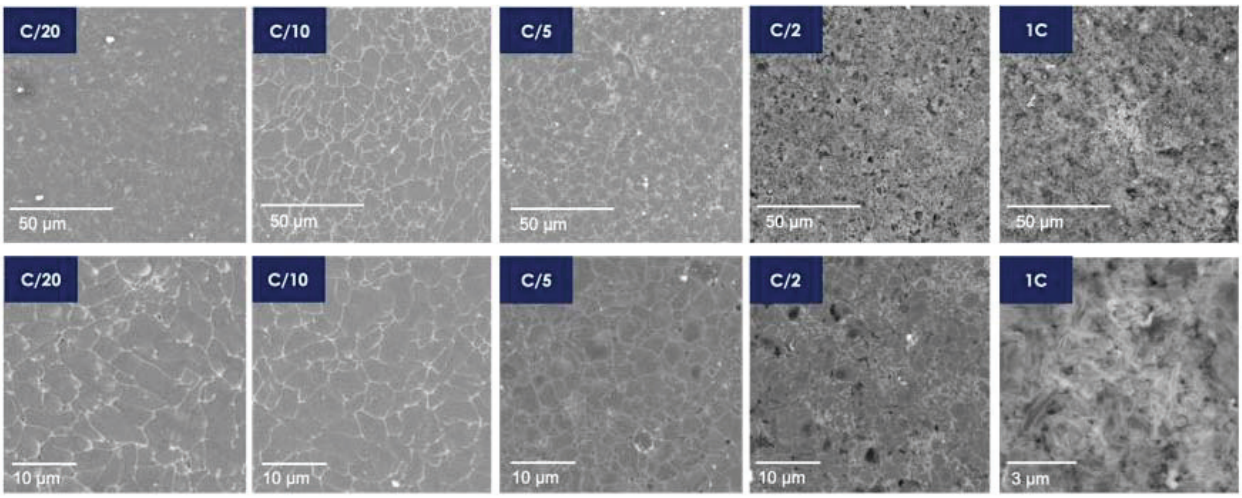


## Post-mortem SEM analysis: First Plating

Li platelet size decreases with C-rate

At 1C dendrites are observed (in agreement with low CE)

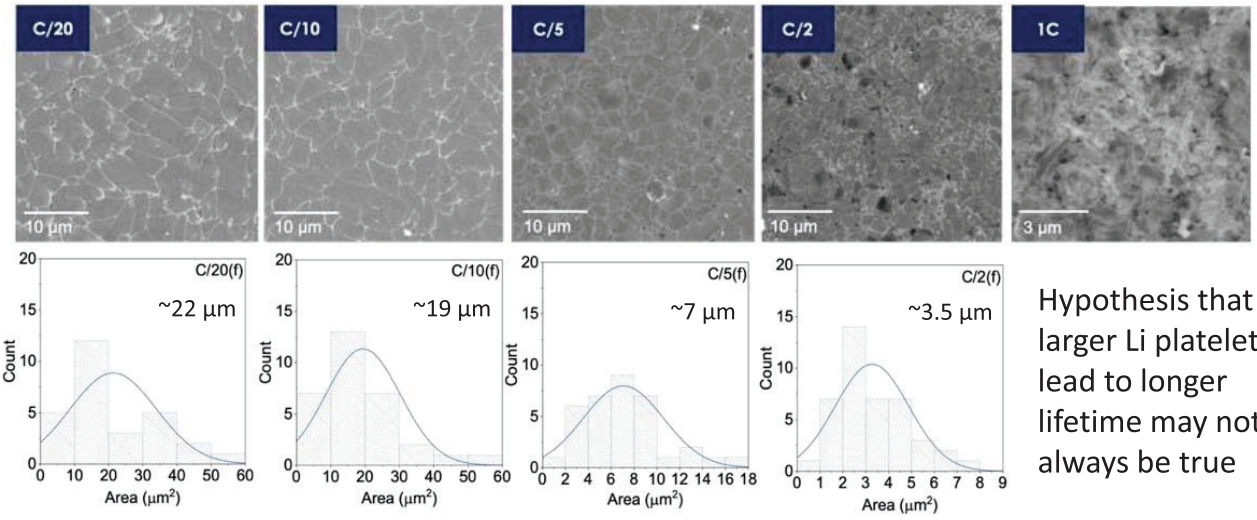


Hypothesis that larger Li platelets lead to longer lifetime may not always be true

## Post-mortem SEM analysis: First Plating

Li platelet size decreases with C-rate

At 1C dendrites are observed (in agreement with low CE)

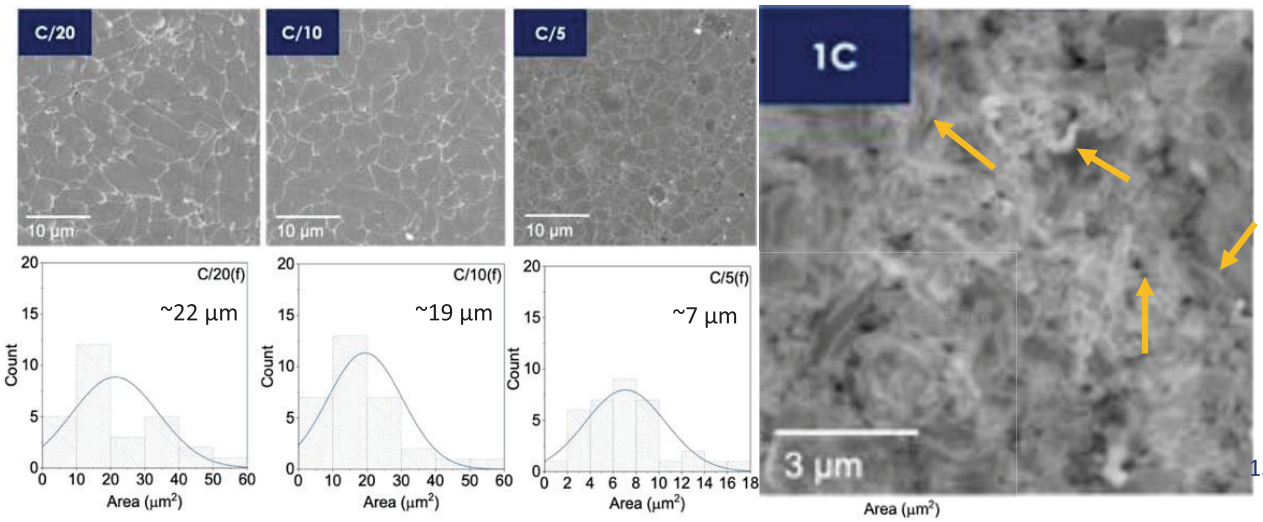


15

## Post-mortem SEM analysis: First Plating SEI

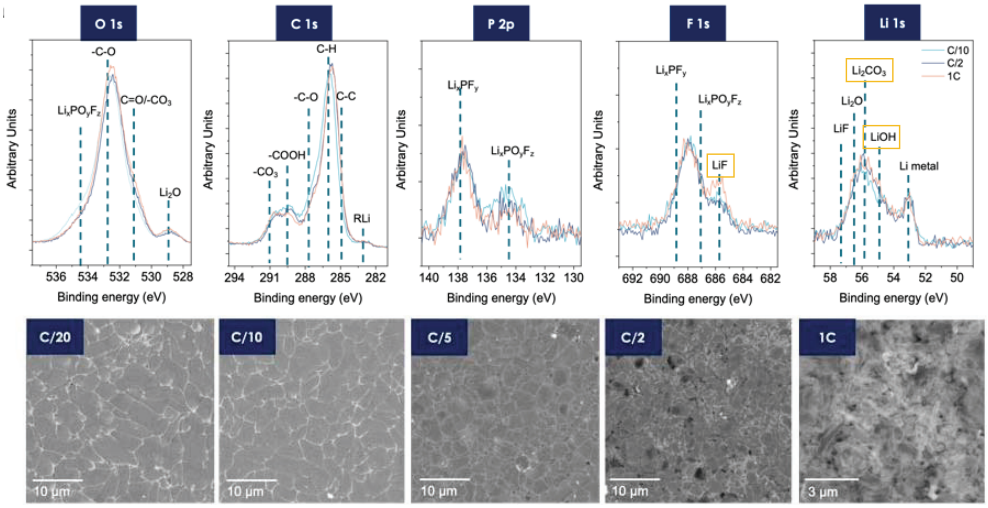


*[XPS by Weatherup group]*

High rate, LiF, $Li_2CO_3$, and LiOH, signal increases.

Inorganic SEIs are known to improve anode-less LIB cycling stability.

This is reflected in higher CE

16

## Post-mortem SEM analysis: First Stripping

Stripped Li after formation at different C-rates

At low C-rate Cu is exposed, which may lead to preferential deposition on Li residues

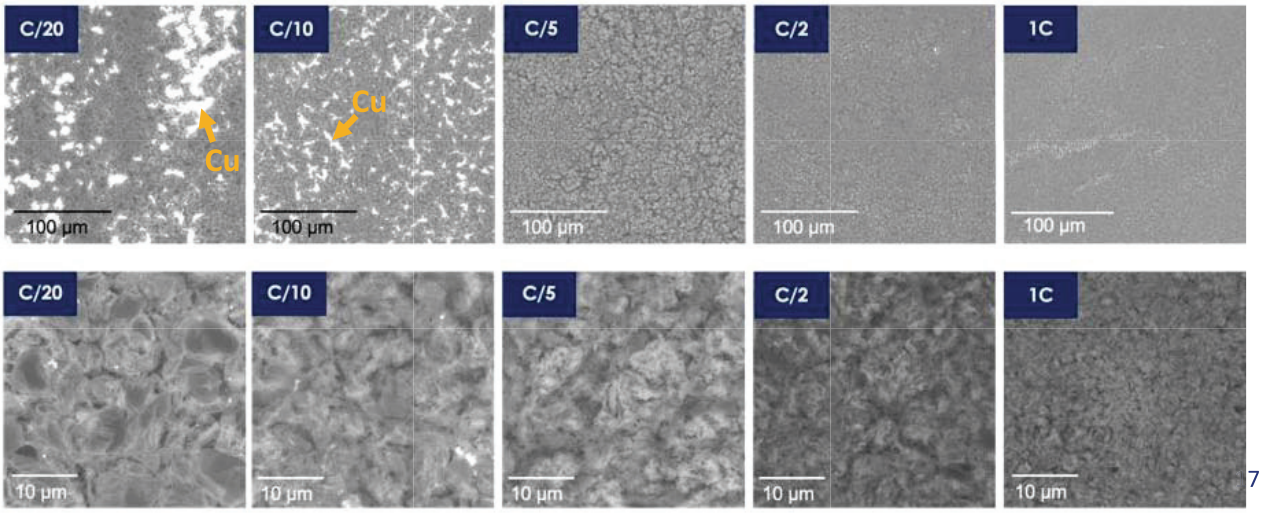


7

## Cross-section SEM @ 2nd Charge

Differences in substrate after first formation, lead to very different second plating

These Cross section after second plating **all @ C/5**

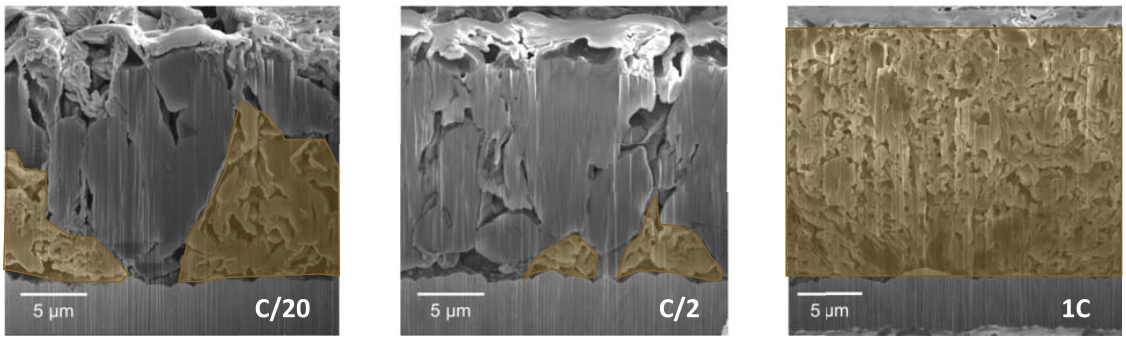


High surface area Li

First cycle has large impact in subsequent cycles which explains differences in CE

18

## Proposed Li morphology evolution

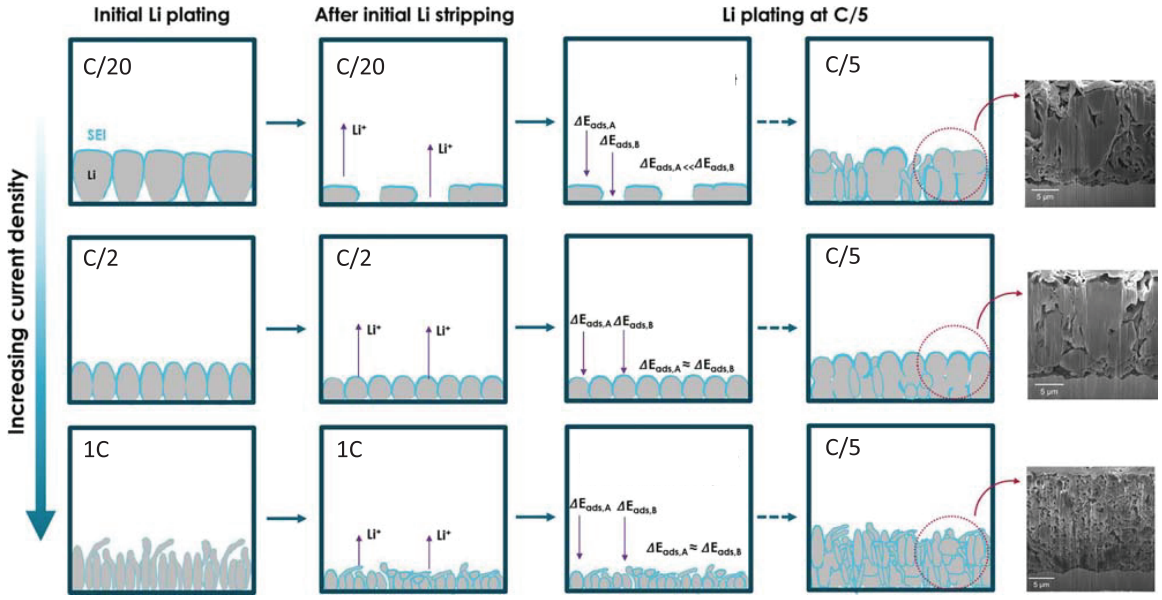


20

## Is this trend universal or specific to one electrolyte?

Repeated formation and cycling protocol on:

- Dual Salt LiDFOB-LiBF4
- Localised high concentration LiFSI-1.2DME-3TTE (M47)

Optimal formation rates are different

- C/5 for dual salt
- C/10 for M47

for 3 mAh/cm$^2$ cells

Are the trends on the Li morphology the same as observed previously?

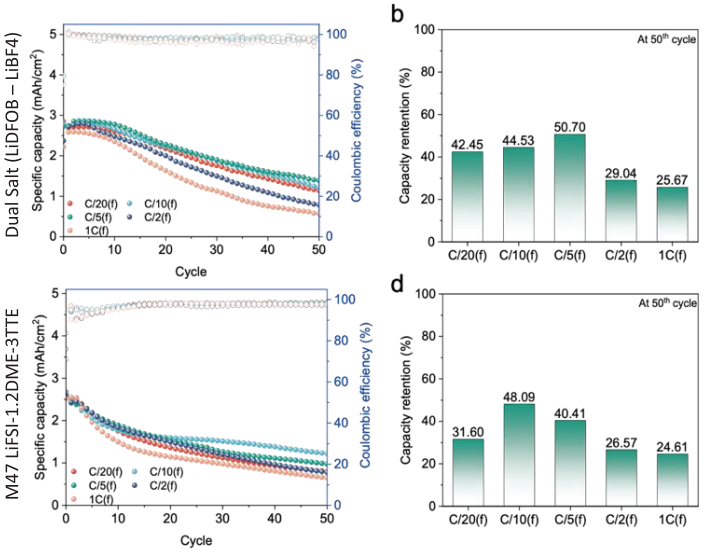


21

## Li plating morphology

Electrolyte influences plated Li morphology

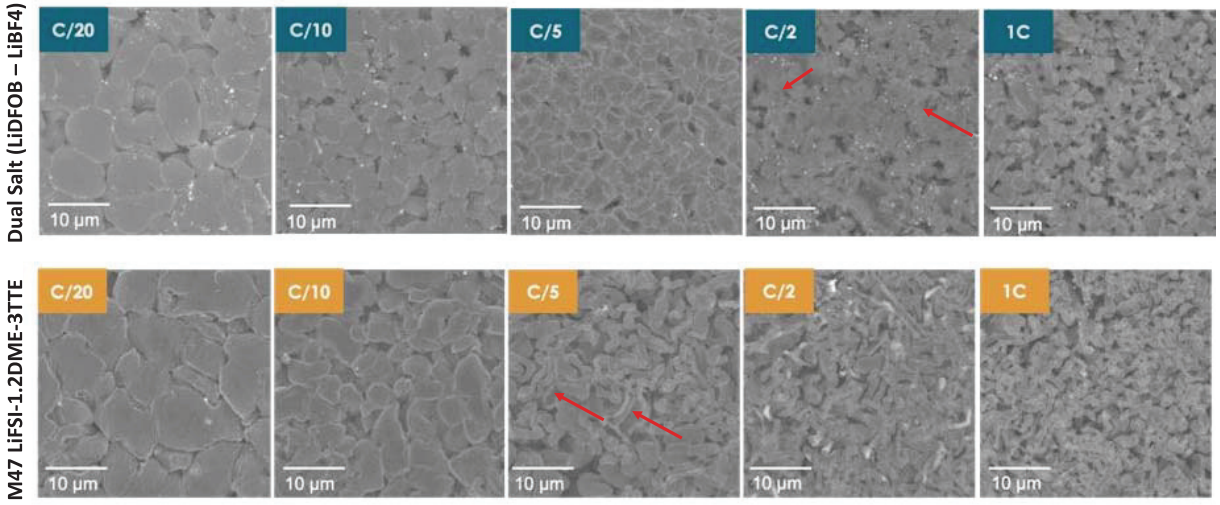


Largest platelets do not lead to best cycling performance

Best formation always at fastest rate prior to dendrite formation

22

## Summary: The secret life of anode-less batteries

**Anode less batteries are very different from Graphite and Li-metal cells!**

- ~~Formation cycles should be as slow as possible~~
- Fastest rate that does not lead to dendrite formation gives best capacity retention for 3 families of electrolytes tested
- The initial plating and stripping dictates plating behaviour in subsequent cycles
- Optimised formation can double battery life-time

UNIVERSITY OF CAMBRIDGE

23

# Thank you!

## Acknowledgements

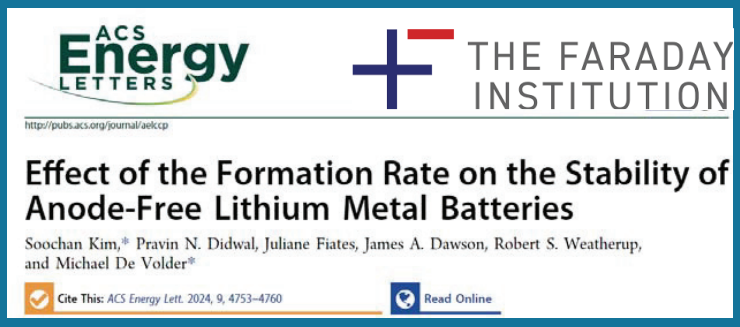

MEMO

MEMO

MEMO

令和６(2024)年11月発行
発行者　東北大学金属材料研究所
　　先端エネルギー材料理工共創研究センター

〒980-8577　宮城県仙台市青葉区片平２－１－１
TEL　022－215－2072
FAX　022－215－2073
E-Mail　e-imr@grp.tohoku.ac.jp
URL　http://www.e-imr.imr.tohoku.ac.jp/

東北大学金属材料研究所
先端エネルギー材料理工共創研究センター

Institute for Materials Research, Tohoku University
Collaborative Research Center on Energy Materials (E-IMR)

# E-IMR International Workshop 2024

## 2024.11.26 （Tue）

## 12:55 – 17:30

**Maximization of solar energy utilization and innovative materials for heat, electricity, and hydrogen storages**

**Venue**

Institute for Materials Research, Tohoku University Auditorium, Bldg. 2(Online)

**Free of charge**

**Click here to register**

https://docs.google.com/forms/d/1uWs7S1WE4sCDZxz5cum9jFtuAzOA6COiBoHJQTBdTgM/edit

私たちは持続可能な開発目標（SDGs）を支援しています

【 Contact us 】
Institute for Materials Research, Tohoku University
E-IMR Research Support Office
Phone: 022-215-2072
E-mail: e-imr*grp.tohoku.ac.jp Please change * to @.

# E-IMR International Workshop 2024 11.26 Thu. 12:55-17:30

| Hours | Content & Speakers |
|---|---|
| 12:40 | opening |
| 12:55 - 13:05 | Opening Remarks<br>Tetsu Ichitsubo　[Center Director, E-IMR Center] |
| 【research publication】 | |
| 13:05 – 13:20 | 「On the dynamics of magnets and ferroelectrics」<br>Bauer Gerritt E.W　[Solar Energy Conversion Materials Research Unit / Advanced Institute for Materials Research Professor] |
| 13:20 – 13:45 | 「Recent Progresses in Skyrmionic Materials and Devices」<br>Wanjun Jiang　[Tsinghua University Professor] |
| 13:45 – 14:00 | 「Dissociative Oxygen Adsorption and Incorporation in $Co_3O_4$-Dispersed PCFC Cathodes」<br>Hitoshi Takamura　[Energy Storage Materials Research Unit / School of Engineering Tohoku University Professor] |
| 14:00 – 14:25 | 「Revealing the Surface Termination Effect of Perovskite for Oxygen Exchange Reaction」<br>Di Chen　[Tsinghua University Associate Professor] |
| 14:25 – 14:50 | 「Mobility and clustering of O and anion vacancies in perovskites as energy materials」<br>Francesco Cordero　[CNR-ISM Istituto di Struttura della Materia　Primo Ricercatore] |
| 14:50 – 15:00 | Break (10 minutes) |
| 15:00 – 15:15 | 「Nanostructure and chemical state imaging of energy materials by coherent X-ray diffraction」<br>Yukio Takahashi　[Materials Evaluation and Analysis Research Unit / International Center for Synchrotron Radiation Innovation Smart Professor] |
| 15:15 – 15:30 | 「Layered Manganese Dioxide as a Heat-Storage Material Utilizing Environmental Water Vapor」<br>Norihiko Okamoto　[Solar Energy Conversion Materials Research Unit / Institute for Materials Research Associate Professor] |
| 15:30 – 15:45 | 「A new AB3-based alloy with reversible hydrogen absorption and desorption reactions and less degradation」<br>Toyoto Sato　[Energy Storage Materials Research Unit / Institute for Materials Research Associate Professor] |
| 15:45 – 16:00 | 「Interface Design for Room-Temperature Rechargeable Magnesium Batteries with Transition Metal Oxide Cathodes」<br>Hongyi Li　[Energy Storage Materials Research Unit/ Institute for Materials Research Project Assistant Professor] |
| 16:00 – 16:10 | Break (10 minutes) |
| 16:10 – 16:35 | 「Recent advances of silicon cystal for solar cells」<br>Deren Yang　[Zhejlang University Professor] |
| 16:35 – 17:00 | 「Probing the Multipolar Structure of Berry Curvature in Magnetization Space by the In-plane Anomalous Hall Effect」<br>Dazhi Hou　[University of Science and Technology of China Professor] |
| 17:00 – 17:25 | 「Formation Rate as a Key Factor in Enhancing the Stability of Anode-Less Lithium Metal Batteries」<br>Michael De Volder　[University of Cambridge Professor] |
| 17:25 – 17:30 | Closing Remarks<br>Tetsu Ichitsubo　[Center Director, E-IMR Center] |